

BIOCHEMICAL CHARACTERIZATION OF SELF-SACRIFICING *P*-AMINOBENZOATE SYNTHASES FROM *CHLAMYDIA TRACHOMATIS* AND *NITROSOMONAS EUROPAEA*

Spenser H. Stone

Thesis submitted to the faculty of the Virginia Polytechnic Institute and State University in partial fulfillment of the requirements for the degree of

Master of Science in Life Sciences

In

Biochemistry

Kylie Allen, Chair

Justin Lemkul

Peter Kennelly

April 28th, 2023

Blacksburg, VA

Keywords: *Chlamydia trachomatis*, *Nitrosomonas europaea*, self-sacrificing enzyme, folate biosynthesis, *p*-aminobenzoate, oxygenase, metalloenzyme

BIOCHEMICAL CHARACTERIZATION OF SELF-SACRIFICING *P*-AMINOBENZOATE SYNTHASES FROM *CHLAMYDIA TRACHOMATIS* AND *NITROSOMONAS EUROPAEA*

Spenser H. Stone

ABSTRACT

Tetrahydrofolate (THF) is an essential cofactor for one-carbon transfer reactions in various biochemical pathways including DNA and amino acid biosynthesis. This cofactor is made up of three distinct moieties: a pteridine ring, *p*-aminobenzoate (pABA), and glutamate residues. Most bacteria and plants can synthesize folate *de novo*, unlike animals that obtain folate from their diet. An established pathway for THF biosynthesis exists in most bacteria, but there is evidence of some organisms such as *Chlamydia trachomatis* and *Nitrosomonas europaea* which do not contain the canonical THF biosynthesis genes, despite still being able to synthesize THF *de novo*. Previous studies have shown that these organisms do not contain the *pabABC* genes, normally required to synthesize the pABA portion of THF, and can circumvent their presence with just a single gene: *ct610* and *ne1434* from *C. trachomatis* and *N. europaea*, respectively. Interestingly, these novel enzymes for pABA synthesis do not use the canonical substrates, chorismate or other shikimate pathway intermediates. The gene product of *ct610* was named Chlamydia Protein Associating with Death Domains (CADD) due to its established role in host mediated apoptosis, while the crystal structure showed an architecture similar to known diiron oxygenases. However, we provide evidence of a moonlighting function in pABA synthesis. Isotopic labeling experiments to understand what substrate might be used by CADD found that isotopically labeled tyrosine was incorporated into the final pABA product. Compellingly, CADD was able to produce pABA in the

presence of molecular oxygen and a reducing agent alone without the addition of any exogenous substrate, implicating this unusual enzyme as a self-sacrificing pABA synthase from *C. trachomatis*. Here, we provide strong evidence for Tyr27 being a sacrificial residue that is cleaved from the protein backbone to serve as the pABA scaffold. Furthermore, we also provide evidence that K152 is an internal amino donor for this pABA synthase reaction performed by CADD. In the case of NE1434, we have conducted initial experiments such as site-directed mutagenesis and our findings suggest that these self-sacrificing residues are conserved between two distantly related organisms. Finally, the pABA synthase activity is reliant on an oxygenated dimetal cofactor and despite the crystal structure of CADD depicting a diiron active site, we have demonstrated that CADD's pABA synthase activity is dependent on a heterodinuclear Mn/Fe cofactor. Conversely, NE1434 demonstrates no preference for manganese and likely employs a more traditional Fe/Fe cofactor for catalysis. Our results implicate the CADD and NE1434 as self-sacrificing pABA synthases that have diverging metal requirements for catalysis.

BIOCHEMICAL CHARACTERIZATION OF SELF-SACRIFICING *P*-AMINOBENZOATE SYNTHASES FROM *CHLAMYDIA TRACHOMATIS* AND *NITROSOMONAS EUROPAEA*

Spenser H. Stone

GENERAL AUDIENCE ABSTRACT

Folate is a molecule used by all organisms that is necessary for survival. Many kinds of bacteria are able to make this molecule with proteins called enzymes, which help by quickening the rate of a reaction. Enzymes are catalysts that usually work by binding a molecule, called a substrate, and will act on this substrate to generate a product; the enzyme remains unchanged in this process, which allows it to facilitate many more of these reactions. *Chlamydia trachomatis*, which is a leading cause of sexually transmitted infections (STIs) in the United States, and *Nitrosomonas europaea*, an environmental bacterium, are able to use enzymes to make their own folate, but not in the way that many other bacteria do. These organisms contain enzymes that use a part of their own structure as a substrate, making them “sacrificial lambs”. Our study provides evidence of how these organisms carry out an abnormal chemical reaction to make folate which can help scientists target this pathway for the development of antibiotics.

Acknowledgements:

I have been extremely fortunate to have an incredible network of supporters who have made my academic career possible. Thank you to Dr. Kylie Allen, who has mentored me for the duration of my project and shown me what it means to be an inquisitive scientist. Thank you to my committee members, Dr. Justin Lemkul, Dr. Peter Kennelly, and Dr. Glenda Gillaspay for your additional support and insight. Thank you to Eric Truong and Logan Peters for your help with my project and allowing me to grow as a mentor. I would also like to thank Ash VanWinkle, Kayla Kester, Kaleb Boswinkle, Paul Kavanaugh, and Thuc-Anh Dinh for your friendships and accountability to being better scientists. Thank you to my best friend Ariel, for your unwavering support since we were young- you influence me to always strive for a better version of myself. To my mom, dad, Cami, and Chelsea- thank you also for your love and support since I was young. Finally, thank you to my love, Cameron, for standing by me through every moment and pushing me to pursue what brings me joy.

Contents

Abstract.....	ii
General audience abstract.....	iv
Acknowledgements.....	v
Contents.....	vi
List of figures.....	viii
List of tables.....	ix
Attributions.....	x
1. Introduction	
1.1 A non-canonical route for tetrahydrofolate biosynthesis in <i>Chlamydia trachomatis</i>	1
1.2 CADD is a moonlighting protein with at least two distinct functions in <i>C. trachomatis</i>	2
1.3 Dimetal Oxygenases.....	11
1.4 Class I RNR's and Its Subclasses.....	15
1.5 R2-like Ligand Binding Oxidase (R2lox).....	21
1.6 Summary.....	22
References.....	30
2. Identification of metal preference and amino acid residues sacrificed for <i>p</i>-aminobenzoate synthesis by a metalloxygenase from <i>Chlamydia trachomatis</i>	35
2.1 Abstract.....	35
2.2 Introduction.....	36
2.3 Materials and Methods.....	38
2.4 Results.....	44
2.5 Discussion.....	50
References.....	63
3. Initial biochemical characterization of a putative self-sacrificing <i>p</i>-aminobenzoate synthase from <i>Nitrosomonas europaea</i>	67
3.1 Abstract.....	67
3.2 Introduction.....	68
3.3 Materials and Methods.....	70

3.4 Results.....	74
3.5 Discussion.....	78
References.....	87
4. Future Directions	88
References.....	93

List of Figures

1.1 Canonical biosynthesis of Tetrahydrofolate	23
1.2 <i>Chlamydiae</i> exist as an EB and an RB during host parasitism.....	24
1.3 The extrinsic and intrinsic apoptotic pathways.....	25
1.4 The crystal structure of CADD.....	26
1.5 Abbreviated shikimate pathway.....	26
1.6 Potential aromatic and amino donors for CADD dependent pABA synthesis	27
1.7 Structural comparison of relevant HDOs and FDOs to CADD	28
2.1 The active site of CADD.....	56
2.2 Scheme for self-sacrificing pABA synthesis by CADD.....	56
2.3 SDS-PAGE gel of a typical CADD purification.....	57
2.4 pABA synthase activity of CADD with and without DTT.....	57
2.5 Metal dependence of CADD pABA synthase activity	58
2.6 pABA synthase activity of CADD expressed with 1,10-phenanthroline	58
2.7 Influence of superoxide and hydrogen peroxide on CADD pABA synthase activity	59
2.8 LC-MS analysis of modified amino acids in the CADD reaction	60
2.9 SDS-PAGE analysis of putative cross-link forming conditions in CADD.....	61
2.10 pABA synthase activity of K152A and K152R in the presence of an exogenous amino source	61
3.1 AlphaFold structural prediction of NE1434	81
3.2 SDS-PAGE gel of a typical NE1434 purification.....	82
3.3 LC-MS analysis of pABA production by NE1434	82
3.4 Site-directed mutagenesis studies in NE1434.....	83
3.5 <i>In vitro</i> enzymatic assays of NE1434 in the presence and absence of iron	83
3.6 pABA synthase activity of NE1434 WT from various growth conditions.....	84
3.7 Metal dependence of NE1434 pABA synthase activity	84
3.8 Incorporation of molecular oxygen into NE1434-derived pABA	85
4.1 Residues of interest for a radical translocation pathway in CADD	92

List of Tables

1.1 Summary of major THF biosynthesis genes.....	29
2.1 ICP metal analysis of CADD apo preparation methods	62
2.2 Observed masses of Tyr and Lys modifications via LC-MS/MS analysis	62
3.1 NE1434 site-directed mutagenesis primers	86

Attributions

The chapters of this thesis were written by Spenser Stone, with content and grammatical changes made by the primary research advisor for this project, Dr. Kylie Allen. Initials provided below will be used to denote the contributions of each author for the chapters.

Spenser Stone (SS)

Dr. Kylie Allen (KA)

Rowan Wooldridge (RW)

Andrew Pedraza (AP)

Eric Truong (ET)

Aleksei Gendron (AG)

Keith Ray (KR)

Richard Helm (RH)

Chapter 1:

Attribution: SS wrote the entirety of the chapter with content and grammatical suggestions provided by KA.

Chapter 2:

Attribution: SS and RW performed wet lab experiments relevant to the manuscript and contributed equally to the work. AP and ET performed minor wet lab experiments under the guidance of RW and SS, respectively. KR and RH performed LC-MS/MS experiments and data analysis. KA wrote the published version of this manuscript, which was adapted and edited by SS for this thesis. Content suggestions and insight were provided by KA.

Chapter 3:

Attribution: AG and RW performed initial wet lab experiments for this project and ET performed wet lab experiments under the guidance of SS. SS designed and oversaw all wet lab experimental work after the initial experiments. All data analysis was performed by SS. SS wrote this chapter with guidance and suggestions from KA.

Chapter 4:

Attribution: SS wrote this chapter with insight and suggestions provided by KA.

Chapter 1:

Introduction

1.1 A non-canonical route for tetrahydrofolate biosynthesis in *Chlamydia*

trachomatis

Tetrahydrofolate (THF, Figure 1.1A) is an essential cofactor that is required for one-carbon transfer reactions in purine biosynthesis and amino acid biosynthesis, as well as for methylation reactions in several other pathways [1]. Because this cofactor is involved in basic cellular processes, it is necessary for all forms of life; however, animals obtain THF from their diet, whereas most bacteria and plants synthesize it *de novo* [1,2]. THF is a tripartite molecule that is composed of a pteridine ring, *p*-aminobenzoate (pABA), and a varying number of glutamate residues in the form of a γ -linked poly-glutamylated tail (Figure 1.1A) [1]. The canonical pathway for *de novo* THF biosynthesis is well-characterized, especially due to the evolutionary distinction between how mammals and bacteria acquire it, making this pathway an important antimicrobial target [1]. Typical THF biosynthesis proceeds with FoleQBK enzymes to produce the pterin portion using GTP as a substrate. pABA is synthesized from chorismate by PabA/B (ADC synthase) and PabC (ADC lyase). Finally, FolPCA performs the ligation of the pterin and pABA portions, as well as the glutamylation and reduction steps to produce the active form of the cofactor (Figure 1.1B) [2].

Although the canonical THF biosynthesis genes are generally highly conserved, there are examples of alternative routes for THF biosynthesis in select organisms. For example, the intracellular pathogen, *Chlamydia trachomatis*, as well as the ammonia-oxidizing bacterium, *Nitrosomonas europaea*, contain several unique genes for THF biosynthesis (Table 1.1). Chapter 2 and 3 of this thesis describe a novel route to produce the pABA portion of THF in these organisms. Because *C. trachomatis* is a pathogenic organism with implications for human health, more work has been done thus far to characterize this unusual pathway. Interestingly, *C. trachomatis* is sensitive to drugs that target the uptake of exogenous THF but is also able to survive in folate-depleted environments, which suggests this organism can synthesize THF in addition to scavenging the cofactor from the environment [2,3]. Despite the ability to synthesize THF *de novo*, many of the canonical genes used for THF biosynthesis are missing from the genome of *C. trachomatis* [2]. Previous work demonstrated that FolE and FolQ were functionally replaced by RibA (GTP cyclohydrolase II) and TrpF (*N*'-5'-phosphoribosylanthranilate isomerase), respectively, to produce the pterin portion of THF in *C. trachomatis* [1,2]. Additionally, a γ -glutamyl ligase with archaeal origins is recruited to replace FolC and add a varying number of glutamate residues to the joined pterin and pABA moieties [2]. Finally, instead of utilizing *pabABC*, *C. trachomatis* complements its need for pABA with a single gene, *ct610* [4]. *N. europaea* is also described to bypass typical pABA biosynthesis in a mechanism similar to *C. trachomatis* and will be discussed in further detail in Chapter 3 of this thesis.

1.2 CADD is a moonlighting protein with at least two distinct functions in *C. trachomatis*

***Chlamydiae* as intracellular pathogens.** *Chlamydiae* are obligate intracellular bacteria known to cause a wide range of diseases [5]. This genus is comprised of 13 species that infect

various types of hosts. In particular, *C. trachomatis* continues to be one of the leading sexually transmitted infections (STIs) reported in the United States and is the causative agent of trachoma - blindness due to bacterial origins. Unfortunately, trachoma is entirely curable, yet extremely prevalent in areas with low access to preventative care [6]. Another species, *C. abortus*, is an enzootic disease that specifically attacks the placenta of ruminant animals and can have devastating consequences for livestock [6].

To decrease metabolic burden, intracellular pathogens often experience a genomic decay over time to eliminate redundant biosynthetic genes of metabolites they could otherwise uptake from their host [1,7]. With one of the smallest bacterial genomes, *Chlamydiae* pathogens are able to maximize their infectious efficiency through reliance on their host for essential nutrients. *Chlamydiae* have streamlined their replicative cycles to manipulate host machinery, but also remain sheltered while not actively dividing. The unique life cycle of *Chlamydiae* is defined by a dimorphic life cycle: the infectious, metabolically inactive elementary body (EB) and the metabolically active, non-infectious reticulate body (RB) [8]. Outside a host cell, *Chlamydiae* exist as EBs, which are structurally rigid to allow the pathogen to remain protected until it is within a host [9]. Upon attachment and ingestion, the crosslinked disulfide bonds of the EB's outer shell are reduced, allowing for differentiation into the more fluid RB; the RB is able to scavenge essential nutrients from the host, recruit host proteins, and actively divide within the protective membrane (Figure 1.2) [3,9,10].

CADD modulates host cell apoptotic activity. The dimorphic life cycle of *C. trachomatis* is a key aspect in this intracellular pathogen's ability to maintain an infection in its host. For the organism to perpetuate an infection, it must re-differentiate into a RB and then can exit the host cell in either of two modes: release of the inclusion body or host cell lysis [11]. An

important mechanism for the successful reproduction and evasion of host detection is modulation of host cell apoptosis, an irreversible programmed cell death in response to stimuli or stress [12,13].

There are two main pathways that apoptosis within a cell can occur: the extrinsic/death receptor pathway or the intrinsic/mitochondrial pathway (Figure 1.3) [12]. In the extrinsic pathway, members of the Tumor Necrosis Factor (TNF) receptor family are responsible for transmitting a death signal from the cell surface to the inside to initiate apoptosis; each receptor is composed of cysteine-rich extracellular domains, a transmembrane domain, and a cytoplasmic domain which is also known as the “death domain” [12]. First, death receptors localized to the membrane will bind a death signaling ligand that initiates the signal transduction pathway [14]. This binding event triggers the recruitment of the respective intracellular apoptotic inducing ligands which will oligomerize at the effector death domain, allowing for the additional recruitment of apoptosis associated proteins such as FADD, Fas Associated Death Domain protein [12,14]. Dimerization of FADD is the final step needed to recruit pro-apoptotic proteases such as caspase-8 and caspase-10 [14]. The Death Inducing Signal Complex (DISC) is formed and intracellular proteases are activated to induce apoptosis by cleaving proteins within the cell [12,14]. Caspases are also linked to the intrinsic apoptotic pathway through the cleavage of a pro-apoptotic BH3-domain only protein, BID [15]. The truncated form of BID, tBID, activates other pro-apoptotic proteins such as BAX and BAK, where each will oligomerize and translocate to the mitochondrial membrane to create pores [15,16]. The permeabilization of the mitochondrial membrane leads to loss of membrane potential and the subsequent release of cytochrome c into the cytoplasm, a key indication of apoptosis [12,15,16]. Cytochrome c then binds to apoptotic peptidase activating factor-1 (Apaf-1) and initiates the oligomerization of these subunits to form

an apoptosome [12]. This active complex allosterically activates caspase-9, an initiator caspase that stimulates other caspases [17].

Because *Chlamydiae* rely heavily on a host cell for metabolism, it was originally thought that the bacteria would independently encode apoptotic signals in order to regulate apoptosis of the host cell [18]. Bioinformatic analysis of *Chlamydial* genomes for proteins that share sequence homology with death domains of mammalian TNF receptor family proteins revealed CADD, *Chlamydia* Associating with Death Domains, encoded by the gene *ct610* of *C. trachomatis* [18]. CADD shares 37% similarity to the death domains of human DR5 and DR4, and 33% similarity to human Fas; the degree of similarity between CADD and these human death domain receptors is comparable to the similarity between human TNF receptor family members [18]. Results from initial experiments showed that CADD interacted with cytosolic death domains of TNF receptors and was able to induce apoptosis without the native ligand [18]. Additionally, it was found that even as CADD co-localized with Fas, apoptosis was not induced, which suggests that the recruitment of Fas to the inclusion body rather than to its respective death domain ligand prevents host-induced apoptosis to limit infection of other healthy host cells [19,20]. There is evidence of CADD-like genes in other clinically significant *Chlamydiae* species, which suggests an advantageous mode of survival from the conservation of these genes [18].

Structural analysis of CADD. The crystal structure of CADD was solved not long after it was shown to play a role in host-mediated apoptosis (Figure 1.4A). Although the structure of CADD was expected to be similar to death domain associating proteins due to its role in apoptosis, it instead revealed a dimer of a seven-helix bundle, an architecture first observed in heme-oxygenases [21]. Additionally, the structure contained a diiron active site comparable to the hydroxylase component of soluble methane monooxygenase (sMMOH) and the β -subunit of class

Ia ribonucleotide reductases (RNRs). Since the structural characterization of CADD, several related proteins have been identified, which together comprise an emerging protein family termed Heme-oxygenase like Diiron Oxidases (HDO's) [22,23].

CADD shares sequence identity with PqqC (18%), human-heme oxygenase (11%), R2 subunit of RNR (12%), and the α -subunit of sMMOH (9%) [23]. Although not all of the active sites of these enzymes are conserved, each possesses redox function, which suggests this fold is an appropriate fit for redox chemistry [23]. The active site is formed by a narrow cavity and there are six residues that coordinate the two metal atoms: Glu-81, His-88, Glu-142, His-174, Asp-178, and His-181 (Figure 1.4B); these residues are conserved in CADD-like proteins across *Chlamydiae* species [23]. Interestingly, when the metal coordinating residues were altered by site-directed mutagenesis, apoptotic activity of CADD decreased by more than 60% [18]. The active site of CADD was found to be most similar to that of RNR-R2 but did not contain any of the conserved residues that this enzymes uses to initiate catalysis, suggesting that these two enzymes might not carry out the same reaction [23]. Additionally, it was shown that CADD housed a narrow internal cavity adjacent to the diiron center, similar to the active site cavity of sMMOH [23]. Because the active site cavity is so narrow, the only accessible molecules to this space is restricted to small molecules such as: O₂, H₂O₂, CH₄, CH₃OH, CO, or CO₂ [23]. Products and substrates are expected to access the cavity via a tunnel in conserved locations for both enzymes, which suggested that CADD has similar function to sMMOH [23]. Despite being originally annotated as “PqqC like” based on sequence similarity, CADD does not share a conserved active site with PqqC and is not likely functionally related [23].

CADD's involvement in a novel THF biosynthesis pathway. Previous work identified that *C. trachomatis* synthesizes THF *de novo*, despite missing the canonical THF biosynthetic

genes [3,4]. A comparative genomic analysis of *Chlamydial* genomes uncovered a conserved cluster containing homologs of *folBKPA*, *folC2* (an archaeal γ -glutamyl ligase), and *ct610*, the gene encoding CADD [2]. Since the enzyme responsible for generating the pABA portion of THF in *C. trachomatis* was unknown, it was hypothesized that CADD may be the missing pABA synthase. Although CADD was shown to have a function in inducing host cell apoptosis, its similarity to known redox enzymes suggested a potential moonlighting function [18].

Thus, an *E. coli* $\Delta pabABC$ mutant was used to test the potential role of CADD in pABA synthesis. Indeed, the $\Delta pabABC$ mutant was complemented by the addition of a plasmid containing *ct610* in the absence of exogenous pABA, suggesting that CADD was responsible for the production of pABA in these cells [4]. Once CADD was identified as a possible pABA synthase in *C. trachomatis*, the first task was to pinpoint the substrate used in the reaction.

Under the assumption that CADD might be able to use canonical pABA precursors as substrates, various *E. coli* mutants were created for complementation studies. The typical pABA biosynthetic pathway starts with chorismate and glutamine [2]. However, CADD was able to also complement the growth of *E. coli* $\Delta aroA$ mutants that were unable to synthesize chorismate and otherwise needed the supplementation of aromatic amino acids, 4-hydroxybenzoate, and pABA to grow [2]. This result demonstrated that CADD did not utilize the typical pABA substrate, chorismate [2].

Although this result was surprising, it seemed possible that CADD instead used a metabolite that precluded chorismate. Shikimate and 3-dehydroquinate are metabolic precursors to chorismate, so these compounds were also investigated as potential substrates [2]. Chorismate biosynthesis starts with the cyclization of 3-deoxy-D-arabino-heptulosonate-7-phosphate to form 3-dehydroquinate by AroB (Figure 1.5) [2]. AroD then acts on this molecule to produce 3-

hydroshikimate, which is finally reduced to shikimate by AroE [2]. *E. coli* Δ *aroD* Δ *pabA* and *E. coli* Δ *aroB* Δ *pabA* mutants were surprisingly complemented by CADD, thus determining CADD likely does not utilize any intermediates from the shikimate pathway to produce pABA [2].

Once chorismate metabolites were ruled out as possible substrates for CADD, another potential aromatic precursor, ubiquinone, and its precursor, *p*-hydroxybenzoate (pHB), were investigated as substrates for CADD-dependent pABA synthesis [2]. Once again, CADD complemented *E. coli* Δ *ubiC* Δ *pabA* mutants that were unable to synthesize the first metabolite of ubiquinone biosynthesis, pHB, in addition to pABA [2]. Results concluded from these experiments indicated that CADD did not employ chorismate, shikimate, ubiquinone, or any of these respective molecules' precursors as substrates for pABA synthesis.

Although CADD was able to rescue the growth of several shikimate pathway *E. coli* deletion strains described above, these experiments required the supplementation of aromatic amino acids and *p*-hydroxybenzoate (pHB), which lead to the hypothesis that either pHB or L-tyrosine could be the precursor for CADD-dependent pABA biosynthesis [2,24]. To test if either of these molecules were incorporated, the *E. coli* Δ *pabA*+*CADD* strain was cultured with either *p*-[3,5-²H₂]HB or L-[3,5-²H₂]tyrosine, where both compounds contain two deuterium atoms on the aromatic ring [24]. The incorporation of each isotopically labeled substrate was determined by the increase in mass of the final pABA produced from the cultures; it was determined that there was 15% incorporation of *p*-[3,5-²H₂]HB and 40% incorporation of L-[3,5-²H₂]tyrosine into the final pABA product [24]. Because the reaction containing labeled L-tyrosine was supplied with 50% unlabeled L-tyrosine, 40% incorporation of labeled L-tyrosine was a significant finding and suggested that L-tyrosine was likely a precursor for CADD produced pABA [24].

As a novel pABA synthase, CADD's initial biochemical characterization relied heavily on structural comparisons. Noting that the established structure of CADD was similar to sMMOH and class Ia RNRs, enzymes that use molecular oxygen as a substrate, it was hypothesized that CADD would also be dependent on molecular oxygen for catalysis [24]. Thus, anaerobic cultures of *E. coli* $\Delta pabA+CADD$ were grown with or without additional pABA supplementation. Anaerobic cultures that were supplemented with pABA were able to grow whereas those without exogenous pABA retained no growth [24]. This finding started to piece together a potential mechanism by determining that O₂ was needed for successful CADD-dependent pABA production. Further, *in vitro* experiments with purified CADD showed that pABA was produced in the presence of molecular oxygen and a reducing agent alone. Interestingly, the addition of exogenous substrates such as pHB or L-tyrosine did not increase the amount of pABA produced by CADD *in vitro*. Combined with the isotope-labeling data that showed L-tyrosine was incorporated into pABA produced by CADD, this result suggested that CADD is a novel self-sacrificing enzyme that uses a tyrosine residue for the production of pABA. Careful interrogation of CADD's crystal structure identified five tyrosine residues in the active site that could possibly engage in the self-sacrificing reaction: Y27, Y43, Y47, Y141, and Y170 [24]. Additionally, an amino group source would be required, so it was hypothesized that a lysine residue, K152, near the active site played a role in this step [24]. Thus, site-directed mutagenesis studies in which each tyrosine was mutated to a phenylalanine revealed that Y27F and Y43F, which are located nearly 14Å away from the di-metal cofactor, were completely inactive in the pABA synthase assay, suggesting that one of these residues could be the sacrificial substrate (Figure 1.6) [23,24]. The study also found that CADD's pABA synthase activity was substantially decreased for the

K152R mutant, which implied that it was important for catalysis and could be the amino group source since no exogenous amino donors were added [24].

The *in vitro* assays for the initial characterization of the pABA synthase activity of CADD yielded poor turnover of only 0.3% [24]. Iron quantitation indicated that only ~10% of the purified enzyme contained a complete diiron cofactor that was presumably necessary for catalysis based upon the diiron cofactor observed in the crystal structure [24]. Thus, it was hypothesized that the addition of excess Fe(II) to allow for more complete incorporation of this metal into the active site would enhance CADD's pABA synthase activity [24]. On the contrary, the addition of Fe(II) to reactions did not improve CADD's pABA synthase activity [24]. The culmination of this work raised the question if iron is the true cofactor required for CADD's self-sacrificing pABA synthase activity. Thus, Chapter 2 of this thesis describes further biochemical studies to identify the cofactor of CADD as well as to identify the amino acid residue(s) sacrificed as substrates in the reaction.

A related self-sacrificing pABA synthase in *Nitrosomonas europaea*. Chapter 3 of this thesis is focused on the characterization of a pABA synthase from *Nitrosomonas europaea* orthologous to CADD. *Nitrosomonas* are gram negative bacteria that are key players in the first step of nitrification of the nitrogen cycle. These organisms are ammonia-oxidizing bacteria (AOB) that oxidize ammonia (NH_3) to nitrite (NO_2^-), where ammonia is one of their main energy sources and CO_2 is their primary source of carbon; therefore, these bacteria are formally known as obligate chemolithoautotrophs [25,26]. Because these organisms are responsive to fluxes of nitrogen in the environment, they can live in a wide variety of landscapes such as freshwater, sewage, soil, or regions with high levels of pollution and are crucial to increasing the availability of nitrogen to plants [25,27]. As several industrial processes produce high levels of nitrogenous

waste, more attention is being drawn to bioremediation, the exploitation of natural processes to degrade harmful pollutants into less toxic products [28]. It is presumed that ammonia oxidation is the rate-limiting step of the nitrogen cycle, due to the low abundance of nitrite in the environment [26].

Although *N. europaea* is distantly related to *C. trachomatis*, it also lacks *pabA*, *pabB*, and *pabC*, and rescues the growth of *E. coli* $\Delta pabABC$ strains with the complementation of a single gene, *ne1434* [4]. It was confirmed that like CADD, *E. coli* $\Delta pabABC+ne1434$ strains did not need the addition of any exogenous substrates for pABA biosynthesis such as chorismate or shikimate, implying that *N. europaea* employs a similar self-sacrificing pABA biosynthesis pathway [4,24].

1.3 Dimetal Oxygenases

Both CADD and NE1434 are classified as heme-oxygenase-like diiron oxidases (HDOs), a relatively new superfamily of enzymes that retain a conserved 3-helix bundle motif that is distinct from the more well known 4-helix bundles seen in ferritin-like nonheme diiron oxidases and oxygenases (FDOs) [22,29]. Members of this family are able to catalyze diverse reactions including *N*-oxygenation during streptozotocin biosynthesis (SznF [22,30,31]), oxidative bond cleavages (UndA [32], and BesC [33]), and methylene excision (FlcD [34]). These enzymes have a heme-oxygenase-like fold that houses a diiron cofactor coordinated by carboxylate-containing and histidine residues [35]. Molecular oxygen is reduced at the Fe₂(II) site, creating the active metal cofactor, forming a μ -peroxo-Fe₂(III/III) intermediate [29,35]. Additional turnovers of this cofactor can occur by reduction of the μ -(hydr)oxo-Fe₂(III/III) cluster [35]. Current evidence

indicates that the detailed catalytic mechanism can vary widely amongst HDO superfamily members. Additionally, class I RNRs and R2lox present similar and diverging dimetal cofactor chemistry that may guide further characterization of HDOs. Thus, the acknowledgment of functionally similar metal coordination motifs that catalyze such diverse reactions presents many fascinating questions concerning structural differences that arrange diverging cofactor assembly. The following paragraphs will summarize what is currently known about HDO superfamily members as well as related enzymes with similar chemistry (Figure 1.7).

SznF. SznF is an HDO involved in the biosynthesis of the nitrosourea pharmacophore streptozotocin (SZN), an approved chemotherapeutic drug [30]. Over the course of three subsequent Fe(III) dioxygen dependent steps, SznF modifies the guanidino group of *N*^ω-methyl-L-arginine (L-NMA) to eventually produce *N*^δ-hydroxy- *N*^ω'-methyl- *N*^ω-nitroso-L-citrulline (L-HMNC), a precursor to SZN [30]. Although the mechanism in which this occurs has not yet been described in detail, spectroscopic studies have demonstrated that SznF targets two N atoms for hydroxylation utilizing the same μ -Fe₂(III/III) intermediate [35]. Results identified a μ -1,2-peroxo-Fe₂(III/III) intermediate in complex with L-NMA suggesting two possible mechanisms.

The central domain of SznF contains the six carboxylate metal coordinating residues that are conserved in other HDO enzymes, CADD and UndA, and the mutation of any of these given residues results in negligible activity [30,35]. Similarly to UndA (see below), initial attempts to co-crystallize SznF with an occupied diiron site were unsuccessful and only a fraction of the crystals retained complete diiron active sites [22]. Surprisingly, further X-ray crystallographic studies comparing the apo enzyme with its iron occupied structure revealed that iron site 2 of the HDO domain was not preformed, unlike what is seen in FDO's; residues 311 to 318, which contains three of the metal coordinating ligands, is ordered but non-helical. In the iron-bound

form of SznF, this same segment adopted an alpha-helical structure and other metal coordinating residues were seen to shift from the outside of the protein to face in to the diiron cavity [22]. These large structural shifts upon iron binding combined with the difficulty in capturing metal-loaded preparations of SznF raises the question of why this flexibility in the metal binding core is necessary.

UndA. Characterization of the enzyme UndA was first described in the search for enzymes involved in the production of the semivolatile metabolite, 1-undecene, from *Pseudomonas aeruginosa* [36]. It is the first member of the diverse HDO family to have been prescribed a function; UndA catalyzes the oxidative decarboxylation of the medium-chained fatty acid (FA), lauric acid, to produce 1-undecene and carbon dioxide [32,36].

Originally, UndA was incorrectly assigned to contain a mononuclear Fe(II) cofactor based on the metal loading efficiency seen in the crystal structure [32,37]. An oxygen-activated diferric cluster was eventually confirmed through the use of Mössbauer spectroscopy, but an intact diiron form has yet to be crystallized [22,32,37]. Although CADD and UndA share 24% sequence similarity as well as the residues necessary for diiron metal coordination, CADD appears to be the outlier of the HDOs characterized thus far and to date is the only structure of this family to demonstrate stable metal assembly [22,23,32]

Although the details of the UndA mechanism have not been fully described, the proposed catalytic mechanism draws inspiration from sMMO, due to the striking similarities in the resulting diferric states of the cofactor during Mössbauer characterization and single turnover studies performed by Manley et al, 2019 [32]. Unlike SznF, which can initiate catalysis in the absence of a bound substrate, UndA starts with a FA-ligated to the oxygenated diferric cluster which can then proceed to form the bis-Fe(IV) “Q” intermediate in the open or closed form [32,37]. In either

case, post-oxygen cleavage, this Q intermediate would then be able to perform a hydrogen atom transfer (HAT) from either the β -carbon or COO- group of the FA [32]. The starting dimeric state could be restored by single electron transfer (SET) performed by the $\text{Fe}^{\text{III}}\text{Fe}^{\text{IV}}$ species to produce either a carbocation or substrate biradical that could undergo rearrangement to form CO_2 and undercene [32]. Further reduction would then be needed to reform the diferrous state [32]. Furthermore, UndA was able to convert myristic acid (C14:0) and capric acid (C10:0) to their respective 1-alkenes, which further emphasizes the substrate flexibility seen in this enzyme [32,37].

BesC. BesC is an enzyme that resides in the β -ethynyl-L-serine biosynthetic pathway of *Streptomyces cattleya* and catalyzes the carbon-carbon bond cleavage of 4-chloro-L-lysine to produce 4-chloro-L-allyglycine, formaldehyde, and ammonia [33]. The complex fragmentation requires substrate binding to activate O_2 by the enzyme's diferrous cofactor in a manner similar to FA-UndA ligation [33,38]. There are confounding interpretations of the ordered assembly of the diiron cofactor and substrate binding; Manley et al. identified through Mössbauer spectroscopy a stable dinuclear iron site in BesC that was not bound to substrate [33]. However, McBride et al. was unable to corroborate these findings through crystallographic interpretations and found rather that the substrate binding event induces a conformational change of α_3 to properly orient residues that will then coordinate the iron in site 2, parallel to the structural change seen in iron-bound SznF [22,33,38].

Crystallization of apo BesC confirmed the presence of a flexible α_3 , which can also be seen in previously described HDO's (SznF and UndA) [38]. Comparable to intermediates found in SznF and UndA, a μ -peroxodiiron (III) intermediate forms post substrate binding to BesC which allows for the reduced diiron (II) cofactor to efficiently trap molecular oxygen [33].

Notably, the formation of the μ -peroxodiiron (III) intermediate is long-lived and the substrate is free to dissociate as well as rebind the intermediate, owing this ability to the dynamic scaffold of this HDO [33]. Additionally, during crystallization attempts, residues 203-212 of $\alpha 3$, which contribute to the coordination of iron in site 2, did not present reliable electron density when the protein was exposed to iron; these findings are similar to the respective residues found in SznF and UndA [30,32,38]. The inability of several HDO members to retain a stable diiron cofactor as predicted suggests that these enzymes operate via a mechanism that does not require a tightly bound diiron cofactor or the diiron cofactor is recycled for subsequent reactions [22]. Moreover, the flexibility of the metal binding core coupled with the instability of oxidized diiron cofactors alludes to the possibility that these versatile HDO enzymes were programed in this way to allow for active site lability.

1.4 Class I RNRs and Its Subclasses

Ribonucleotide reductases (RNRs) are essential enzymes in nucleic acid metabolism of all living organisms and catalyze the reduction of ribonucleotide 5'-di- or triphosphates (NDPs or NTPs) to deoxynucleotide 5'-di- or triphosphates (dNDPs or dNTPs) [39]. Because these enzymes play a crucial role in regulating levels of dNDPs and dNTPs, they are controlled by allosteric and transcriptional regulation mechanisms; activity of RNRs can be manipulated by nucleotide binding sites that are sensitive to substrate reduction ("S" site) as well as their overall activity ("A" site) [39]. RNR's share a universal mechanism to generate a cysteine thiyl radical that initiates abstraction of the 3'-hydrogen atom [40–42]. These enzymes can be further segregated into one of three classes depending on the cofactor used to generate the catalytic cysteine radical [42]. Class I enzymes utilize a dinuclear oxygen dependent cluster and are found

in all domains of life. Class II enzymes use adenosylcobalamin (vitamin B₁₂) to directly oxidize the active site cysteine. Lastly, class III enzymes are found only in microbes and use a [4Fe-4S] cluster associated with *S*-adenosylmethionine (SAM) that initiates the formation of a stable glycy radical in the enzyme active site [39]. Irrespective of the metallocofactor, this transient oxidation of the cysteine residue allows the resulting radical to activate the inert 3' C-H bond in the ribose ring, allowing the reduction mechanism to occur [39].

Given the similarities between CADD and class Ia RNRs, the remainder of the section will focus exclusively on class I RNRs. Class I RNRs are heterodimers comprised of an α and a β subunit; α contains the catalytic cysteine radical and is where the ribonucleotide reduction occurs, and β houses the metallocofactor necessary to initiate the reaction by generating the cysteine radical [39]. Although class I enzymes seem to have a simple architecture, the reaction involves an impressive long-range radical translocation from the β subunit to the active site of the α subunit, an estimated 35-40 Å [39,42]. Additionally, class I RNRs are assorted into different subclasses depending on: 1) the number and type of metal ions used in the β subunit, 2) the source of oxidant needed to generate the active cofactor, 3) accessory proteins needed to assemble the cofactor, and 4) the identity of the radical-initiator used in the β subunit to generate the Cys• in the α subunit (tyrosyl radical [Y•] or metal-based) [39,42]. It is likely that the divergence of radical initiation chemistry in class I RNRs derived from bacterial pathogenesis and this hypothesis will be described further below [43].

Class Ia. More than 30 years ago, class Ia RNRs were first described and to date, their metallocofactor is the best characterized of the class I enzymes [42]. These enzymes contain a diiron metal center and the activation of the catalytic cysteine residue in the α subunit is derived from a Fe₂(III/III)-Y• [39,42]. β subunits of class Ia RNR enzymes all have a symmetrical four-

helix bundle core to coordinate two Fe (II) molecules, making them members of the ferritin structural superfamily, a conserved structure similar to CADD from *C. trachomatis* [23,42]. Because the helices are arranged head to tail, molecular oxygen has a direct pathway via a hydrophobic channel to oxidize the Fe₂(II/II) cluster to the activated Fe₂(III/IV) cofactor [42]. The assembled Fe₂(III/III)-Y• oxidant is fully protected from the solvent which allows for the subsequent radical transfer to be carefully controlled [42].

E. coli class Ia RNR assembles in an $\alpha_2\beta_2$ complex with an α - β interface that modulates a reversible radical translocation from β to α [42]. Dynamic radical translocation over this interface is governed by an asymmetric transient interaction between one α subunit and β_2 , which previously made detection of pathway radical intermediates nearly impossible [44]. The tail of one β subunit extends into the cavity of α , forming a binding pocket with the substrate; this sequestered cavity facilitates β departure as soon as product is released and thus the quick dissociation of the proton-coupled electron transfer (PCET) pathway [44]. Despite experimental difficulties, the radical translocation pathway was impressively established by Stubbe and coworkers [45–47]. Tyr122 is oxidized in the β subunit active site which forms Fe₂(III/III)-Y•; this activated cofactor quickly forms a peroxo-Fe₂(III/III) that is reductively cleaved by an electron from Trp48 [42]. The radical is transiently passed along a hydrogen bonding network of aromatic amino acids (Tyr356 in β ; Tyr731 and Tyr730 in α) to generate the final thiyl radical at Cys439 in the α subunit active site [44,47].

Class Ib. Although diiron-dependent class Ia RNRs are found across all domains of life, newer subclasses of RNRs are being discovered in bacteria and archaea. Unlike humans and animals that utilize Fe-dependent RNRs, prokaryotes living in nutrient depleted environments are presented with metabolic challenges that necessitate the need for adaptation [42]. Interestingly,

E. coli encodes both class Ia and Ib RNRs and it was found that expression of class Ib RNR is the only RNR expressed in mutants with deficient iron sensing and uptake systems [39,48,49].

Class Ib RNR radical chemistry is distinctive in that a $\text{Mn}_2(\text{III/III})\text{-Y}\cdot$ is formed for radical initiation [42]. Unlike $\text{Fe}_2(\text{II})$, $\text{Mn}_2(\text{II})$ is inert with O_2 and needs a reactive form of oxygen to create the active cofactor; therefore, class Ib requires a reduced flavoprotein (NrdI) to produce its active metallocofactor complex [42]. The structure of the class Ib β subunit unveiled a hydrophilic channel that is the necessary link between NrdI and the dimanganese site, indicating that NrdI could be responsible for generating a reduced form of molecular oxygen [42]. Further experimentation confirmed that NrdI was essential for the survival of pathogens with class Ib RNRs and the substitution of iron for manganese was unsuccessful [50,51]. The biological divergence within this class of essential enzymes demonstrates the countermeasures pathogens have evolved to circumvent iron-depleted environments.

Class Ic. The class Ic RNR from *Chlamydia trachomatis* was an important discovery to the class I RNRs; it was the first RNR shown to not utilize a $\text{Y}\cdot$ for cysteine radical initiation, but rather a metal-based oxidant [52]. Sequence alignments revealed the absence of the tyrosine that normally forms the stable $\text{Y}\cdot$ conserved in class Ia and Ib RNRs, and it was shown to be replaced by a redox-inert phenylalanine residue; all other PCET pathway and active site residues were conserved in class Ic [40,42].

The emergence of class Ic RNRs presented additional divergent cofactor requirements that seemed to provide auxiliary modes of achieving the same thiyl radical seen in class Ia and Ib. Class Ic RNRs are defined by a $\text{Mn}^{\text{IV}}\text{Fe}^{\text{III}}$ active cofactor complex formed from $\text{Mn}(\text{II})$, $\text{Fe}(\text{II})$ and either O_2 or $2\text{H}_2\text{O}_2$ [42]. The insertion of Mn into the heterodinuclear site is presumed to be the pathogenic evolutionary advantage compared to diiron dependent RNRs, which are able to

initially react rapidly with H₂O₂, but subsequently reacts very slowly for additional turnover to produce the Fe₂(III/III)-Y• cofactor [53]. Minimal structural differences have been identified to discern the differences seen between class I RNR metal preferences. Furthermore, the substitution of a glutamate for an aspartate at a conserved residue corresponding to coordination at metal site 1 is seen across class Ic enzymes, indicating that there may only be minor structural rearrangements needed to fine tune metal preferences between class I RNRs [42]. Because of the important implications for the chemistry that proceeds, mismetallation of active site metals may provide selective advantages for pathogens.

Class Id. The enzymes in class Id RNR are similar to class Ic in that the activated metal cluster is the initial source of the cysteine radical needed for ribonucleotide reduction [42]. Class Id RNRs are characterized by the presence of an active Mn₂^{III/IV} cluster, but unlike class Ib RNRs which require NrdI for complete assembly of the active cofactor, class Id enzymes appear to assemble independently [54,55]. Cofactor assembly of class Id enzymes is relatively simple and only requires an apo β subunit, Mn(II), and a form of superoxide [54,55].

Class Id enzymes have structural flexibility that was not seen in other subclasses [55]. The class Id β subunit from *Flavobacterium johnsoniae* was the first solved structure of this subclass which showed an unwinding in helix 1 that created a large cavity exposing the metal center to the solvent [55]. Interestingly, apo preparations of the respective metal-loaded enzyme showed that helix 1 had retained order; the differences seen between the metal loaded and apo Id enzyme suggest metal binding induces a large conformational change that increases the access of the metal center to the solvent [54]. Furthermore, the significant structural changes associated with this metal loading may emphasize the divergence seen within class I RNRs.

Class Ie. Class I RNRs discussed thus far all share the requirement of a dinuclear metal cofactor for the activation of catalysis. It is hypothesized that because iron-dependent class Ia RNRs are only found in eukaryotes, manganese-dependent classes I(b-d) have appeared specifically in pathogenic bacteria as a means of survival against iron-directed innate immunity by a host [43]. The emergence of class Ie metal independent RNRs are shown to be present in parasitic and opportunistic pathogens and might be the most effective countermeasure against host defense that targets transition metals [43].

Conserved glutamate residues that have been established in metal coordination for class I(a-d) RNRs are absent in class Ie. These metal coordinating residues have been replaced by two hydrophobic residues that vary between organisms and a positively charged lysine [43,56]. The replacement of these key residues results in the complete absence of metal. Interestingly, *Streptococcus pyogenes* encodes both class Ib and Ie RNRs and a study of this organism's RNRs found that increased exposure to extracellular Fe or Mn downregulated expression of the class Ie RNR [42,57].

Surprisingly, the absence of a dimetal cofactor is not the only distinguishing factor of class Ie from classes Ia-Id. Although the details of the class Ie mechanism have yet to be established, current evidence has determined the cysteine radical initiator to be a 3,4-dihydroxyphenylalanine radical (DOPA•) which requires NrdI for assembly [42,43,56]. Interestingly, DOPA• is the result of a post-translational modification of a tyrosine residue in the same position that the Tyr• is formed in class Ia and Ib [42]. This finding is striking due to the inadequate redox potential of DOPA• to independently oxidize the catalytic cysteine residue [42]. There are still many pieces of information missing regarding DOPA• maturation and radical transfer for this unusual subclass of RNRs.

1.5 R2-like Ligand Binding Oxidase (R2lox)

The R2-like ligand-binding oxidase (R2lox) was named according to its sequence homology with the β (R2) subunit of class Ic RNRs. However, it was found to lack RNR activity, and the true function remains unknown [58]. Despite possessing an unknown function, R2lox assembles a heterobimetallic Mn/Fe cofactor similar to class Ic RNRs; however, unlike class Ic RNRs, it contains a long, hydrophobic channel that leads directly to the metal center, which is coordinated by a carboxylate motif and an exogenous fatty acid [58]. Investigation of this protein thus far has definitively shown its Mn/Fe cofactor requires O₂ activation to form a tyrosine-valine ether crosslink near the active site, but the reason behind this crosslink is unclear [58]. Unlike diiron oxidases which can easily perform this two-electron oxidation for crosslink formation, this is the first Mn/Fe cofactor described to carry out this chemistry [58].

Interestingly, R2lox challenges what is understood regarding the Irving-Williams series of divalent metal stability. The Irving-Williams series is a trend seen in first row transition metal complexes in which stability increases across the period until it reaches copper and is independent of the type of ligand present [59]. Spectroscopic investigations of metal binding found that R2lox consistently bound Mn(II) more tightly in metal site 1 than Fe(II), even though R2lox can also assemble a Fe₂(II) cofactor *in vitro* [58,60]. The selective metal assembly seen in this dimetal oxidase raises the question of how similar enzymes are able to fine tune metal assembly for catalytic processes.

1.6 Summary

As previously reported, CADD from *C. trachomatis* has been implicated in a novel, self-sacrificial pABA synthase pathway [24]. Genomic analysis and subsequent experimentation demonstrated that an ortholog of CADD, NE1434 from *N. europaea*, also complements pABA synthase activity in a mechanism that does not require canonical pABA substrates such as chorismate or shikimate [4,24]. Macias-Orihuela significantly progressed our understanding of the unique mechanistic details for CADD; primary isotopic labeling experiments implicated L-tyrosine as a likely substrate for CADD derived pABA [24]. Successive site-directed mutagenesis studies would eventually narrow down the sacrificial aromatic donor(s) to Y27 or Y43 and a potential internal amino donor to K152. Our work in chapter 2 of this thesis aims to exhibit evidence of modifications that would be indicative of a self-sacrificial mechanism performed by CADD. Additionally, the inability to reconstitute an active enzyme in the presence of Fe(II) raises the possibility that CADD may be dependent on a different metal cofactor. Although HDO members are defined by a diiron cofactor, previous work from our lab indicated that CADD utilized an alternative metal cofactor that is uncovered in Chapter 2 of this thesis.

Notably, CADD and its ortholog, NE1434, are from two distinct organisms but both contain conserved residues implied to be involved in the sacrificial mechanism. This leads to the question of whether each of these enzymes retain similar metal requirements as well as self-sacrificing residues. Initial characterization of NE1434 will be described in chapter 3 of this thesis.

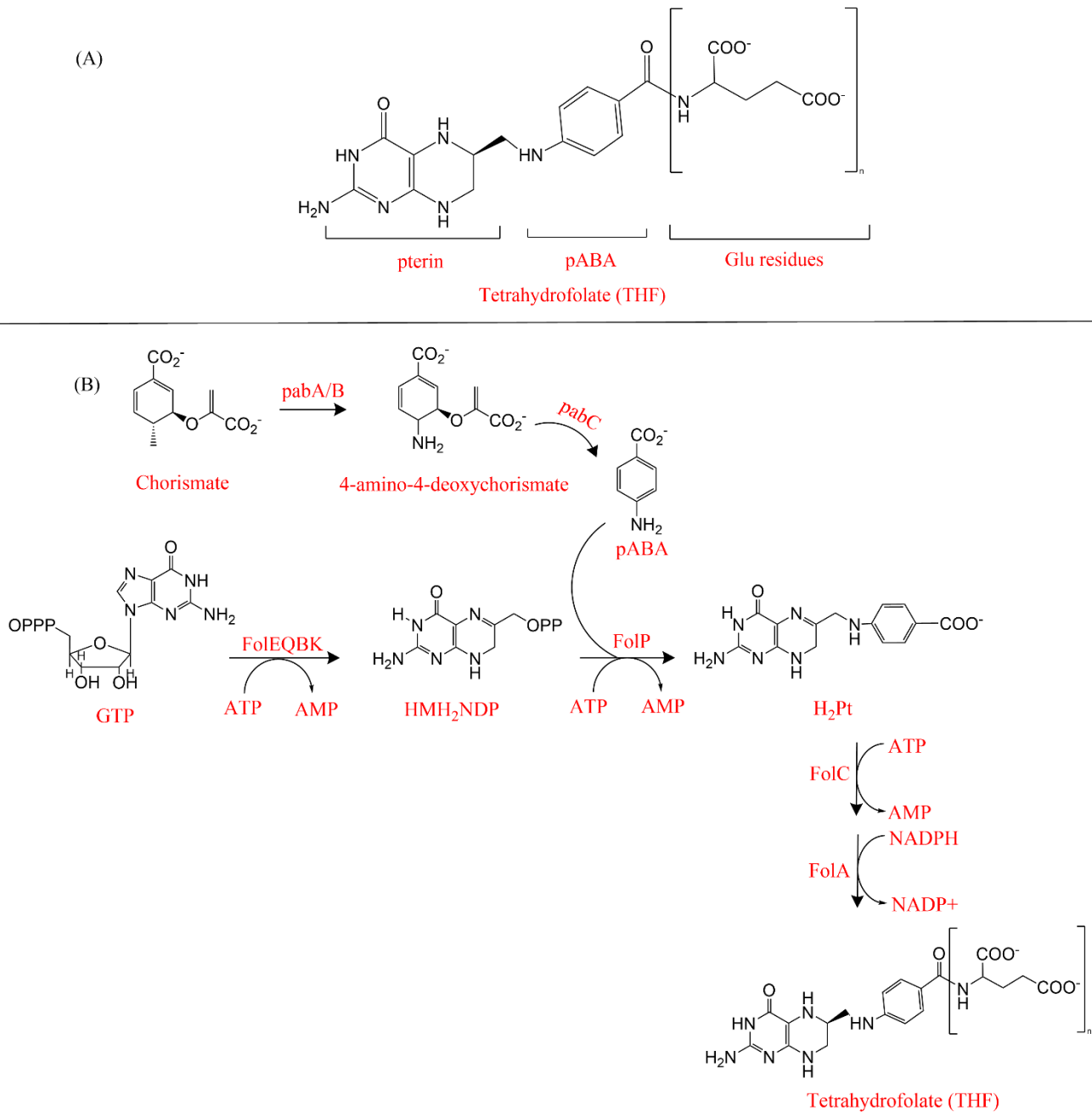


Figure 1.1: Canonical biosynthesis of Tetrahydrofolate (THF) **A)** The structure of THF **B)** The canonical biosynthesis of THF with FolEQBK, PabABC, and FolPCA. The FolEQBK enzymes are responsible for synthesizing 6-hydroxymethyl-7,8-dihydroneopterin diphosphate (HMH_2NDP) which is the pterin portion of THF. Once PabA/B and PabC create pABA from chorismate, these two portions are ligated together by FolP. Finally, FolC and FolA are responsible for the final glutamylation and reduction steps, respectively, to produce the active cofactor.

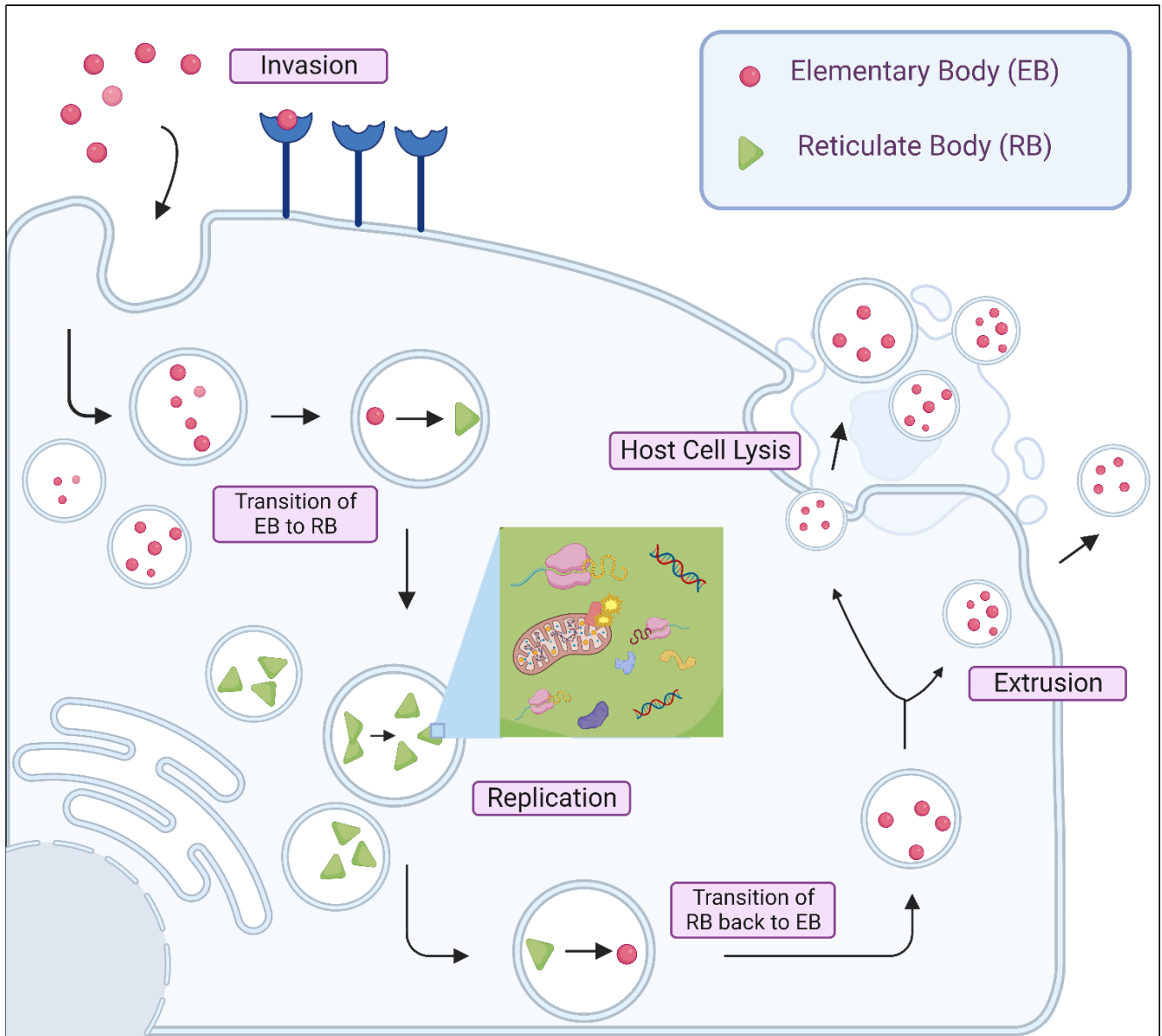


Figure 1.2: *Chlamydiae* exist as an EB and an RB during host parasitism. The invasion of a host cell involves a metabolically inactive EB entering through receptor-mediated endocytosis. Within the inclusion body, the EB will differentiate into a metabolically active RB and now be able to actively divide and uptake nutrients from the host. At the end of the developmental cycle, the RB will re-differentiate back into an EB and leave via host cell lysis or extrusion of the inclusion body. Adapted from Elwell et al, 2016. Created with BioRender.com.

Apoptosis

Extrinsic vs Intrinsic Pathways

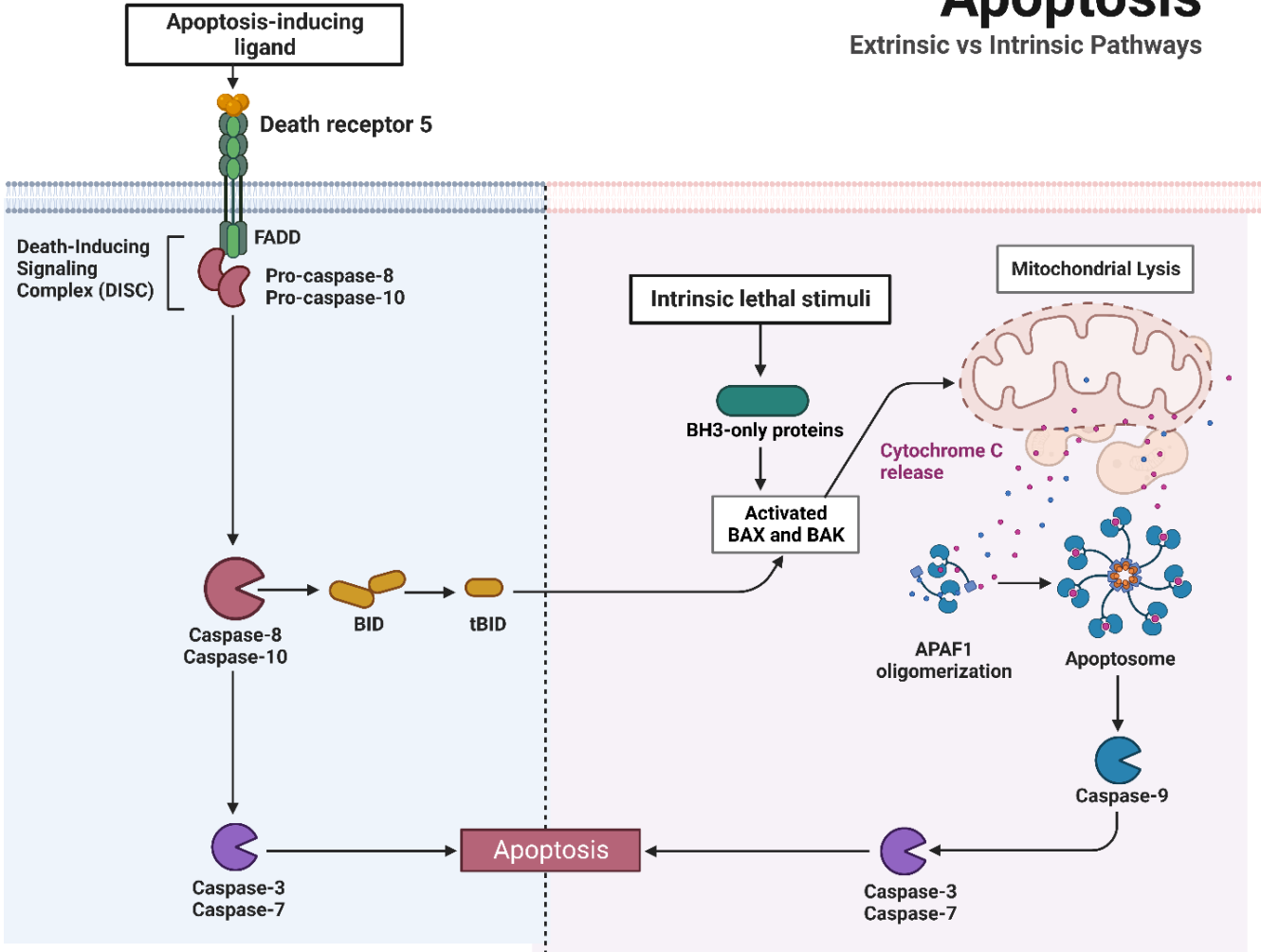


Figure 1.3: The extrinsic and intrinsic apoptotic pathways. Initiation of apoptosis can come from outside of a cell or within a cell, both of which trigger a cascade of apoptosis inducing events. Adapted from Yamada et al, 2017. Created with BioRender.com.

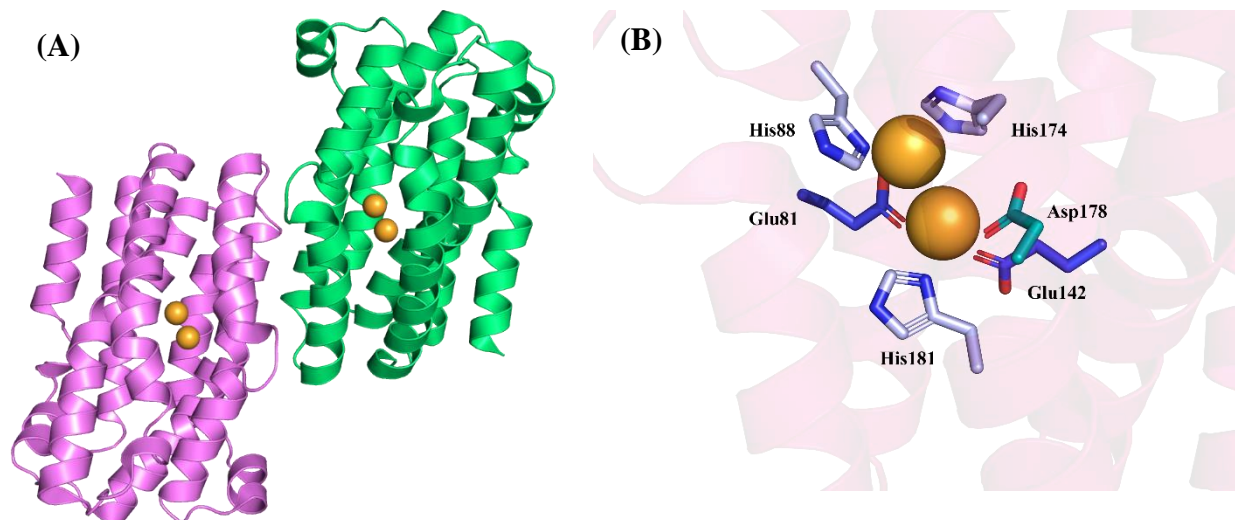


Figure 1.4: The crystal structure of CADD (PDB: 1RCW). A) CADD as a dimer with a diiron active site depicted in orange, chain A in pink, and chain B in green. B) The diiron active site of CADD is coordinated by residues Glu-81, His-88, Glu-142, His-174, Asp-178, and His-181.

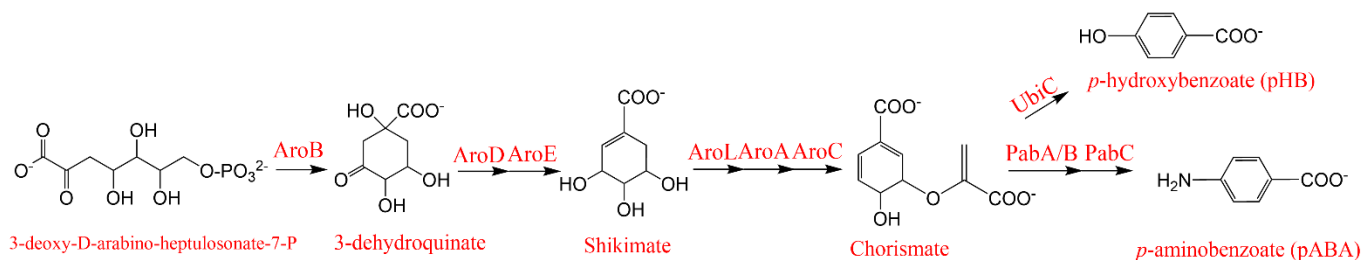


Figure 1.5: An abbreviated shikimate pathway detailing aromatic precursors that are utilized in the typical pABA biosynthetic pathway.

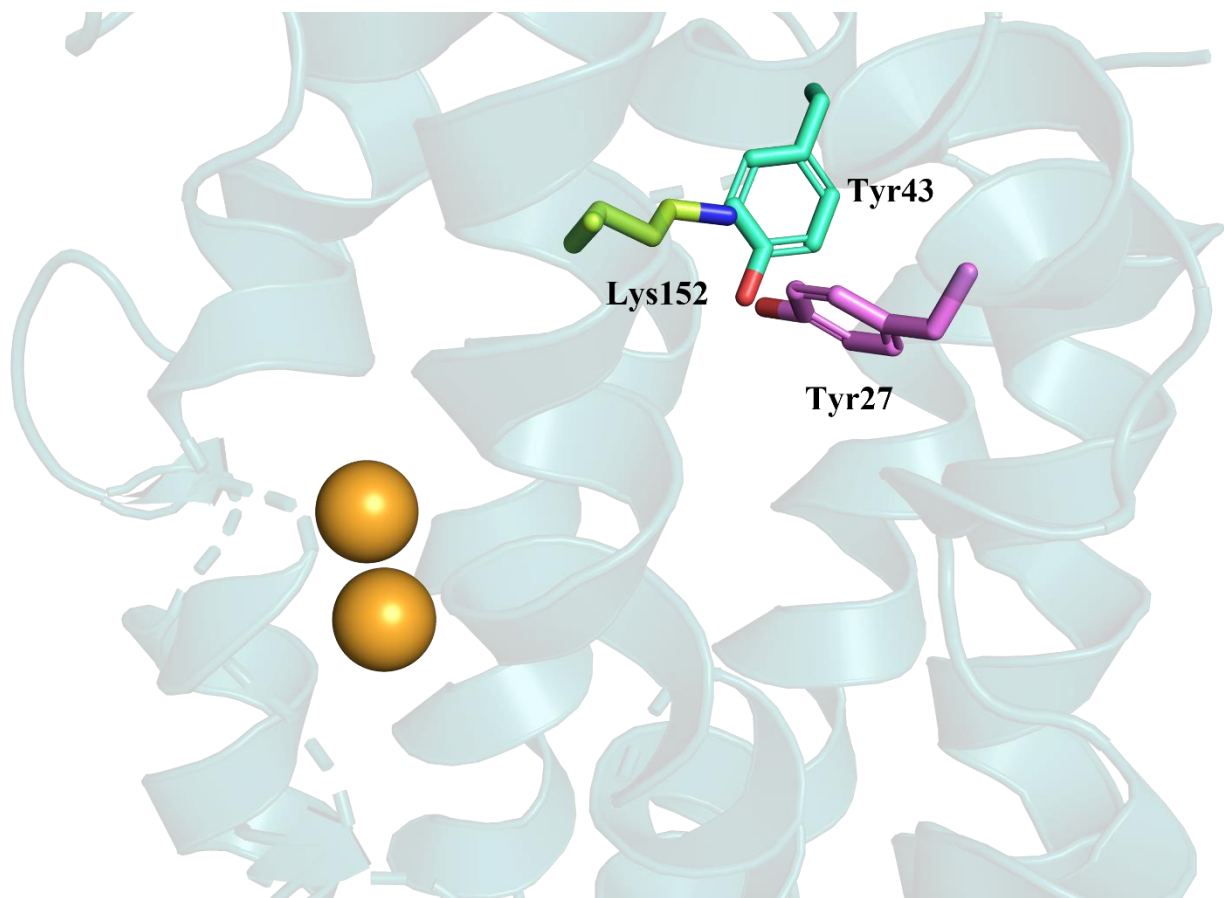


Figure 1.6: Tyrosine residues identified as potential aromatic donors for CADD dependent pABA synthesis. A lysine residue near these tyrosine residues was hypothesized to be the amino donor for the reaction.

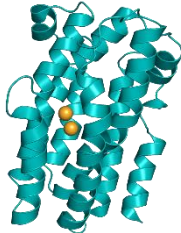
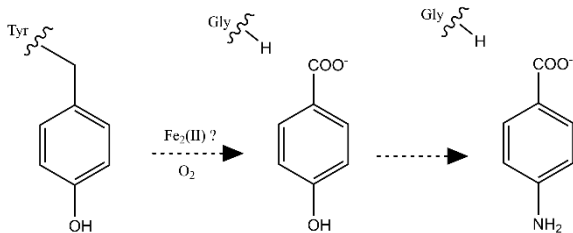
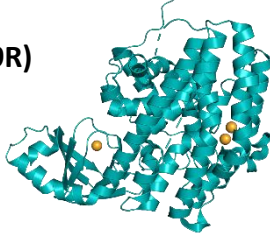
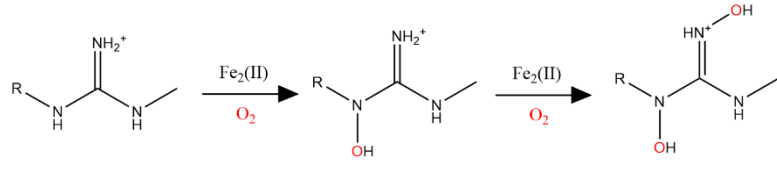

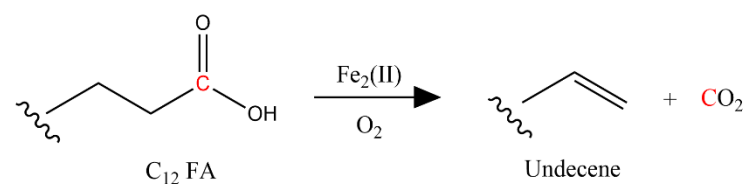
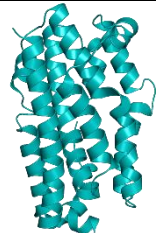
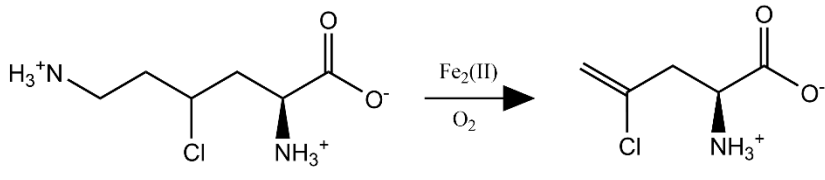
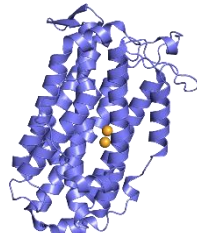
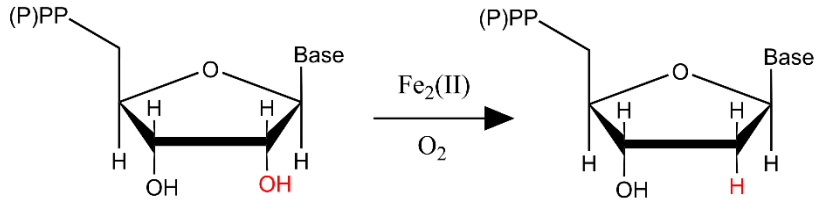
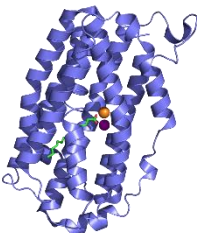
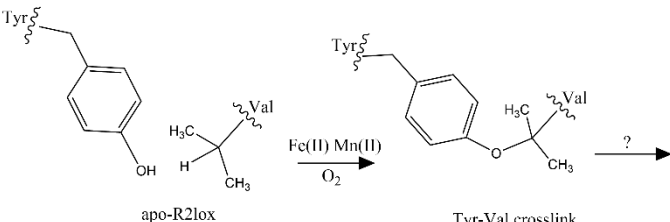
Enzyme:	Reaction Catalyzed:
CADD (PDB: 1RCW) 	
SznF (PDB: 6M9R) 	
UndA (PDB: 4WWZ) 	
BesC (PDB: 7TWA) 	
Class Ia RNR (PDB: 6W4X) 	
R2lox (PDB: 4HR4) 	

Figure 1.7: A structural comparison of HDOs (colored in teal) and FDOs (colored in purple) with CADD. For metals and colored within the structures, iron is shown in orange, manganese is shown as purple, and any various ligands are colored in bright green.

	Pteridine Ring	pABA	Glutamate
Canonical Gene	<i>folE + folQ</i>	<i>pabA/B + pabC</i>	<i>folC</i>
<i>C. trachomatis</i>	<i>ribA + trpF</i>	<i>ct610</i>	γ-glutamyl ligase
<i>N. europaea</i>	<i>ne1163 + ne2150</i>	<i>ne1434</i>	<i>ne0696</i>

Table 1.1: Summary of major THF biosynthesis genes. Organisms that can synthesize THF *de novo* typically possess a well-characterized THF biosynthetic gene cluster. However, organisms such as *C. trachomatis* and *N. europaea* have demonstrated novel pathways to synthesize THF.

References:

- 1 de Crécy-Lagard V, El Yacoubi B, de la Garza RD, Noiriél A & Hanson AD (2007) Comparative genomics of bacterial and plant folate synthesis and salvage: predictions and validations. *BMC Genomics* **8**, 245.
- 2 Adams NE, Thiaville JJ, Proestos J, Juárez-Vázquez AL, McCoy AJ, Barona-Gómez F, Iwata-Reuyl D, de Crécy-Lagard V & Maurelli AT (2014) Promiscuous and Adaptable Enzymes Fill “Holes” in the Tetrahydrofolate Pathway in Chlamydia Species. *mBio* **5**, e01378-14.
- 3 Fan H, Brunham RC & McClarty G (1992) Acquisition and synthesis of folates by obligate intracellular bacteria of the genus Chlamydia. .
- 4 Satoh Y, Kuratsu M, Kobayashi D & Dairi T (2014) New gene responsible for para-aminobenzoate biosynthesis. *J Biosci Bioeng* **117**, 178–183.
- 5 CDC (2021) STI Prevalence, Incidence, and Cost Estimates Infographic. *Cent Dis Control Prev*.
- 6 Cheong HC, Lee CYQ, Cheok YY, Tan GMY, Looi CY & Wong WF (2019) Chlamydiaceae: Diseases in Primary Hosts and Zoonosis. *Microorganisms* **7**, 146.
- 7 Zomorodipour A & Andersson SGE (1999) Obligate intracellular parasites: Rickettsia prowazekii and Chlamydia trachomatis. *FEBS Lett* **452**, 11–15.
- 8 Oehme A, Musholt PB & Dreesbach K (1991) Chlamydiae as pathogens — An overview of diagnostic techniques, clinical features, and therapy of human infections. *Klin Wochenschr* **69**, 463–473.
- 9 Moulder JW (1991) Interaction of chlamydiae and host cells in vitro. *Microbiol Rev* **55**, 143–190.
- 10 Elwell C, Mirrashidi K & Engel J (2016) Chlamydia cell biology and pathogenesis. *Nat Rev Microbiol* **14**, 385–400.
- 11 Kun D, Xiang-lin C, Ming Z & Qi L (2013) Chlamydia inhibit host cell apoptosis by inducing Bag-1 via the MAPK/ERK survival pathway. *Apoptosis* **18**, 1083–1092.
- 12 Elmore S (2007) Apoptosis: A Review of Programmed Cell Death. *Toxicol Pathol* **35**, 495–516.
- 13 Hybiske K & Stephens RS (2007) Mechanisms of host cell exit by the intracellular bacterium Chlamydia. *Proc Natl Acad Sci* **104**, 11430–11435.
- 14 Yamada A, Arakaki R, Saito M, Kudo Y & Ishimaru N (2017) Dual Role of Fas/FasL-Mediated Signal in Peripheral Immune Tolerance. *Front Immunol* **8**.
- 15 Korsmeyer SJ, Wei MC, Saito M, Weiler S, Oh KJ & Schlesinger PH (2000) Pro-apoptotic cascade activates BID, which oligomerizes BAK or BAX into pores that result in the release of cytochrome c. *Cell Death Differ* **7**, 1166–1173.
- 16 Wang Y & Tjandra N (2013) Structural Insights of tBid, the Caspase-8-activated Bid, and Its BH3 Domain. *J Biol Chem* **288**, 35840–35851.

- 17 Bao Q & Shi Y (2007) Apoptosome: a platform for the activation of initiator caspases. *Cell Death Differ* **14**, 56–65.
- 18 Stenner-Liewen F, Liewen H, Zapata JM, Pawlowski K, Godzik A & Reed JC (2002) CADD, a Chlamydia Protein That Interacts with Death Receptors*. *J Biol Chem* **277**, 9633–9636.
- 19 Fischer SF, Vier J, Kirschnek S, Klos A, Hess S, Ying S & Häcker G (2004) Chlamydia Inhibit Host Cell Apoptosis by Degradation of Proapoptotic BH3-only Proteins. *J Exp Med* **200**, 905–916.
- 20 Fan T, Lu H, Hu H, Shi L, McClarty GA, Nance DM, Greenberg AH & Zhong G (1998) Inhibition of Apoptosis in Chlamydia-infected Cells: Blockade of Mitochondrial Cytochrome c Release and Caspase Activation. *J Exp Med* **187**, 487–496.
- 21 Poulos TL (2014) Heme Enzyme Structure and Function. *Chem Rev* **114**, 3919–3962.
- 22 McBride MJ, Pope SR, Hu K, Okafor CD, Balskus EP, Bollinger JM & Boal AK (2021) Structure and assembly of the diiron cofactor in the heme-oxygenase-like domain of the N-nitrosourea-producing enzyme SznF. *Proc Natl Acad Sci U S A* **118**, e2015931118.
- 23 Schwarzenbacher R, Stenner-Liewen F, Liewen H, Robinson H, Yuan H, Bossy-Wetzel E, Reed JC & Liddington RC (2004) Structure of the Chlamydia Protein CADD Reveals a Redox Enzyme That Modulates Host Cell Apoptosis*. *J Biol Chem* **279**, 29320–29324.
- 24 Macias-Orihuela Y, Cast T, Crawford I, Brandecker KJ, Thiaville JJ, Murzin AG, de Crécy-Lagard V, White RH & Allen KD (2022) An Unusual Route for p-Aminobenzoate Biosynthesis in Chlamydia trachomatis Involves a Probable Self-Sacrificing Diiron Oxygenase. *J Bacteriol* **202**, e00319-20.
- 25 Chain Patrick, Lamerdin Jane, Larimer Frank, Regala Warren, Lao Victoria, Land Miriam, Hauser Loren, Hooper Alan, Klotz Martin, Norton Jeanette, Sayavedra-Soto Luis, Arciero Dave, Hommes Norman, Whittaker Mark, & Arp Daniel (2003) Complete Genome Sequence of the Ammonia-Oxidizing Bacterium and Obligate Chemolithoautotroph Nitrosomonas europaea. *J Bacteriol* **185**, 2759–2773.
- 26 Kowalchuk GA & Stephen JR (2001) Ammonia-Oxidizing Bacteria: A Model for Molecular Microbial Ecology. *Annu Rev Microbiol* **55**, 485–529.
- 27 Arp DJ, Sayavedra-Soto LA & Hommes NG (2002) Molecular biology and biochemistry of ammonia oxidation by Nitrosomonas europaea. *Arch Microbiol* **178**, 250–255.
- 28 Sayavedra-Soto LA, Gvakharia B, Bottomley PJ, Arp DJ & Dolan ME (2010) Nitrification and degradation of halogenated hydrocarbons—a tenuous balance for ammonia-oxidizing bacteria. *Appl Microbiol Biotechnol* **86**, 435–444.
- 29 Jasniewski AJ & Que L (2018) Dioxygen activation by nonheme diiron enzymes: diverse dioxygen adducts, high-valent intermediates, and related model complexes. *Chem Rev* **118**, 2554.
- 30 Ng TL, Rohac R, Mitchell AJ, Boal AK & Balskus EP (2019) An N-nitrosating metalloenzyme constructs the pharmacophore of streptozotocin. *Nature* **566**, 94.

- 31 He H-Y, Henderson AC, Du Y-L & Ryan KS (2019) Two-Enzyme Pathway Links l-Arginine to Nitric Oxide in N-Nitroso Biosynthesis. *J Am Chem Soc* **141**, 4026–4033.
- 32 Manley OM, Fan R, Guo Y & Makris TM (2019) Oxidative Decarboxylase UndA Utilizes a Dinuclear Iron Cofactor. *J Am Chem Soc* **141**, 8684–8688.
- 33 Manley OM, Tang H, Xue S, Guo Y, Chang W & Makris TM (2021) BesC Initiates C–C Cleavage through a Substrate-Triggered and Reactive Diferric-Peroxo Intermediate. *J Am Chem Soc* **143**, 21416–21424.
- 34 Patteson JB, Putz AT, Tao L, Simke WC, Bryant LH, Britt RD & Li B (2021) Biosynthesis of fluopsin C, a copper-containing antibiotic from *Pseudomonas aeruginosa*. *Science* **374**, 1005–1009.
- 35 McBride MJ, Sil D, Ng TL, Crooke AM, Kenney GE, Tysoe CR, Zhang B, Balskus EP, Boal AK, Krebs C & Bollinger JM Jr (2020) A Peroxodiiron(III/III) Intermediate Mediating Both N-Hydroxylation Steps in Biosynthesis of the N-Nitroso-urea Pharmacophore of Streptozotocin by the Multi-domain Metalloenzyme SznF. *J Am Chem Soc* **142**, 11818–11828.
- 36 Rui Z, Li X, Zhu X, Liu J, Domigan B, Barr I, Cate JHD & Zhang W (2014) Microbial biosynthesis of medium-chain 1-alkenes by a nonheme iron oxidase. *Proc Natl Acad Sci* **111**, 18237–18242.
- 37 Zhang B, Rajakovich LJ, Van Cura D, Blaesi EJ, Mitchell AJ, Tysoe CR, Zhu X, Streit BR, Rui Z, Zhang W, Boal AK, Krebs C & Bollinger JM (2019) Substrate-triggered formation of a peroxo-Fe₂(III/III) intermediate during fatty acid decarboxylation by UndA. *J Am Chem Soc* **141**, 14510.
- 38 McBride MJ, Nair MA, Sil D, Slater JW, Neugebauer M, Chang MCY, Boal AK, Krebs C & Bollinger JM (2022) A Substrate-triggered μ -Peroxodiiron(III) Intermediate in the 4-Chloro-L-Lysine-Fragmenting Heme-Oxygenase-like Diiron Oxidase (HDO) BesC: Substrate Dissociation from, and C4 Targeting by, the Intermediate. *Biochemistry* **61**, 689–702.
- 39 Cotruvo JA & Stubbe J (2011) Class I Ribonucleotide Reductases: Metallocofactor Assembly and Repair In Vitro and In Vivo. *Annu Rev Biochem* **80**, 733–767.
- 40 Bollinger JM, Jiang W, Green MT & Krebs C (2008) The manganese(IV)/iron(III) cofactor of *Chlamydia trachomatis* ribonucleotide reductase: structure, assembly, radical initiation, and evolution. *Curr Opin Struct Biol* **18**, 650–657.
- 41 Kolberg M, Strand KR, Graff P & Kristoffer Andersson K (2004) Structure, function, and mechanism of ribonucleotide reductases. *Biochim Biophys Acta BBA - Proteins Proteomics* **1699**, 1–34.
- 42 Ruskoski TB & Boal AK (2021) The periodic table of ribonucleotide reductases. *J Biol Chem* **297**, 101137.
- 43 Blaesi EJ, Palowitch GM, Hu K, Kim AJ, Rose HR, Alapati R, Lougee MG, Kim HJ, Taguchi AT, Tan KO, Laremore TN, Griffin RG, Krebs C, Matthews ML, Silakov A, Bollinger JM, Allen BD & Boal AK (2018) Metal-free class Ie ribonucleotide reductase from pathogens

- initiates catalysis with a tyrosine-derived dihydroxyphenylalanine radical. *Proc Natl Acad Sci* **115**, 10022–10027.
- 44 Kang G, Taguchi AT, Stubbe J & Drennan CL (2020) Structure of a trapped radical transfer pathway within a ribonucleotide reductase holocomplex. *Science* **368**, 424–427.
- 45 Minnihan EC, Nocera DG & Stubbe J (2013) Reversible, Long-Range Radical Transfer in E. coli Class Ia Ribonucleotide Reductase. *Acc Chem Res* **46**, 2524–2535.
- 46 Yokoyama K, Uhlin U & Stubbe J (2010) A Hot Oxidant, 3-NO₂ Y₁₂₂ Radical, Unmasks Conformational Gating in Ribonucleotide Reductase. *J Am Chem Soc* **132**, 15368–15379.
- 47 Seyedsayamdost MR & Stubbe J (2006) Site-Specific Replacement of Y356 with 3,4-Dihydroxyphenylalanine in the β₂ Subunit of E. coli Ribonucleotide Reductase. *J Am Chem Soc* **128**, 2522–2523.
- 48 Cotruvo JA & Stubbe J (2010) An Active Dimanganese(III)–Tyrosyl Radical Cofactor in Escherichia coli Class Ib Ribonucleotide Reductase. *Biochemistry* **49**, 1297–1309.
- 49 Martin JE & Imlay JA (2011) The alternative aerobic ribonucleotide reductase of Escherichia coli, NrdEF, is a manganese-dependent enzyme that enables cell replication during periods of iron starvation. *Mol Microbiol* **80**, 319–334.
- 50 Rhodes DV, Crump KE, Makhlynets O, Snyder M, Ge X, Xu P, Stubbe J & Kitten T (2014) Genetic Characterization and Role in Virulence of the Ribonucleotide Reductases of Streptococcus sanguinis. *J Biol Chem* **289**, 6273–6287.
- 51 Puccio T, Kunka KS, Zhu B, Xu P & Kitten T (2020) Manganese Depletion Leads to Multisystem Changes in the Transcriptome of the Opportunistic Pathogen Streptococcus sanguinis. *Front Microbiol* **11**.
- 52 Jiang W, Yun D, Saleh L, Barr EW, Xing G, Hoffart LM, Maslak M-A, Krebs C & Bollinger JM (2007) A Manganese(IV)/Iron(III) Cofactor in *Chlamydia trachomatis* Ribonucleotide Reductase. *Science* **316**, 1188–1191.
- 53 Jiang W, Xie J, Nørgaard H, Bollinger JM & Krebs C (2008) Rapid and Quantitative Activation of *Chlamydia trachomatis* Ribonucleotide Reductase by Hydrogen Peroxide. *Biochemistry* **47**, 4477–4483.
- 54 Rozman Grinberg I, Berglund S, Hasan M, Lundin D, Ho FM, Magnuson A, Logan DT, Sjöberg B-M & Berggren G (2019) Class Id ribonucleotide reductase utilizes a Mn₂(IV,III) cofactor and undergoes large conformational changes on metal loading. *JBIC J Biol Inorg Chem* **24**, 863–877.
- 55 Rose HR, Maggiolo AO, McBride MJ, Palowitch GM, Pandelia M-E, Davis KM, Yennawar NH & Boal AK (2019) Structures of Class Id Ribonucleotide Reductase Catalytic Subunits Reveal a Minimal Architecture for Deoxynucleotide Biosynthesis. *Biochemistry* **58**, 1845–1860.
- 56 Srinivas V, Lebrette H, Lundin D, Kutin Y, Sahlin M, Lerche M, Eirich J, Branca RMM, Cox N, Sjöberg B-M & Högbom M (2018) Metal-free ribonucleotide reduction powered by a DOPA radical in Mycoplasma pathogens. *Nature* **563**, 416–420.

- 57 Do H, Makthal N, Chandrangu P, Olsen RJ, Helmann JD, Musser JM & Kumaraswami M (2019) Metal sensing and regulation of adaptive responses to manganese limitation by MtsR is critical for group A streptococcus virulence. *Nucleic Acids Res* **47**, 7476–7493.
- 58 Kisgeropoulos EC, Griese JJ, Smith ZR, Branca RMM, Schneider CR, Högbom M & Shafaat HS (2020) Key Structural Motifs Balance Metal Binding and Oxidative Reactivity in a Heterobimetallic Mn/Fe Protein. *J Am Chem Soc* **142**, 5338–5354.
- 59 Irving H & Williams RJP (1953) 637. The stability of transition-metal complexes. *J Chem Soc Resumed*, 3192–3210.
- 60 Kutin Y, Srinivas V, Fritz M, Kositzki R, Shafaat HS, Birrell J, Bill E, Haumann M, Lubitz W, Högbom M, Griese JJ & Cox N (2016) Divergent assembly mechanisms of the manganese/iron cofactors in R2lox and R2c proteins. *J Inorg Biochem* **162**, 164–177.

Chapter 2:

Identification of metal preference and amino acid residues sacrificed for *p*-aminobenzoate synthesis by a metalloxygenase from *Chlamydia trachomatis*

*A modified version of this chapter was recently published in *FEBS letters*[1]

2.1 Abstract

CADD (chlamydia protein associating with death domains) is a *p*-aminobenzoate (pABA) synthase involved in a non-canonical route for tetrahydrofolate biosynthesis in *Chlamydia trachomatis*. Although previously implicated to employ a diiron cofactor, here we show that pABA synthesis by CADD requires manganese and the physiological cofactor is most likely a heterodinuclear Mn/Fe cluster. Isotope labeling experiments revealed that the two oxygen atoms in the carboxylic acid portion of pABA are derived from molecular oxygen. Finally, mass spectrometry-based proteomic analyses of CADD-derived peptides demonstrated a glycine substitution at Tyr27, providing strong evidence that this residue is sacrificed for pABA synthesis. Additionally, Lys152 was deaminated and oxidized to aminoadipic acid, supporting its proposed role as a sacrificial amino group donor.

2.2 Introduction

Tetrahydrofolate (THF, Figure 1.1A) and its derivatives – collectively referred to as folates – are essential cofactors for one-carbon transfer reactions in all domains of life. Animals are dependent on their diet for folate acquisition; however, most bacteria, plants, and fungi synthesize folates de novo. *Chlamydia trachomatis* is an intracellular bacterial pathogen that utilizes several non-canonical enzymes for THF biosynthesis [2,3]. The *p*-aminobenzoate (pABA) portion of THF is normally synthesized via chorismate by two enzymes – the bifunctional aminodeoxychorismate synthase (encoded by *pabA* and *pabB*) and aminodeoxychorismate lyase (encoded by *pabC*). However, *C. trachomatis* is missing these three genes and instead utilizes the product of a single gene, *ct610*, in a route that does not directly employ chorismate [3]. Before the discovery of its role in THF biosynthesis, the *ct610* gene product was named CADD (*C*hlamydia protein associating with death domains) due to its role in inducing host cell apoptosis via interacting with death domains of mammalian tumor necrosis factor family receptors [4]. Thus, the *ct610* gene product appears to be a “moonlighting” protein with at least two distinct functions.

The crystal structure of CADD revealed a dimer of seven-helix bundles [5], an architecture first observed in heme oxygenase [6], with an active site containing a diiron cofactor (Figure 1.4A) similar to the hydroxylase component of soluble methane monooxygenase (sMMOH) and the β subunit of class Ia ribonucleotide reductase (RNR) [5]. Thus, CADD is a member of the emerging heme-oxygenase-like diiron oxidase (HDO) superfamily, of which ~10,000 members are bioinformatically proposed, but only a handful have defined enzymatic activities [7]. Characterized HDOs catalyze diverse reactions including *N*-oxygenation (SznF [7–10], RohS [11] and FlcE [12]), oxidative C-C bond cleavage (UndA [13–15], BesC [16–18], and FlcE [12]), and methylene excision (FlcD) [12].

Although CADD was the first HDO superfamily member with a reported crystal structure [5], its enzymatic activity(ies) and physiological function(s) remain unclear. Previous work in our lab utilized isotope feeding studies in an *E. coli* $\Delta pabA$ strain expressing CADD to demonstrate that L-tyrosine is the likely substrate for CADD-dependent pABA biosynthesis [19]. Further, *in vitro* studies demonstrated that the purified enzyme produces pABA in a reaction that requires a reducing agent and molecular oxygen, but does not appear to utilize free L-tyrosine as a substrate. Site-directed mutagenesis identified two active site tyrosine residues (Tyr27 and Tyr43) as being essential for pABA synthesis and, thus, suggested that CADD is a self-sacrificing enzyme that cleaves an active site tyrosine residue from the protein backbone to serve as a substrate for pABA biosynthesis (Figure 2.1) [19]. Additionally, mutating a conserved lysine residue (Lys152) to arginine resulted in a dramatic decrease in pABA production, suggesting it could be the missing amino group donor in the reaction (Figure 2.2).

Here, we further characterize this novel pABA synthase to assess its metal-dependence and elucidate key details of the proposed self-sacrificing reaction. Surprisingly, we found that the pABA synthase activity is dependent on manganese and the results indicate that the most likely physiological cofactor is a heterodinuclear Mn/Fe site analogous to the class Ic RNR used in *C. trachomatis* [20]. Isotope-labeling studies show that the final pABA product contains two oxygen atoms incorporated from molecular oxygen, indicating that CADD is an oxygenase and that both carboxylic acid oxygens are derived from molecular oxygen. Finally, mass spectrometric analyses of CADD-derived peptide reaction products showed the conversion of Tyr27 to Gly as well as Lys152 to amino adipic acid, supporting the roles of these two amino acids as sacrificial aromatic and amino group donors during the pABA synthase reaction, respectively.

2.3 Materials and Methods

Materials. Dithiothreitol (DTT), isopropyl- β -D-thiogalactopyranoside (IPTG), and ampicillin were acquired from GoldBio (St. Louis, MO, USA). EDTA disodium salt and Miller's Luria Broth were from Research Products International (RPI, Mount Prospect, IL, USA). All other chemicals and reagents were from Millipore Sigma (Burlington, MA, USA) unless otherwise specified. Metals – Ferrous ammonium sulfate was acquired from Sigma Aldrich and manganese(II) sulfate monohydrate was from Alfa Aesar (Haverhill, MA, USA). Oxygen $^{18}\text{O}_2$ was from MilliporeSigma, and all other reagents were from Genesee Scientific unless otherwise specified.

Overexpression and purification of CADD. The *ct610* gene cloned into pET19b (CT610_pET19b) with the downstream proteomics predicted start codon - originally obtained from Professor Anthony Maurelli (University of Florida). Site-directed mutagenesis was used to modify one codon to be consistent with the sequence from *C. trachomatis* 434/Bu listed in the NCBI database (Accession: CAP04311) [18].

For overexpression of CADD with an N-terminal 10X-His tag, the CT610_pET19b plasmid was transformed into *E. coli* BL21 and a single colony from a LB/Amp plate was used to inoculate 20 mL of LB broth supplemented with 100 $\mu\text{g}/\text{mL}$ ampicillin, which was incubated at 37°C with shaking at 200 rpm overnight. An aliquot (15 mL) of this overnight culture was used to inoculate 1.5 L of LB broth supplemented with 100 $\mu\text{g}/\text{mL}$ ampicillin and was incubated at 37°C with shaking at 200 rpm. When the optical density at 600 nm reached ~ 0.7 , expression of CADD was induced by the addition of 0.5 mM IPTG. The cells were cultured for 4 hours at 37°C, harvested by centrifugation, and stored at -20°C until the pellet was needed for purification. When cells were grown in the presence of 1,10-phenanthroline, it was added to LB-grown cells at a

concentration of 0.5 mM at the same time as induction with IPTG as described [21], and cells were grown at 37°C for an additional 4 hours before harvesting.

A routine purification was performed from 3 L of culture resulting in a cell pellet of ~12 g. The pellet was resuspended in 30 mL 50 mM sodium phosphate, 300 mM NaCl, and 20 mM imidazole (pH 7.4) (buffer A: 20 mM imidazole). The cells were then sonicated on ice and the insoluble cell debris was removed by centrifugation at 27 000 g for 45 mins. The cell lysate was loaded into a gravity flow column (1 by 3 cm, ~2 mL of resin) of Ni-nitrilotriacetic acid metal affinity resin (Prometheus), equilibrated with 20 mL buffer A. The column was then washed with 10 mL of buffer A followed by 10 mL of buffer A containing 100 mM imidazole. CADD was then eluted from the column with buffer A containing 500 mM imidazole.

After concentrating the CADD-containing fractions to 2.5 mL using an Amicon centrifuge concentrator (10-kDa cutoff, 15 mL; EMD Millipore), the protein was exchanged into 20 mM HEPES (pH 7.5) using a PD-10 desalting column (Cytiva). The final purified protein in 3.5 mL had an average concentration of ~700 μ M monomer (~20 mg/mL). The protein was flash frozen and stored at -80°C until needed for assays. Protein concentrations were determined by the Bradford method with bovine serum albumin as a standard.

***In vitro* enzymatic assays and pABA detection by LC-MS.** Purified CADD was thawed on ice. A typical assay was a 500 μ L reaction carried out in 20 mM Sodium HEPES (pH 7.5) and contained 154 μ M monomer (4.5 mg/mL) protein and 10 mM DTT. Negative control (protein only) reactions contained 154 μ M protein in 20 mM HEPES (pH 7.5). The enzyme reactions were incubated at 37°C for 1 hour before being quenched with 1.5 mL CH₃CN. The protein was removed by high-speed centrifugation, the supernatant concentrated under vacuum to 100 μ L, and finally analyzed by LC-MS. When performing these assays with anaerobically reconstituted

protein (see below), the reconstituted sample was first oxygenated by gently pipetting up and down in an aerobic environment as well as using oxygenated 20 mM HEPES (pH 7.5) to dilute the protein for the reactions. DTT was then added, and the reactions proceeded as described above.

For LC-MS analysis of pABA produced by CADD, a Waters Acquity TQD mass spectrometer with a Waters Acquity UPLC equipped with an Acquity Premier HSS T3 column (2.1 x 100 mm, 1.8 μ m particle size) was used with solvent A as 0.1% formic acid in water and solvent B as 100% methanol. The LC program consisted of 3 min at 95% A followed by a 10-min linear gradient to 50% B at a flow rate of 0.30 mL/min and the injection volume was 10 μ L. The MS method was a multiple reaction-monitoring method scanning two pairs: 138.1 and 120.4, 138.1 and 94.4 with a collision energy of 15 V and a cone voltage of 30 V. The source temperature was 150°C, the desolvation temperature was 500°C, the desolvation gas flow was 800 L/hr, and the cone gas flow was 50 L/hr. MassLynx was used for system operation and data processing. The pABA produced in CADD reactions was quantified using a standard curve.

Metal reconstitution. Three methods were employed for assessing the metal dependence of pABA synthesis by CADD. In the first method (Method A), as-purified CADD expressed in LB medium was treated with various metals in anaerobic conditions followed by removal of unbound metals before assaying for pABA synthesis. Thus, a sample containing 5-10 mg/mL protein was deoxygenated in a Coy anaerobic chamber (~98% N₂/~2% H₂) by gently stirring for 2 hours. Then, an aliquot of a stock solution containing the metal ion(s) of interest was introduced to the sample and gently stirred in the anaerobic chamber for another two hours. Unless otherwise indicated, 2 equivalents of each metal were added per monomer of protein. Unbound metal was removed using a PD-10 desalting column (Cytiva Life Sciences) eluting the reconstituted protein with deoxygenated 20 mM HEPES (pH 7.5). This sample was capped to maintain anaerobic

conditions and stored at 4°C overnight or used for in vitro enzymatic assays immediately. Experiments showed no significant decrease in activity when the enzyme was left at 4°C overnight. For mixed metal reconstitutions, aliquots of stock solutions of the two metals were combined together first before being added to the protein. The various metal ion salts used were: $\text{Fe}(\text{NH}_4)_2(\text{SO}_4)_2$, CuSO_4 , ZnSO_4 , and MnSO_4 . In a second method (Method B), an EDTA treatment was employed before reconstitution. Purified CADD (~5 mg/mL) was gently stirred in the presence of 1 mM EDTA for one hour and then exchanged into 20 mM HEPES (pH 7.5) using a PD-10 desalt column. After concentrating the protein using an Amicon 10 kDa MWCO centrifuge concentrator, pABA synthase assays were performed with the resulting CADD and the remaining portion of the protein was transferred into the anaerobic chamber, deoxygenated with gentle stirring, and reconstituted with Mn, Fe, or Mn/Fe followed by a final buffer exchange step into 20 mM HEPES (pH 7.5) before performing pABA synthase assays. Finally, in the third method (Method C), the metal ion of interest was added directly to the pABA synthase assay containing apo-CADD. The unbound metals were not removed in this method, which is distinct from Methods A and B.

Metal analysis. A colorimetric ferrozine assay [22] was used for initial iron determination of as-purified vs. Fe-reconstituted CADD. For subsequent metal analysis of various preparations of CADD (Table 2.1), inductively coupled plasma atomic emission spectroscopy (ICP-AES) was employed. The protein sample was acidified with 50% trace metal grade nitric acid and incubated at room temperature for ~16 hours followed by incubation at 90°C for two hours. The samples were then diluted with deionized water to produce a final solution containing 3% nitric acid. The sample solutions were analyzed for Fe, Cu, Mn, and Zn content, using a Spectro ARCOS II MV inductively coupled plasma atomic emission spectrometer and a Teledyne ASX-560 autosampler

maintained by the Virginia Tech Soil Testing Laboratory. Sample quantification was achieved through a standard calibration curve of each element listed and a yttrium internal standard.

Superoxide and hydrogen peroxide assays. To determine the potential involvement of superoxide and/or peroxide in the CADD pABA synthase reaction, reactions were carried out with hydroquinol (HQ, 0.5 mM) or H₂O₂ (1 mM or 10 mM) in the presence of 10 mM DTT. For the HQ experiments, the HQ was first added to the reaction buffer and pipetted up and down to aerate for ~40 minutes as previously described [21]. Then, CADD and DTT were added to complete the reaction components. The H₂O₂ experiments were carried out under anaerobic conditions in the presence of DTT. For these ROS experiments, reactions were quenched after 5 min (as opposed to the normal 60 min) to ensure meaningful comparisons. Two forms of CADD were used in these experiments – EDTA-treated and Mn-reconstituted (Method B) compared to apo-CADD with Mn/Fe added directly to the enzyme assay (Method C). Separate experiments were also performed with Mn-reconstituted CADD (Method B) compared to Mn/Fe CADD (Method C) in the presence of superoxide dismutase (SOD, 15 U) or catalase (15 U). The enzymes were first added to the reaction buffer, incubated for 15 minutes at room temperature, then the remaining reaction components were added.

LC-MS/MS experiments to identify amino acid modifications. Mn-reconstituted CADD was used to prepare two standard pABA synthase assays in the presence of 10 mM DTT. After incubating these reactions for 1 hour, 25 µg of protein from each sample was diluted to 1 µg/µl in 50 mM triethylammonium bicarbonate, pH 8.5 (TEAB) followed by digestion overnight with 0.5 µg Glu-C endoproteinase MS grade (Thermo Scientific). The digest was diluted in 2: 98 LC-MS grade acetonitrile: water containing 0.1% (v/v) formic acid (solvent A) to 100 ng/µL and 500 ng was analyzed by LC-MS/MS utilizing an Easy-nLC 1200 autosampler/liquid

chromatography system, a μ PAC compatible nanospray emitter, an Easy Spray nanospray source and a tribrid Orbitrap Fusion Lumos mass spectrometer (Thermo Scientific).

The sample was loaded onto an Acclaim PepMap 100 (100 μ m x 2 cm, nanoViper C18 5 μ m, Thermo Scientific) serving as a precolumn followed by valve switching to a second Acclaim PepMap 100 (100 μ m x 2 cm, nanoViper C18 5 μ m, Thermo Scientific) that served as an analytical column. Flow rate during peptide separation was maintained at 250 nL/min. The LC gradient began at 2:98 solvent A: solvent B (80: 20 LC-MS grade acetonitrile: water containing 0.1% (v/v) formic acid), increased to 15% B over 2 min then 50% B over 20 min and finally up to 98% B in 1 min with a 2 min hold then back to 2% over 1 min with a 1 min hold at 2% for a total 27 min. Spray voltage was 1800 V, ion transfer temperature was 275°C, the RF lens was set to 30% and the default charge state was set to 2.

MS data for the m/z range of 400-1500 was collected using the orbitrap at 120000 resolution in positive profile mode with an AGC target of 4.0e5 and a maximum injection time of 50 ms. Peaks were filtered for MS/MS analysis based on having isotopic peak distribution expected of a peptide with an intensity above 2.0e4 and a charge state of 2-5. Peaks were excluded dynamically for 60 seconds after 2 scans with the MS/MS set to be collected at 55% of a chromatographic peak width with an expected peak width (FWHM) of 20 seconds. MS/MS data starting at m/z of 150 was collected using the orbitrap at 15000 resolution in positive centroid mode with an AGC target of 1.0e5 and a maximum injection time of 200 ms. Activation type was HCD stepped from 25% to 35%. For validation of the modification observed at Lys152, a second run utilized a targeted mass list with the m/z value of 416.23. If a fragment mass of 249.11 was observed in the MS/MS using HCD activation, this triggered a second MS/MS scan utilizing ETD activation with supplemental HCD activation set at 15% using previously calibrated charge-

dependent ETD parameters determined using the MRFA 524.3 peak of the Flex Mix tuning mix (Thermo Scientific). Proteome Discoverer v. 2.5 (Thermo Scientific) was used to generate a mascot generic format peak lists which were then searched using Mascot search engine v. 2.7 (Matrix Science) with the following parameters: precursor mass tolerance of ± 10 ppm, fragment mass tolerance of ± 0.1 Da, variable modifications of N-terminal Gln to pyro-Glu and oxidation of Met with Glu-C specificity and error-tolerant searching set to true. The databases searched were the common laboratory contaminant protein list included with Proteome Discover and a reference protein for *E. coli* with the recombinant CADD protein sequence with an N-terminal His-tag appended.

Addition of ammonium to rescue K152 mutant activities. In order to better understand the amino source for CADD-derived pABA, pABA synthase assays were carried out with K152A and K152R mutants in the presence of 1mM NH₄Cl [19]. The protein used for these reactions was expressed and purified from LB and then concentrated down for a typical *in vitro* assay (described above). If metal solution or ammonium was used for the assay, the mixed Mn/Fe metal solution or 1mM NH₄Cl was added to the diluted protein and gently pipetted before the addition of the reducing agent to initiate the reaction. Three conditions were tested for both K152A and K152R: 1) +NH₄Cl, -Mn/Fe 2) -NH₄Cl, +Mn/Fe 3) +NH₄Cl, +Mn/Fe.

2.4 Results

Overexpression and purification of CADD. CADD containing an N-terminal 10X-His-tag was heterologously expressed and purified from *E. coli* (Figure 2.3) [19]. As-purified, CADD contained $\sim 0.05 - 0.07$ Fe ions per monomer, indicating that the majority of the enzyme population

lacked the expected diiron cofactor. This result is consistent with other HDO family members [7,8,10,13,14,16], where the metallocofactor is apparently highly unstable and does not tend to remain intact.

Metal dependence of CADD. As a defining characteristic of HDOs, poor metal loading of the dimetal cofactor was thought to be the source of low *in vitro* activity. LC-MS analysis of reactions containing as-purified CADD (154 μM) under aerobic conditions showed the production of $\sim 3 \mu\text{M}$ pABA when the enzyme was incubated with dithiothreitol (DTT) versus $\sim 1 \mu\text{M}$ pABA detected when incubated without a reducing agent (Figure 2.4). Thus, we reconstituted the enzyme with 2 equivalents of Fe(II) (per monomer) under anaerobic conditions, followed by removal of excess metal with a buffer exchange step. This resulted in nearly complete incorporation of a diiron cofactor (1.7 ± 0.3 mol Fe per mol monomer) as measured by a ferrozine iron determination assay. Surprisingly, however, Fe-reconstituted CADD exhibited substantially decreased pABA synthase activity compared to the as-purified enzyme (Figure 2.4) thus leading us to hypothesize that an alternative metal cofactor was required.

To test this, CADD was reconstituted with Cu(II), Zn(II), and Mn(II) as well as Fe(II) paired with each of these three metals. In these reconstitution experiments, the purified protein was incubated with the metal ion(s) of interest under anaerobic conditions, followed by removal of the unbound metals with a buffer exchange step (Method A). Our initial experiments using equimolar Fe with other metals resulted in very low pABA synthase activity, likely due to the formation of diiron (Fe/Fe) cofactors. Thus, in subsequent dimetal reconstitutions shown in Figure 2.5A, a sub-stoichiometric amount of Fe was added (0.5 eq.) to mitigate the formation of Fe/Fe cofactors as opposed to a potential heterodimetallic species. In this experiment, CADD

reconstituted with Mn produced the highest amount of pABA, where the Mn-only and Mn/Fe reconstituted samples resulted in similar pABA synthase activities (Figure 2.5A).

To further clarify the identity of the metal cofactor required for pABA synthesis, as-purified CADD was treated with EDTA in an effort to remove existing metals followed by reconstitution with Fe or Mn, or combinations thereof (Method B). After removal of unbound metal ions with a buffer exchange step, the resulting enzyme was assayed for pABA synthase activity. The Mn-reconstituted protein showed ~30-fold higher pABA synthase activity compared to the Fe-reconstituted protein (Figure 2.5B), thus demonstrating a strong preference for Mn as opposed to Fe. Additionally, reactions with 2 eq. Mn showed the highest activity, while 1 eq. Mn, 1 eq. Mn/0.5 eq. Fe, and 1 eq. Mn/1 eq. Fe all produced significantly less pABA (Figure 2.5B). Metal analysis revealed that although the EDTA-treatment does not completely remove bound Fe from as-purified CADD, the Mn-only reconstituted protein lacks Fe and the Mn/Fe reconstituted protein incorporates both metals (Table 2.1). This would suggest that both Mn/Mn and Mn/Fe cofactors can support pABA synthesis by CADD.

During the course of these experiments, a study was published by Manley et al. that reported the use of a Mn/Fe cofactor by CADD [23]. Since there were discrepancies between this newly published work and our results, we performed further experiments to help shed light on the physiologically relevant cofactor for pABA synthesis by CADD. To confirm that we were working with an initial apo form of CADD in metal reconstitution experiments, we expressed the enzyme in the presence of the chelator, phenanthroline. Metal analysis revealed that the resulting purified CADD was indeed the apo form (Table 2.1). We then performed metal addition experiments following two different methods. In Method A, the enzyme was reconstituted with the indicated metal and the excess metal was removed with a buffer exchange step under anaerobic conditions

as done in the experiments described above and reported in Figure 2.6. In Method C, the indicated metals were added directly to the pABA synthase assay which is analogous to the method reported for metal dependence studies by Manley et al. [23].

Interestingly, the results for Method A showed about 2-fold higher pABA synthase activity by the Mn-only reconstituted enzyme compared to the Mn/Fe form, while Method C resulted in dramatically enhanced pABA synthesis in the presence of Mn/Fe compared to Mn-only (Figure 2.6). Despite the increase in activity with the Mn/Fe form in Method C, sub-stoichiometric product formation is still observed, with only about 0.2 pABA formed per CADD monomer. Surprisingly, the Mn-only experiment with Method C resulted in significantly decreased pABA production compared to Mn-only in Method A (Figure 2.5A), which is difficult to explain. One explanation is that a minor amount of Fe remains in the protein preparation (below the ICP detection limit) that is used to generate Mn/Fe cofactors for pABA synthase activity; but, when excess Mn is present in the sample, this blocks the formation of the presumably active Mn/Fe cofactor and results in the very low activity observed in the Mn-only Method C reactions (Figure 2.6). Given the relatively high level of activity observed in the Mn-only Method A reactions, this explanation would require the putative minor amount of Fe to cycle through multiple CADD subunits to facilitate the reaction. In summary, these metal dependence data are most consistent with the physiological cofactor for the pABA synthase activity of CADD being a Mn/Fe site as recently reported [23]. However, we cannot yet rule out that a Mn/Mn cofactor is also capable of facilitating the pABA synthase reaction.

Potential involvement of reactive oxygen species in the pABA synthase reaction. Given the use of a Mn-containing cofactor for pABA synthesis by CADD, we next considered the nature of the oxygen species involved in production of the active cofactor. To gain insight into the nature

of the oxygen species involved in activation of CADD, we first investigated the potential activation of Mn-reconstituted CADD (Method B) by ROS. Thus, reactions were carried out in the presence of HQ, which generates O_2^- from O_2 , as well as H_2O_2 under anaerobic conditions. We found that both ROS stimulate the pABA synthase reaction, where the addition of HQ or 10 mM H_2O_2 results in about 2-fold higher pABA synthase activity compared to the control, which consisted of the standard Mn-reconstituted CADD reaction in the presence of DTT under aerobic conditions (Figure 2.7A).

We also tested the activity of Mn/Fe CADD (Method C) in the presence of HQ and H_2O_2 (Figure 2.7B). We observed similar activities in the absence vs. presence of HQ, indicating that superoxide is not involved in cofactor activation. A low concentration (1 mM) of H_2O_2 in anaerobic conditions did not support activity, but 10 mM H_2O_2 could activate the enzyme, although not to the same extent as O_2 (Figure 2.7B). As expected, the addition of catalase or SOD to Mn/Fe CADD did not affect the pABA synthase activity (Figure 2.7D).

Identification of sacrificial residues for pABA synthesis by CADD. Previous work in our lab identified two tyrosine residues (Tyr27 and Tyr43) and a lysine residue (K152) that could be potential sacrificial substrates for CADD-derived pABA [19]. To provide evidence for the proposed self-sacrificing reaction, peptides resulting from protease-digested CADD were subjected to LC-MS analysis (Figure 2.8A). Intriguingly, Tyr27 was found to be converted to glycine in some HTFY27VKWSKGE peptides (monoisotopic mass for unmodified peptide is 1380.672 compared to 1274.640 for Tyr to Gly modification). The intensity of the $[M + 3H]^+$ ion (425.8862 m/z, Table 2.2) corresponding to the Tyr27 to Gly modification increases ~50-fold in samples from in vitro reactions with Mn-reconstituted CADD in the presence of DTT compared to the absence of DTT (Figure 2.8B), thus providing strong support that this modification is linked

to pABA formation (Figure 2.8C). The MS/MS spectrum shows characteristic fragment ions consistent with the identity of the Tyr27 to Gly modification (Figure 2.8C and Table 2.2). On the other hand, analysis of Tyr43-containing peptides revealed that this tyrosine residue remained intact and no peptides were observed that corresponded to a Tyr to Gly modification. Thus, these data provide strong evidence that Tyr27 serves as a sacrificial substrate for the CADD-catalyzed pABA synthase reaction, while Tyr43 is not used as a sacrificial substrate but is otherwise critical for the reaction.

Further analysis of CADD-derived peptides revealed that the Lys152-containing peptide, K152IRGLTE, also contains a modification, where Lys152 is deaminated and oxidized to aminoadipic acid (Figure 2.8D and Table 2.2). The ion corresponding to the deaminated lysine was found to be ~10X more intense in Mn-reconstituted reactions with DTT compared to without DTT (Figure 2.8D), thus correlating the pABA synthase activity with the lysine modification. Macias-Orihuela et al. previously showed that this lysine residue played a critical role in the pABA synthase reaction via site-directed mutagenesis [19], so the finding of deaminated Lys152 provides further evidence for the potential use of this residue as an internal amino group donor (Figure 2.8C).

Addition of an exogenous amino source to rescue lysine mutants. Based upon our previous results which identified Lys152 as the likely internal amino donor for CADD's pABA synthase activity, we hypothesized that the addition of an external amino source, such as ammonium chloride (NH₄Cl), could rescue the pABA synthase activity of K152A and K152R mutants. With the recent finding that CADD uses a heterodinuclear Mn/Fe cofactor, we decided to perform *in vitro* assays with and without the addition of Mn/Fe solution to compare our data to the most optimal wild type. Although it was hypothesized that an exogenous amino source may

rescue the pABA synthase activity of CADD Lys mutants, there was no difference in the activity of each mutant for all of the conditions tested (-Mn/Fe, +NH₄⁺; +Mn/Fe, -NH₄⁺; and +Mn/Fe, +NH₄⁺) and the pABA synthase activity was negligible.

Preliminary identification of a potential crosslink formed during the CADD reaction.

Previous work in our lab noticed the appearance of a double band when running purified CADD on an SDS-PAGE gel. There are examples in the literature of enzymes such as galactose oxidase which self-assemble a cross-linked cofactor using Cu and molecular oxygen [24]. Interestingly, galactose oxidase also runs as a double band on an SDS-PAGE gel, where the cross-linked form runs slightly below the non-cross-linked form [24]. This led us to hypothesize that we were possibly seeing a cross-linked form of CADD and we wanted to further elucidate the conditions that presented us with a double band on a gel.

We considered that metal assembly may contribute to the formation of this putative cross-link, so the manner in which the metal was added as well as the type was varied. Five microgram samples were taken from *in vitro* enzymatic reactions for Fe/Fe, Fe/Mn, and Mn/Mn in which both Methods A and C were employed and visualized on a SDS-PAGE gel. Although we are unable to definitively conclude what the presence of this band indicates, there was a noticeable increase in double band formation for our manganese only preparations, with Method A producing a visually darker bottom band (Figure 2.9).

2.5 Discussion

CADD is a founding HDO superfamily member involved in an unusual route for pABA biosynthesis in *C. trachomatis* [3]. Based upon the crystal structure [5], which showed a diiron-

containing active site (Figure 2.1), it was assumed that CADD would employ this diiron cofactor for pABA biosynthesis [19]. However, here we showed that pABA formation by purified CADD is drastically enhanced in the presence of manganese as opposed to iron-only and current results are most consistent with the use of a Mn/Fe cofactor, although Mn/Mn may also facilitate the pABA synthase reaction. Most intriguingly, we provide strong evidence that Tyr27 acts as a sacrificial substrate to yield the aromatic portion of pABA and Lys152 may participate as a sacrificial amino group donor.

Sacrificial residues involved in CADD's pABA biosynthetic pathway. The self-sacrifice of an enzyme is unusual and seems quite wasteful in terms of energy requirements; however, examples of such enzymes exist in other cofactor biosynthesis pathways. In thiamine biosynthesis in eukaryotes, a cysteine residue is used as the sulfur source to yield the thiazole ring and a histidine residue serves as a precursor to the pyrimidine portion of the cofactor in reactions catalyzed by THI4 and THI5, respectively [25,26]. Additionally, nickel pincer cofactor biosynthesis involves a cysteine residue as a sulfur donor [27]. Finally, an unusual route for biotin biosynthesis involves a self-sacrificing enzyme that employs a lysine residue as an amino group donor [28]. Thus, since most cofactors are recycled and generally only required in low concentrations, the use of an inefficient self-sacrificing enzyme reaction is likely not highly detrimental for an organism.

One of the major questions regarding the pABA synthase activity of CADD is the identity of the substrate(s). Previous isotope feeding studies showed that the aromatic portion of L-tyrosine was incorporated into pABA in the CADD-dependent route, but the addition of L-tyrosine to *in vitro* reactions did not result in enhanced pABA production [19]. Additionally, site-directed mutagenesis revealed that two conserved tyrosine residues (Tyr27 and Tyr43) and a lysine residue

(K152) were essential for pABA synthesis, leading us to hypothesize that CADD utilizes a self-sacrificing mechanism for pABA synthesis [19], where the aromatic portion of a tyrosine residue is utilized as a scaffold for pABA synthesis and a conserved lysine is used as an internal amino donor (Figure 2.1).

Our findings present evidence of a peptide containing a Tyr27 modification to a glycine, that increases significantly in intensity in the presence of a reducing agent, implicating Tyr27 as the aromatic donor which is cleaved from the protein backbone for CADD's pABA synthase reaction. The other notable finding was the modification of Lys152 to amino adipic acid; Lys residues can undergo non-specific oxidative deamination; however, we did not see any evidence of any other Lys residue being modified/oxidized, thus suggesting a specific role for Lys152 in the pABA synthase reaction. Furthermore, the recent report from Manley et al. used isotope-labeling studies to show that the amino group of pABA is CADD-derived, although the authors did not suggest the specific identity of the amino group donor [23]. Although the activity of the K152A and K152R mutants was not restored by the addition of an exogenous amino donor, this does not rule out that K152 is acting as the internal amino donor. In the case of the K152A mutant, the NH_4^+ added would need to make its way into CADD's constricted active site and be properly oriented to contribute to the overall reaction. Furthermore, it can be speculated that an exogenous amino source did not stimulate the activity of the K152R mutant due to the unlikely prospect of finding both the positively charged amino source and guanidino group juxtaposed to each other. In both cases, we believe that the nature of the amino donor used for CADD's pABA synthase activity is specific. Thus, combined with our data reported here, there is strong evidence for the use of Lys152 as a sacrificial amino group donor in the CADD reaction.

It is important to note that some as-purified CADD expressed in normal LB medium contained modified Tyr27 and Lys152 residues. Thus, a portion of the protein has already reacted *in vivo*, which is consistent with previous results showing that CADD rescues *E. coli* mutants that cannot make pABA via the normal route [3,19]. This indicates that the correct metallocofactor is properly assembled in at least a portion of the heterologously expressed CADD in *E. coli* and results in a portion of purified CADD being in an inherently inactive form since it already reacted and no longer contains the required Tyr27 substrate. This at least partially explains the low *in vitro* activity of the enzyme – we would expect to observe one pABA molecule for every one CADD active site based on the self-sacrificing reaction, but our current *in vitro* assays yield, at most, ~0.2 pABA/CADD.

The formation of an oxygenated dimetal cofactor. The use of Mn in place of Fe has established precedent in related class I RNRs. A dimanganese active site is found in class Ib and Id RNRs, while class Ic RNR harbors a heterodinuclear Mn/Fe active site [20]. In traditional class Ia RNR, the reduced FeII/FeII cofactor in the β subunit reacts with oxygen to produce a $\text{Fe}^{\text{IV}}\text{Fe}^{\text{III}}$ species, which is used to generate a tyrosyl radical that undergoes long-range radical translocation to produce the catalytic cysteinyl radical in the β subunit [29]. The dimanganese RNRs employ an oxygenated $\text{Mn}^{\text{IV}}\text{Mn}^{\text{III}}$ cofactor, where class Ib uses the cofactor to generate a tyrosyl radical and class Id utilizes the oxidized cofactor directly as the cysteinyl radical initiator [20,21,30,31]. Interestingly, *C. trachomatis* has a well-characterized class Ic RNR, in which an oxygenated $\text{Mn}^{\text{IV}}\text{Fe}^{\text{III}}$ complex serves as the cysteinyl radical forming species [32–34]. Thus, it appears that *C. trachomatis* has evolved to use the unique heterodinuclear Mn/Fe cofactor for two key enzymes involved in primary metabolism.

The canonical diiron RNRs react with molecular oxygen to generate the active oxidized cofactor. However, the dimanganese cofactors of class Ib and class Id RNRs are unreactive towards O₂ itself since the reduced Mn^{II}Mn^{II} species does not have sufficient reducing power to react with O₂ directly [31,35]. Instead, superoxide (O₂^{•-}) is required for generation of the active oxidized cofactors [21,36]. Superoxide occurs spontaneously in biological systems, but in the case of class Ib RNRs, this reactive species is specifically generated and delivered to the β subunit by a flavoprotein called NrdI [31,36,37]. In the case of class Id enzymes, the *in vivo* source of superoxide is unclear, but the addition of superoxide-generating compounds such as hydroquinol (HQ) can produce the active Mn^{IV}Mn^{III} cofactor [21,30], and H₂O₂ can also activate the enzyme *in vitro* [30]. Finally, although the Mn/Fe site of class Ic RNR from *C. trachomatis* reacts directly with molecular oxygen to generate the active Mn^{IV}Fe^{III} species, H₂O₂ can also efficiently produce the active cofactor [38].

Our data indicates that the Mn/Fe form of CADD is activated by O₂ directly, while H₂O₂ can also produce the active cofactor, similar to what has been observed for class Ic RNR [38]. The differences in reactivity of the Mn-only compared to Mn/Fe CADD with ROS (Figures 2.7A and 2.7B) indicates that the nature of the metallocofactor is different in these two preparations and thus suggests that Mn-only (i.e. Mn/Mn) may support pABA synthase activity, as opposed to the alternate explanation of Mn-only preparations having minor amounts of Fe that result in a Mn/Fe cofactor. In standard reaction conditions, the reducing agent can react with oxygen to generate the potentially required ROS [30]; thus, these results suggest that the putative dimanganese form of CADD reacts with a ROS, either superoxide and/or H₂O₂, to generate the catalytic oxidized cofactor. However, the pABA synthase activity of Mn-reconstituted CADD was not inhibited by the addition of either catalase or superoxide dismutase (SOD, Figure 2.7C). This suggests that the

formation of the oxygenated cofactor is not the major rate-limiting step for pABA synthesis and/or that CADD can capture the ROS at a rate that outcompetes SOD and catalase.

The Mn-dependency of CADD as well as the class Ic RNR in *C. trachomatis* may provide important insights into the unique metal biology of this intracellular pathogen. The activation of Mn/Fe and Mn/Mn RNRs by ROS as opposed to conventional Fe/Fe RNRs, for which superoxide results in irreversible inactivation via quenching of the tyrosyl radical [39] and H₂O₂ is unable to activate [40], provides interesting insight into the potential evolution of Mn-containing oxo-bridged dimetal cofactors. As an intracellular pathogen, *C. trachomatis* would benefit from mechanisms to cope with ROS produced by host cells in the innate immune response [41]. Thus, this bacterium may have adapted to employ high-valent Mn/Fe and Mn/Mn cofactors as radical initiators in order to avoid inhibition by ROS, a hypothesis previously set forth to explain the use of the unique class Ic RNR in *C. trachomatis* [33,38].

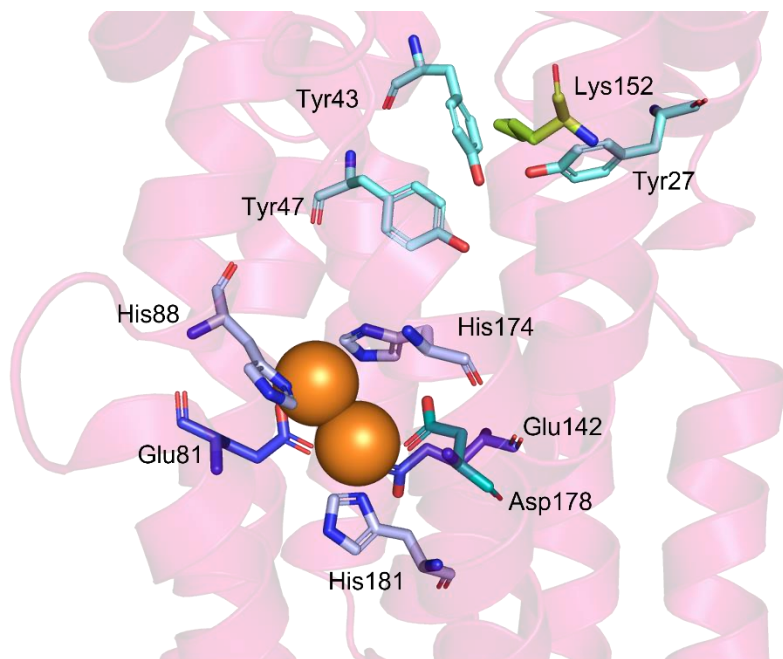


Figure 2.1: The active site of CADD (PDB: 1RCW) with the residues of interest highlighted and the dimetal site shown in orange.

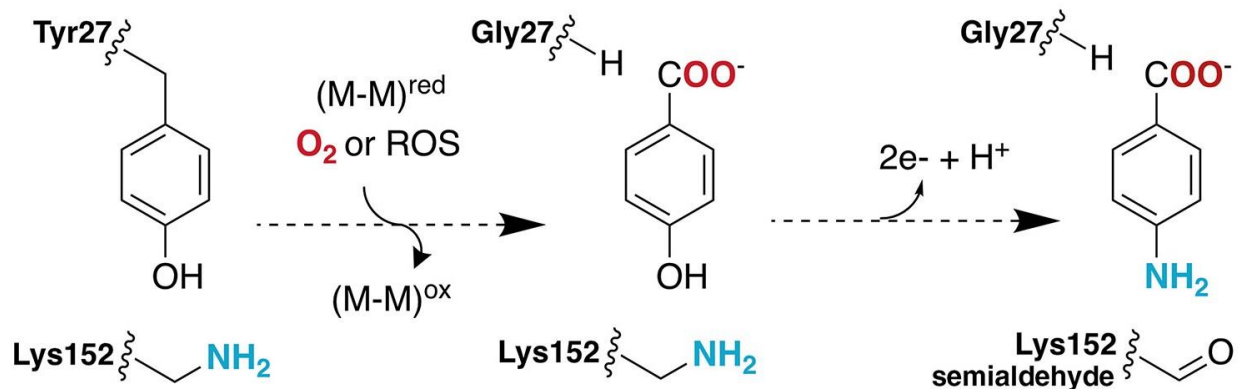


Figure 2.2: Scheme for self-sacrificing pABA synthesis by CADD. ‘M’ represents a metal ion; ROS = reactive oxygen species such as superoxide or hydrogen peroxide.

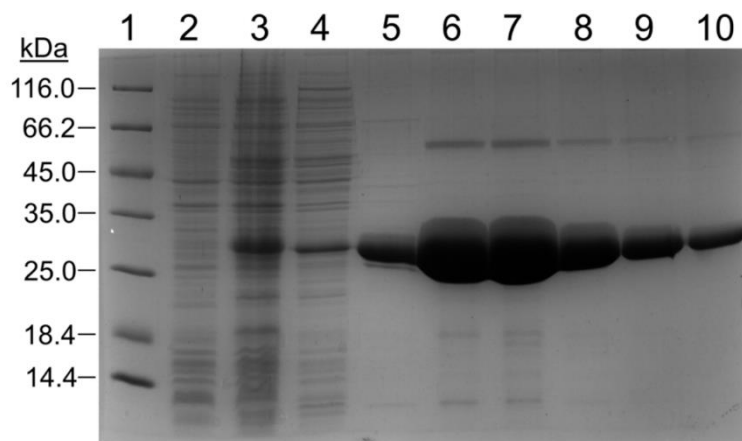


Figure 2.3: SDS-PAGE gel of a typical CADD purification. (1) Molecular weight marker (2) T_0 induction study (3) T_f induction study (4) 20 mM imidazole wash (5-10) 50% and 100% B elution fractions that were pooled and exchanged for subsequent enzyme assays.

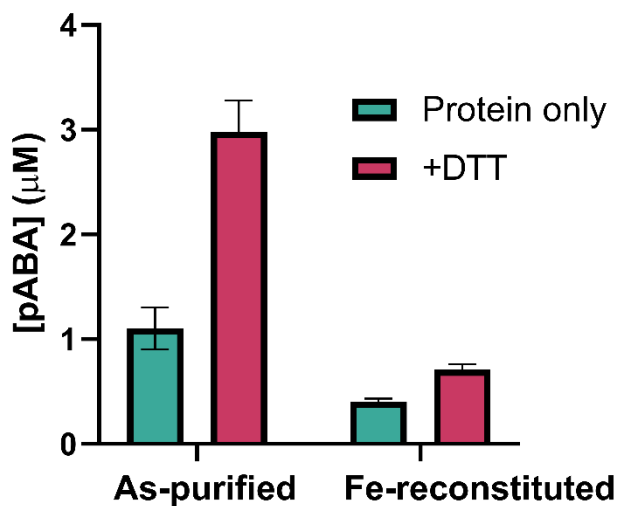


Figure 2.4: pABA synthase activity of CADD with and without DTT purified from LB compared to CADD reconstituted with 2 molar equivalents of iron solution. Each reaction contained 154 μM protein.

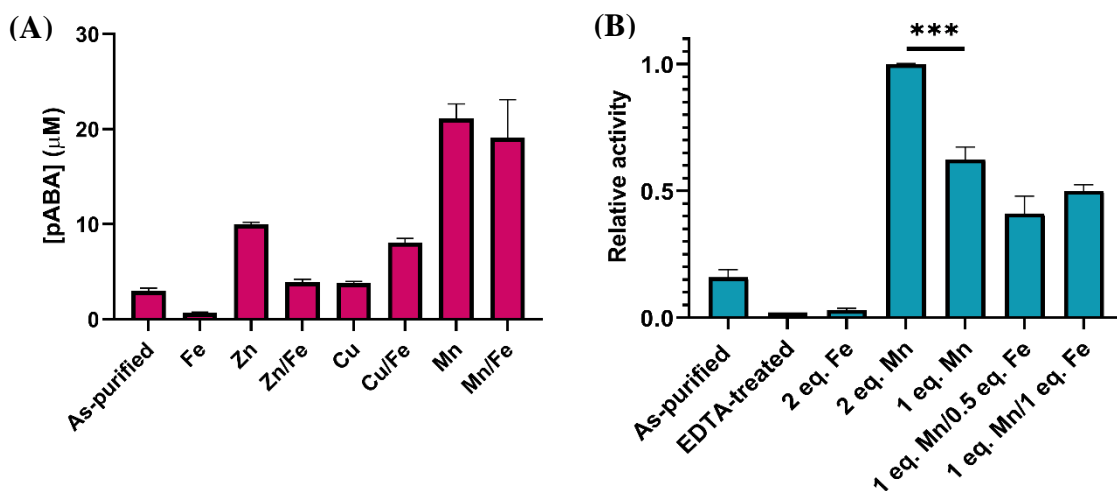


Figure 2.5: Metal dependence of CADD pABA synthase activity treated with and without EDTA. **A)** pABA synthase activity measured from CADD reconstituted with various metals, which was then removed (Method A). **B)** pABA synthase activity from LB purified CADD that was pretreated with EDTA before reconstitution with metals. The excess metal was also removed in the same manner as the non-EDTA treated protein and *in vitro* assays were performed identically. ***The pABA synthase activity of CADD reconstituted with 2 eq. Mn is statistically significantly higher than pABA reconstituted with 1 eq. Mn or with Mn/Fe (P-values < 0.0005). The statistical analysis was performed using a Welch's t-test in graphpad prism 9 (Boston, MA, USA).

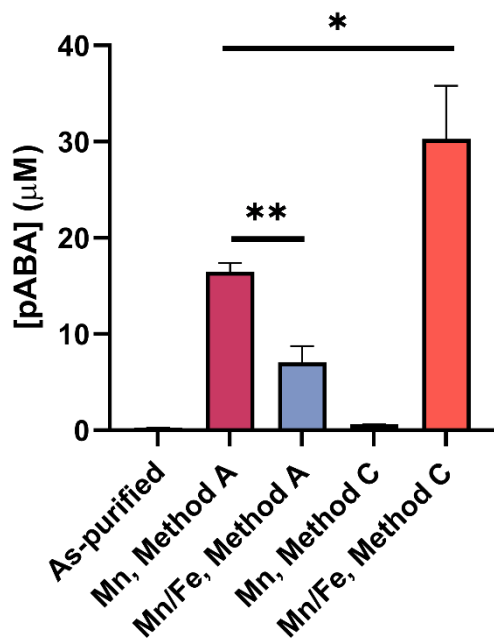


Figure 2.6: pABA synthase activity of CADD expressed with 1,10-phenanthroline. Method A: purified protein was reconstituted with either 2 eq. of Mn or 1 eq. Mn/ 1 eq. Fe and then excess metal was removed by buffer exchange. *In vitro* enzymatic assays were then set up as normal. Method C: 2 eq. of Mn or 1 eq. Mn/ 1 eq. Fe was added directly to the enzymatic assays which were then carried out as normal. All assays contained 154 μM protein and 10 mM DTT and were carried out under aerobic conditions.

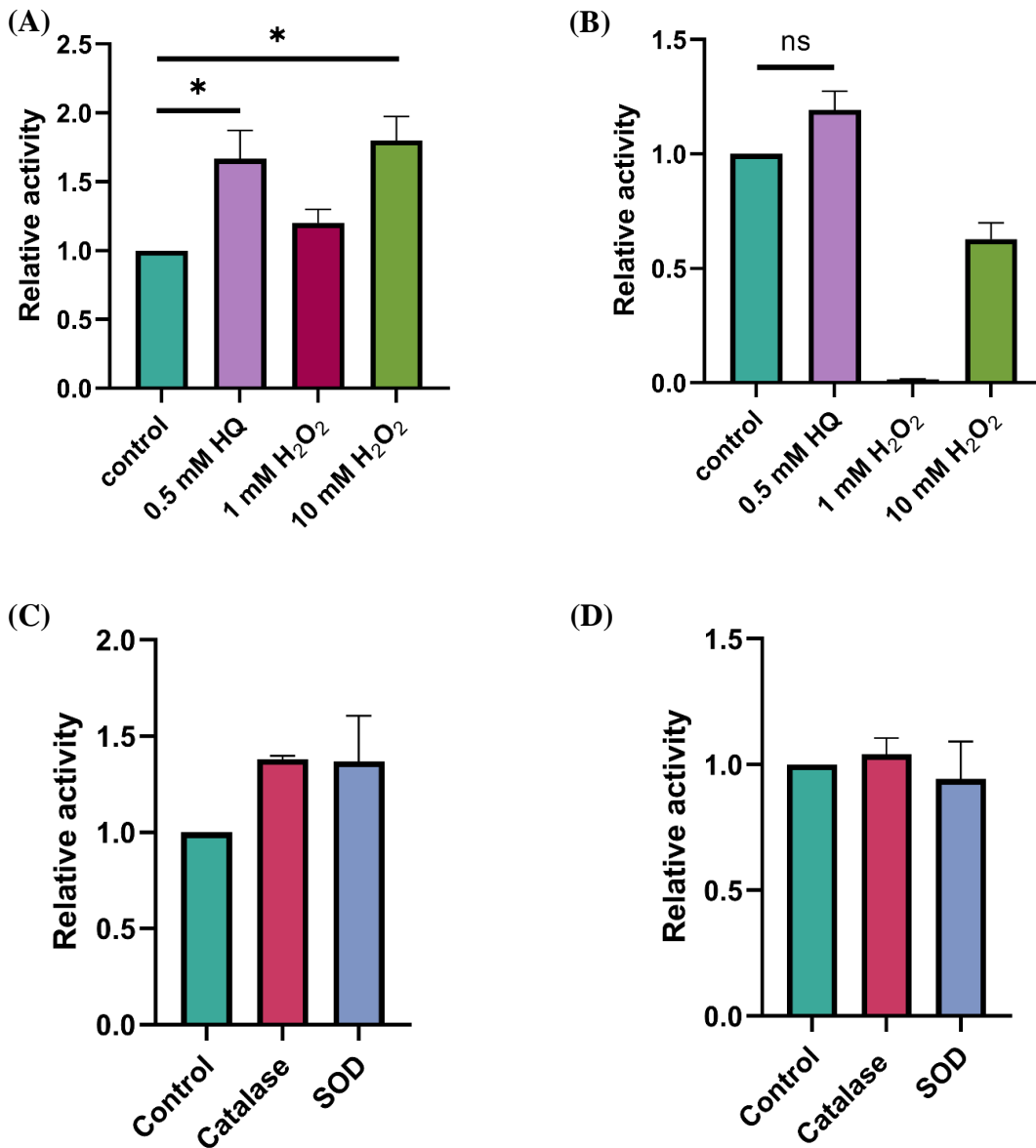


Figure 2.7: Influence of superoxide and hydrogen peroxide on CADD pABA synthase activity. A) Activity of Mn-reconstituted CADD (Method B) in the presence of hydroquinol (HQ, a superoxide-generating compound) and H₂O₂. B) Activity of Mn/Fe CADD (Method C) in the presence of HQ and H₂O₂. C) Activity of Mn/Mn CADD (Method C) in the presence of catalase and superoxide dismutase (SOD). D) Activity of Mn/Fe CADD (Method C) in the presence of catalase and SOD. Control is the standard pABA synthase reaction in aerobic conditions. All reactions contained 10 mM DTT. H₂O₂ reactions were performed in anaerobic conditions. Figures 2.7C and 2.7D both contained 15U of the respective enzyme. Error bars represent the standard deviation of three replicates. *Means are significantly different, p-value < 0.05. ns, non-significant. The statistical analyses were performed using Welch's t-tests in GraphPad Prism 9.

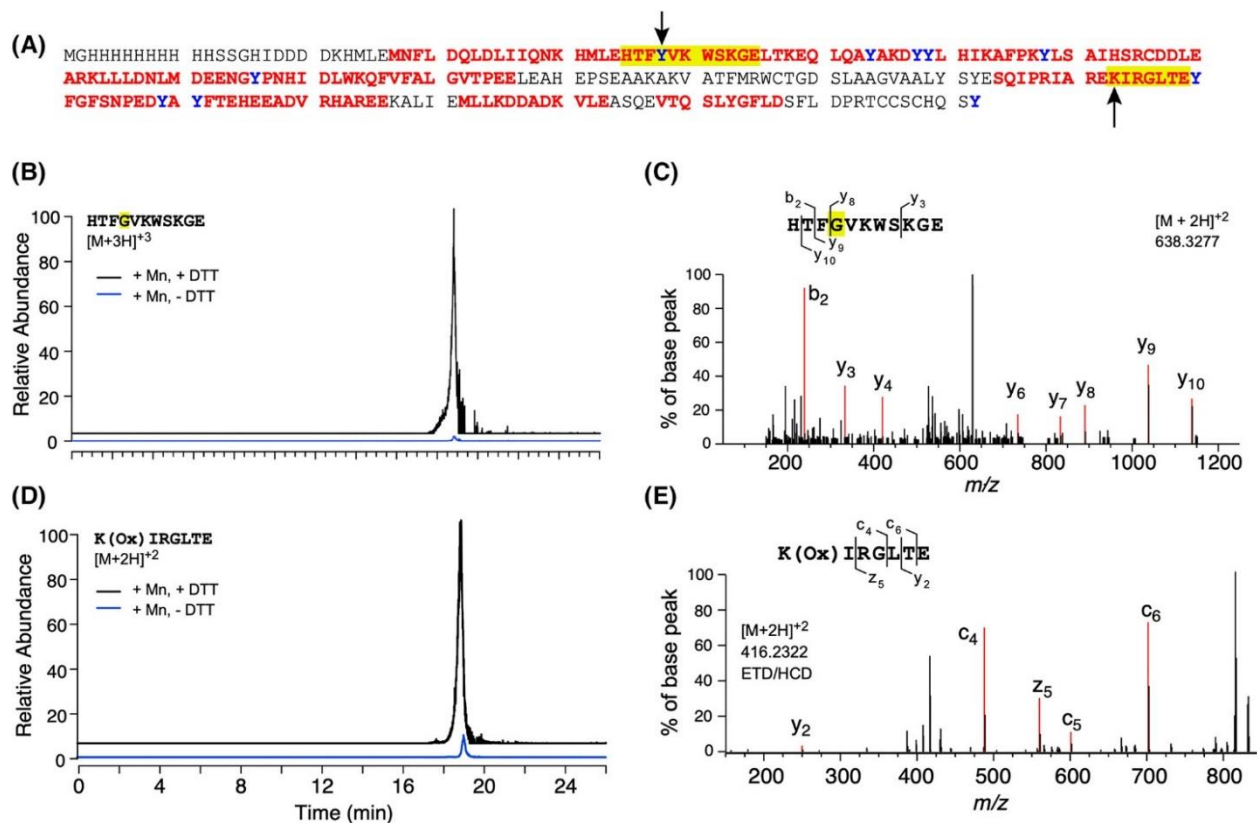


Figure 2.8: LC-MS analysis of modified amino acids in the CADD reaction. **A)** Primary sequence of CADD expressed with a His-tag from pET19b. Peptides identified by LC-MS analysis of GluC-digested CADD are shown in red, peptides of interest containing Tyr27 and Lys152 are highlighted in yellow and arrows indicate specific residues of interest. **B)** Extracted ion chromatogram corresponding to the $[M + 3H]^{+3}$ ion for the peptide containing Tyr27 to Gly modification in Mn-reconstituted CADD reactions with (black) and without (blue) DTT. **C)** MS/MS spectrum of $m/z = 638.3253$, the $[M + 2H]^{+2}$ ion, showing characteristic fragments for Tyr27 to Gly modification. **D)** Extracted ion chromatogram corresponding to the $[M + 2H]^{+2}$ ion for the peptide containing Lys152 to amino adipic acid modification in Mn-reconstituted CADD reactions with (black) and without (blue) DTT. **E)** Electron transfer dissociation/Higher-energy collisional dissociation (ETD/HCD) spectrum of $m/z = 416.2309$, the $[M + 2H]^{+2}$ ion, showing fragments corresponding to the Lys152 to amino adipic acid modification. Corresponding exact masses with errors are shown in Table 2.2.

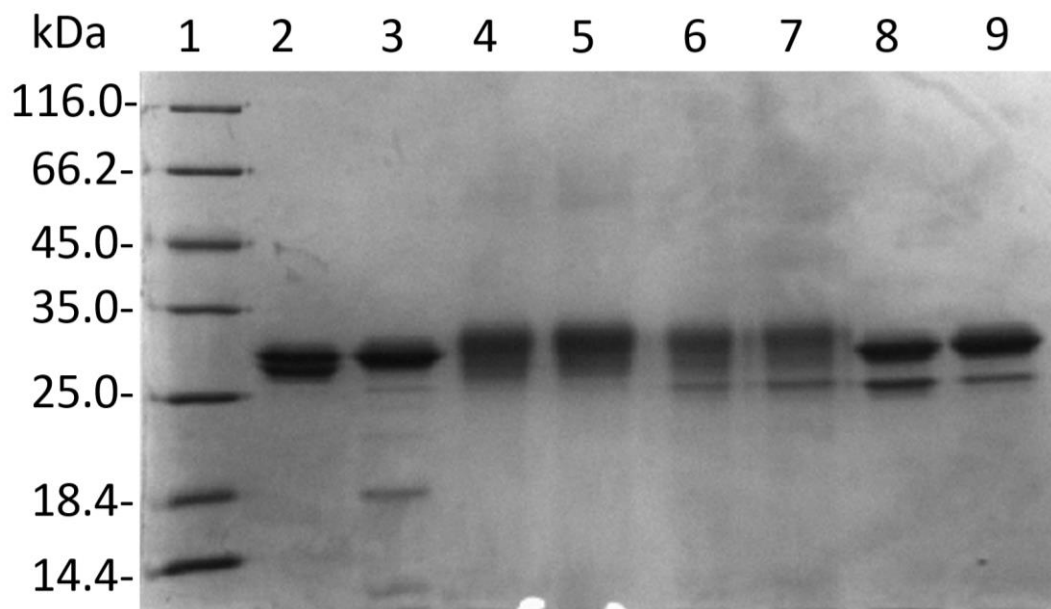


Figure 2.9: Analysis of putative cross-link forming conditions in CADD. 5 μ g samples were collected from various *in vitro* enzymatic assays that will be denoted by the description of the lane (lanes 3-9). Lanes: 1) Protein molecular weight marker. 2) As-purified CADD. 3) No metal, standard *in vitro* assay. 4) Method A, Fe/Fe. 5) Method C. Fe/Fe. 6) Method A, Fe/Mn. 7) Method C, Fe/Mn. 8) Method A, Mn/Mn. 9) Method C, Mn/Mn.

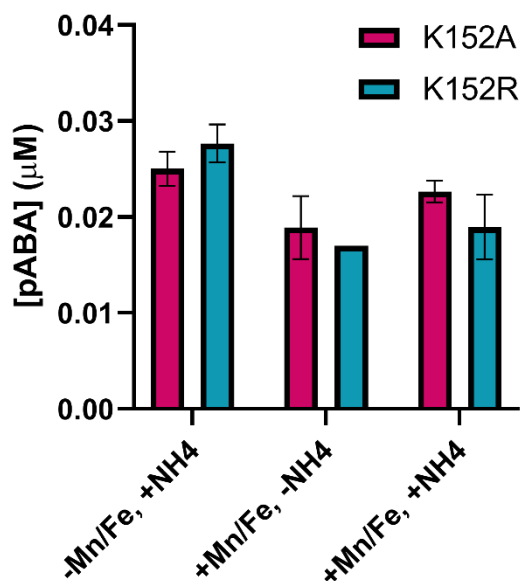


Figure 2.10: pABA synthase of CADD K152A and K152R mutants in the presence and absence of an exogenous amino source. Protein was purified from LB and used for a typical *in vitro* enzymatic assay. Metal solutions or NH₄⁺ was added directly to the assay and the reaction was initiated with DTT.

Protein preparation	mol metal/mol protein	
	Fe	Mn
LB, as-purified	0.07	Below LOD ³
LB, treated with EDTA	0.03	Below LOD ³
LB, treated with EDTA, reconstituted with 2 eq. Mn ¹	Below LOD ²	0.82
LB, treated with EDTA, reconstituted with 1 eq. Mn and 1 eq. Fe ¹	0.81	0.35
LB with 1,10-phenanthroline, as-purified	Below LOD ²	Below LOD ³

Table 2.1: ¹Reconstituted using Method B; ²limit of detection (LOD) for Fe is 0.005 mg/L; ³LOD for Mn is 0.001 mg/L. Concentrations of protein analyzed ranged from 15 – 36 mg/mL depending on the preparation.

Ion	Observed	Theoretical	Error (ppm)
Tyr27 to Gly precursor ion			
[M+H] ⁺³	425.8862	425.8875	3.1
[M+H] ⁺²	638.3253	638.3277	3.8
Tyr27 to Gly MS/MS fragment ions			
b ₂	239.1125	239.1139	5.9
y ₃	333.1755	333.1769	4.2
y ₄	420.2074	420.2089	3.6
z	734.3796	734.3832	4.9
y ₇	833.4602	833.4516	-10.3
y ₈	890.4724	890.4730	0.7
y ₉	1037.5369	1037.5415	4.4
y ₁₀	1138.5832	1138.5891	5.2
Lys152 to aminoadipic acid precursor ion			
[M+H] ⁺²	416.2309	416.2322	3.1
Lys152 to aminoadipic acid ETD/HCD fragment ions			
y ₂	249.1066	249.1081	6.0
c ₄	487.2965	487.2987	4.5
z ₅	559.2935	559.2960	4.5
c ₅	600.3804	600.3828	4.0
c ₆	701.4273	701.4304	4.4

Table 2.2: Masses (observed and theoretical) for ions corresponding to peptides containing the Tyr27 to Gly modification (HTFGVKWSKGE) and the Lys152 to aminoadipic acid modification (K(ox)IRGLTE).

References:

- 1 Wooldridge R, Stone S, Pedraza A, Ray WK, Helm RF & Allen KD (2023) The *Chlamydia trachomatis* p-aminobenzoate synthase CADD is a manganese-dependent enzyme that uses its own amino acid residues as substrates. *FEBS Lett.*
- 2 de Crécy-Lagard V, El Yacoubi B, de la Garza RD, Noiriél A & Hanson AD (2007) Comparative genomics of bacterial and plant folate synthesis and salvage: predictions and validations. *BMC Genomics* **8**, 245.
- 3 Adams NE, Thiaville JJ, Proestos J, Juárez-Vázquez AL, McCoy AJ, Barona-Gómez F, Iwata-Reuyl D, de Crécy-Lagard V & Maurelli AT (2014) Promiscuous and Adaptable Enzymes Fill “Holes” in the Tetrahydrofolate Pathway in *Chlamydia* Species. *mBio* **5**, e01378-14.
- 4 Stenner-Liewen F, Liewen H, Zapata JM, Pawlowski K, Godzik A & Reed JC (2002) CADD, a *Chlamydia* Protein That Interacts with Death Receptors*. *J Biol Chem* **277**, 9633–9636.
- 5 Schwarzenbacher R, Stenner-Liewen F, Liewen H, Robinson H, Yuan H, Bossy-Wetzel E, Reed JC & Liddington RC (2004) Structure of the *Chlamydia* Protein CADD Reveals a Redox Enzyme That Modulates Host Cell Apoptosis*. *J Biol Chem* **279**, 29320–29324.
- 6 Poulos TL (2014) Heme Enzyme Structure and Function. *Chem Rev* **114**, 3919–3962.
- 7 McBride MJ, Pope SR, Hu K, Okafor CD, Balskus EP, Bollinger JM & Boal AK (2021) Structure and assembly of the diiron cofactor in the heme-oxygenase-like domain of the N-nitrosourea-producing enzyme SznF. *Proc Natl Acad Sci U S A* **118**, e2015931118.
- 8 Ng TL, Rohac R, Mitchell AJ, Boal AK & Balskus EP (2019) An N-nitrosating metalloenzyme constructs the pharmacophore of streptozotocin. *Nature* **566**, 94.
- 9 He H-Y, Henderson AC, Du Y-L & Ryan KS (2019) Two-Enzyme Pathway Links l-Arginine to Nitric Oxide in N-Nitroso Biosynthesis. *J Am Chem Soc* **141**, 4026–4033.
- 10 McBride MJ, Sil D, Ng TL, Crooke AM, Kenney GE, Tysoe CR, Zhang B, Balskus EP, Boal AK, Krebs C & Bollinger JMJr (2020) A Peroxodiiron(III/III) Intermediate Mediating Both N-Hydroxylation Steps in Biosynthesis of the N-Nitrosourea Pharmacophore of Streptozotocin by the Multi-domain Metalloenzyme SznF. *J Am Chem Soc* **142**, 11818–11828.
- 11 Hedges JB & Ryan KS (2019) In vitro Reconstitution of the Biosynthetic Pathway to the Nitroimidazole Antibiotic Azomycin. *Angew Chem Int Ed* **58**, 11647–11651.
- 12 Patteson JB, Putz AT, Tao L, Simke WC, Bryant LH, Britt RD & Li B (2021) Biosynthesis of fluopsin C, a copper-containing antibiotic from *Pseudomonas aeruginosa*. *Science* **374**, 1005–1009.
- 13 Zhang B, Rajakovich LJ, Van Cura D, Blaesí EJ, Mitchell AJ, Tysoe CR, Zhu X, Streit BR, Rui Z, Zhang W, Boal AK, Krebs C & Bollinger JM (2019) Substrate-triggered formation of a peroxo-Fe₂(III/III) intermediate during fatty acid decarboxylation by UndA. *J Am Chem Soc* **141**, 14510.

- 14 Manley OM, Fan R, Guo Y & Makris TM (2019) Oxidative Decarboxylase UndA Utilizes a Dinuclear Iron Cofactor. *J Am Chem Soc* **141**, 8684–8688.
- 15 Rui Z, Li X, Zhu X, Liu J, Domigan B, Barr I, Cate JHD & Zhang W (2014) Microbial biosynthesis of medium-chain 1-alkenes by a nonheme iron oxidase. *Proc Natl Acad Sci* **111**, 18237–18242.
- 16 Manley OM, Tang H, Xue S, Guo Y, Chang W & Makris TM (2021) BesC Initiates C–C Cleavage through a Substrate-Triggered and Reactive Diferric-Peroxo Intermediate. *J Am Chem Soc* **143**, 21416–21424.
- 17 McBride MJ, Nair MA, Sil D, Slater JW, Neugebauer M, Chang MCY, Boal AK, Krebs C & Bollinger JM (2022) A Substrate-triggered μ -Peroxodiiron(III) Intermediate in the 4-Chloro-L-Lysine-Fragmenting Heme-Oxygenase-like Diiron Oxidase (HDO) BesC: Substrate Dissociation from, and C4 Targeting by, the Intermediate. *Biochemistry* **61**, 689–702.
- 18 Marchand JA, Neugebauer ME, Ing MC, Lin C-I, Pelton JG & Chang MCY (2019) Discovery of a pathway for terminal-alkyne amino acid biosynthesis. *Nature* **567**, 420–424.
- 19 Macias-Orihuela Y, Cast T, Crawford I, Brandecker KJ, Thiaville JJ, Murzin AG, de Crécy-Lagard V, White RH & Allen KD (2022) An Unusual Route for p-Aminobenzoate Biosynthesis in *Chlamydia trachomatis* Involves a Probable Self-Sacrificing Diiron Oxygenase. *J Bacteriol* **202**, e00319-20.
- 20 Ruskoski TB & Boal AK (2021) The periodic table of ribonucleotide reductases. *J Biol Chem* **297**, 101137.
- 21 Rose HR, Ghosh MK, Maggiolo AO, Pollock CJ, Blaesi EJ, Hajj V, Wei Y, Rajakovich LJ, Chang W, Han Y, Hajj M, Krebs C, Silakov A, Pandelia M-E, Bollinger JM Jr & Boal AK (2018) Structural Basis for Superoxide Activation of *Flavobacterium johnsoniae* Class I Ribonucleotide Reductase and for Radical Initiation by Its Dimanganese Cofactor. *Biochemistry* **57**, 2679–2693.
- 22 Beinert H (1978) [24] Micro methods for the quantitative determination of iron and copper in biological material. In *Methods in Enzymology* pp. 435–445. Academic Press.
- 23 Manley OM, Phan HN, Stewart AK, Mosley DA, Xue S, Cha L, Bai H, Lightfoot VC, Rucker PA, Collins L, Williams TI, Chang W-C, Guo Y & Makris TM (2022) Self-sacrificial tyrosine cleavage by an Fe:Mn oxygenase for the biosynthesis of *para*-aminobenzoate in *Chlamydia trachomatis*. *Proc Natl Acad Sci* **119**, e2210908119.
- 24 Dominy JE, Hwang J, Guo S, Hirschberger LL, Zhang S & Stipanuk MH (2008) Synthesis of Amino Acid Cofactor in Cysteine Dioxygenase Is Regulated by Substrate and Represents a Novel Post-translational Regulation of Activity*. *J Biol Chem* **283**, 12188–12201.
- 25 Lai R-Y, Huang S, Fenwick MK, Hazra A, Zhang Y, Rajashankar K, Philmus B, Kinsland C, Sanders JM, Ealick SE & Begley TP (2012) Thiamin Pyrimidine Biosynthesis in *Candida albicans*: A Remarkable Reaction between Histidine and Pyridoxal Phosphate. *J Am Chem Soc* **134**, 9157–9159.

- 26 Chatterjee A, Abeydeera ND, Bale S, Pai P-J, Dorrestein PC, Russell DH, Ealick SE & Begley TP (2011) *Saccharomyces cerevisiae* THI4p is a suicide thiamine thiazole synthase. *Nature* **478**, 542–546.
- 27 Nickel-pincer cofactor biosynthesis involves LarB-catalyzed pyridinium carboxylation and LarE-dependent sacrificial sulfur insertion | PNAS
- 28 Sakaki K, Ohishi K, Shimizu T, Kobayashi I, Mori N, Matsuda K, Tomita T, Watanabe H, Tanaka K, Kuzuyama T & Nishiyama M (2020) A suicide enzyme catalyzes multiple reactions for biotin biosynthesis in cyanobacteria. *Nat Chem Biol* **16**, 415–422.
- 29 Minnihan EC, Nocera DG & Stubbe J (2013) Reversible, Long-Range Radical Transfer in *E. coli* Class Ia Ribonucleotide Reductase. *Acc Chem Res* **46**, 2524–2535.
- 30 Rozman Grinberg I, Berglund S, Hasan M, Lundin D, Ho FM, Magnuson A, Logan DT, Sjöberg B-M & Berggren G (2019) Class Id ribonucleotide reductase utilizes a Mn₂(IV,III) cofactor and undergoes large conformational changes on metal loading. *JBIC J Biol Inorg Chem* **24**, 863–877.
- 31 Cotruvo JA & Stubbe J (2010) An Active Dimanganese(III)–Tyrosyl Radical Cofactor in *Escherichia coli* Class Ib Ribonucleotide Reductase. *Biochemistry* **49**, 1297–1309.
- 32 Jiang W, Yun D, Saleh L, Barr EW, Xing G, Hoffart LM, Maslak M-A, Krebs C & Bollinger JM (2007) A Manganese(IV)/Iron(III) Cofactor in *Chlamydia trachomatis* Ribonucleotide Reductase. *Science* **316**, 1188–1191.
- 33 Högbom M, Stenmark P, Voevodskaya N, McClarty G, Gräslund A & Nordlund P (2004) The Radical Site in Chlamydial Ribonucleotide Reductase Defines a New R2 Subclass. *Science* **305**, 245–248.
- 34 Jiang W, Bollinger J Martin & Krebs C (2007) The Active Form of *Chlamydia trachomatis* Ribonucleotide Reductase R2 Protein Contains a Heterodinuclear Mn(IV)/Fe(III) Cluster with S = 1 Ground State. *J Am Chem Soc* **129**, 7504–7505.
- 35 Cotruvo JA & Stubbe J (2011) Class I Ribonucleotide Reductases: Metallocofactor Assembly and Repair In Vitro and In Vivo. *Annu Rev Biochem* **80**, 733–767.
- 36 Mechanism of Assembly of the Dimanganese-Tyrosyl Radical Cofactor of Class Ib Ribonucleotide Reductase: Enzymatic Generation of Superoxide Is Required for Tyrosine Oxidation via a Mn(III)Mn(IV) Intermediate | Journal of the American Chemical Society
- 37 Boal AK, Cotruvo JA, Stubbe J & Rosenzweig AC (2010) Structural Basis for Activation of Class Ib Ribonucleotide Reductase. *Science* **329**, 1526–1530.
- 38 Jiang W, Xie J, Nørgaard H, Bollinger JM & Krebs C (2008) Rapid and Quantitative Activation of *Chlamydia trachomatis* Ribonucleotide Reductase by Hydrogen Peroxide. *Biochemistry* **47**, 4477–4483.
- 39 The irreversible inactivation of ribonucleotide reductase from *Escherichia coli* by superoxide radicals - Gaudu - 1996 - FEBS Letters - Wiley Online Library

- 40 Baldwin J, Krebs C, Ley BA, Edmondson DE, Huynh BH & Bollinger JM (2000) Mechanism of Rapid Electron Transfer during Oxygen Activation in the R2 Subunit of *Escherichia coli* Ribonucleotide Reductase. 1. Evidence for a Transient Tryptophan Radical. *J Am Chem Soc* **122**, 12195–12206.
- 41 Yang Y, Bazhin AV, Werner J & Karakhanova S (2013) Reactive Oxygen Species in the Immune System. *Int Rev Immunol* **32**, 249–270.

Chapter 3:

Initial biochemical characterization of a putative self-sacrificing *p*-aminobenzoate synthase from *Nitrosomonas europaea*

3.1 Abstract

Nitrosomonas europaea is a model ammonia-oxidizing bacterium (AOB) that oxidizes ammonia (NH₃) to nitrite (NO₂⁻) in the nitrogen cycle. This organism lacks the canonical genes involved in *p*-aminobenzoate (pABA) biosynthesis, which is an essential component of the tetrahydrofolate cofactor. Previous genetic studies showed that a single gene, *ne1434*, is responsible for pABA production in this organism. Interestingly, NE1434 is a proposed self-sacrificing pABA synthase based upon its homology to the recently characterized metalloxygenase, CADD, from the intracellular pathogen *Chlamydia trachomatis*. Here, we perform initial biochemical characterization of NE1434 to investigate its putative pABA synthase activity and metal preference. Purified NE1434 indeed produces pABA *in vitro* in a reaction that is stimulated by molecular oxygen and a reducing agent. Although CADD was shown to utilize a heterodinuclear Mn/Fe cofactor, NE1434 clearly demonstrated no preference for manganese and likely employs the more traditional Fe/Fe cofactor. Isotope labeling experiments revealed that the two oxygen atoms in the carboxylic acid portion of pABA are derived from molecular oxygen. Finally, site-directed mutagenesis studies followed by pABA synthase activity assays identified

Tyr25, Tyr41, and K159 as potential precursors to the aromatic and amino portions of NE1434 derived pABA. Thus, NE1434 is likely a self-sacrificing pABA synthase similar to CADD, but employs a Fe/Fe instead of Fe/Mn cofactor.

3.2 Introduction

Tetrahydrofolate (THF) is an essential one-carbon carrier cofactor involved in metabolic processes such as DNA and amino acid synthesis biosynthesis (Figure 1.1A) [1]. Humans and mammals are unable to synthesize this cofactor unlike many bacteria and plants, which can synthesize it *de novo*, making this molecule an important antimicrobial target [1]. Due to its essential nature and appeal as a drug target, the typical THF biosynthesis pathway is well defined. THF is a tripartite molecule assembled from a pteridine ring, *p*-aminobenzoate (pABA), and a poly-glutamate tail [1]. *Nitrosomonas europaea* is an ammonia-oxidizing soil bacterium that contains the canonical THF biosynthetic genes, but lacks the *pabABC* orthologs to produce pABA (Table 1.1) [2]. In the canonical pathway, pABA is synthesized from chorismate by the heterodimeric PabA/B (ADC synthase) and PabC (ADC lyase) [1]. However, *N. europaea* bypasses this entire pathway and its intermediates with a single gene, *ne1434* [2].

The role of *ne1434* as a novel pABA synthase in *N. europaea* became apparent during complementation studies conducted by Satoh et al., where *ne1434* was shown to complement an *E. coli* $\Delta pabABC$ strain [2]. In an effort to illuminate the substrate of NE1434, a heterologously expressed version was incubated with the canonical pABA precursor, chorismate. However, even in the presence of various metals, cofactors, and pH conditions, no product was able to be detected [2]. Moreover, a genetic method was used to investigate 3-dehydroquinate, a metabolite in the shikimate pathway that is the predecessor to chorismate (Figure 1.5). The presence of *ne1434* was enough to complement the growth of *E. coli* $\Delta aroB$, $\Delta aroC$, and $\Delta aroD$ mutants, which required

additional aromatic amino acids, 4-hydroxybenzoate, and pABA for their successful growth [2]. The genetic study was complemented by *in vitro* reactions in which aromatic amino acids and 4-hydroxybenzoate were also incubated with NE1434, but again found no detection of pABA formation [2]. These results demonstrated that NE1434 was involved in a novel pABA biosynthesis pathway that did not employ the typical substrates.

Although genomic analysis previously defined NE1434 as a pyrroloquinoline-quinone (PQQ) synthase (PqqC), its low similarity to PqqC in other species as well as the fact it did not contain other PQQ biosynthetic genes brought its true function into question [2]. Compellingly, NE1434 shares 40% identity and 60% similarity with CADD from *Chlamydia trachomatis* (Figure 3.1C) [2]. The crystal structure of NE1434 has yet to be solved, but an AlphaFold predicted model displays a structure that closely resembles the helical bundle fold of CADD (Figure 3.1A). CADD was originally demonstrated to have a role in host-mediated apoptosis, but was later confirmed to possess a moonlighting self-sacrificing pABA synthase function [1,3,4]. Recent work done by our lab has shown that CADD uses an oxygenated heterodinuclear Mn/Fe cofactor for pABA synthase activity. This cofactor is necessary to cleave one of its own Tyr residues (Tyr27) from the protein backbone which serves as the aromatic scaffold for the pABA product. Two molecular oxygen atoms are incorporated into this scaffold and a neighboring Lys residue (Lys152) has been implicated as an internal amino donor.

Here, we are the first to provide experimentation to implicate NE1434 as a putative self-sacrificing pABA synthase similar to CADD. Interestingly, NE1434 does not appear to be dependent on manganese for catalytic activity, but the pABA synthase activity is stimulated in the presence of only iron [5,6]. Oxygenase activity was established through isotopic labeling studies, which showed that $^{18}\text{O}_2$ is incorporated into the carboxylic acid portion of NE1434 derived pABA.

Additionally, our site-directed mutagenesis studies have identified potential tyrosine residues as well as a lysine residue that are the aromatic and amino donors, respectively, for NE1434's self-sacrificing pABA synthase activity.

3.3 Materials and Methods

Materials. Dithiothreitol (DTT), isopropyl- β -D-thiogalactopyranoside (IPTG), and ampicillin were acquired from GoldBio (St. Louis, MO, USA). Ferrous ammonium sulfate was purchased from MilliporeSigma (Burlington, MA, USA) and manganese(II) sulfate monohydrate was from Alfa Aesar (Haverhill, MA, USA). $^{18}\text{O}_2$ was from MilliporeSigma and primers for mutagenesis were from Integrated DNA technologies (IDT). All other reagents were from typical suppliers unless otherwise specified.

Overexpression and purification. The *ne1434* gene (Accession: CAD85345.1) from *N. europaea* was cloned into pet15b with an N-terminal hexahistidine tag. The resulting NE1434_pet15b plasmid was transformed into *E. coli* BL21 and plated on a LB agar plate supplemented with 100 $\mu\text{g}/\text{mL}$ ampicillin. Single colonies were used to inoculate culture tubes with 5 mL of LB and 100 $\mu\text{g}/\text{mL}$ ampicillin, which were incubated overnight at 37°C and shaking at 250 RPM. The next day, a 15 mL aliquot was used to inoculate two 3 L flask containing 1.5 L of LB and 100 $\mu\text{g}/\text{mL}$ ampicillin. The cells were grown at 37°C with shaking at 250 RPM until they reached an OD_{600} of ~ 0.7 . Expression of NE1434 was then induced by adding 0.5 mM isopropyl- β -Dthiogalactopyranoside (IPTG) and the cells were cultured for an additional 4 hours in the same conditions. The cells were then harvested by centrifugation at 8,000 $\times g$ for 15 minutes

and stored at -20°C until purification. If a growth required 1,10-phenanthroline, a concentration of 0.5 mM was added just before induction with IPTG [7].

The 3 L culture typically produced ~12 gram pellet. The pellet was thawed and resuspended in 30 mL of 50 mM sodium phosphate, 300 mM NaCl, and 20 mM imidazole (pH 7.4) (buffer A: 20 mM imidazole). Once the cells were resuspended, they were sonicated on ice and the soluble fraction was separated by centrifugation at $27,000 \times g$ for 50 minutes. The supernatant was loaded into a gravity flow column (1 by 3 cm, ~ 2 mL of resin) of Ni-nitrilotriacetic acid metal affinity resin (Prometheus, Genesee Scientific, El Cajon, CA, USA), equilibrated with 20 mL buffer A. The column was then washed with 50 mL of buffer A : 20 mM imidazole, followed by 5 mL of buffer A containing 100 mM imidazole. NE1434 was then eluted from the column by 10 mL of buffer A containing 250 mM imidazole.

The high imidazole fraction containing NE1434 was concentrated to 2.5 mL using an Amicon centrifuge concentrator (10-kDa cutoff, 15 mL; MilliporeSigma), the protein was exchanged into 20 mM HEPES (pH 7.5) using a PD-10 desalting column (Cytiva Life Sciences, Marlborough, MA, USA). The final purified protein in 3.5 mL had an average concentration of ~700 μM monomer (~20 $\text{mg}\cdot\text{mL}^{-1}$). The protein was flash-frozen and stored at -80°C until needed for assays. Protein concentrations were determined by the Bradford method with bovine serum albumin as a standard.

Overexpression and purification of NE1434 from M9 minimal media. A starter culture of BL21 cells containing NE1434_pet15b was prepared in LB medium as described above. Two 3 L flasks containing 1.5 L of M9 minimal media [50 mM Na_2HPO_4 , 20 mM KH_2PO_4 , 10 mM NaCl, 20 mM NH_4Cl , 0.5% glucose, 0.1 mM CaCl_2 , 2 mM MgSO_4 , 2 μM $\text{Fe}(\text{NH}_4)_2(\text{SO}_4)_2$], 100 $\mu\text{g}/\text{mL}$ ampicillin, and 2 g/L casamino acids were inoculated with 15 mL of the starter culture and

incubated at 37°C while shaking at 250 RPM. Once the cells reached an OD₆₀₀ of ~0.7, the cells were removed from the incubator and cooled on ice for 20 minutes. Expression of NE1434 was then induced by adding 200 µM IPTG and the cells were incubated at 30°C with shaking at 250 RPM overnight. Cells were harvested the next morning by centrifugation at 8 000 g for 15 minutes and stored at -20°C until purification. Purification was then conducted in the same manner described above.

***In vitro* enzymatic assays and pABA detection by LC-MS.** Purified NE1434 from the method described above was thawed on ice and a fresh Bradford assay was conducted. Routine pABA synthase assays were 500 µL reactions containing 154 µM (4.5 mg/mL) protein and 10 mM DTT in 20 mM HEPES buffer (pH 7.5). Control “protein only” reactions contained only 154 µM (4.5 mg/mL) protein in 20 mM HEPES buffer (pH 7.5). Some reactions were carried out in the presence of varying amounts of metal: Fe(NH₄)₂(SO₄)₂, MnSO₄, or CuSO₄ were added directly to the enzyme reaction (1 – 2 molar equivalents compared to the monomeric protein concentration). Mixed metal assays used a 1:1 ratio of metal that was premixed before being added to the assay. Addition of the reducing agent was followed by gentle pipetting to aerate the reaction followed by incubation at 37°C for 2 hours. Reactions were then quenched with 1.5 mL CH₃CN and precipitated protein was removed by high-speed centrifugation. The supernatant was transferred to a new tube and concentrated down to 100 µL by vacuum centrifugation. The 100 µL sample was spun down once again to remove any particulates, transferred to an LC-MS vial, and analyzed by the LC-MS.

For LC-MS analysis, a Waters Acquity TQD mass spectrometer with a Waters Acquity UPLC equipped with an Acquity Premier HSS T3 column (2.1 x 100 mm, 1.8 µm particle size) was used with solvent A as 0.1% formic acid in water and solvent B as 100% methanol. The LC

program consisted of 3 min at 98% A followed by a 10-min linear gradient to 50% B at a flow rate of 0.3 mL/min and the injection volume was 2 μ l. The MS method was a multiple reaction-monitoring method scanning three pairs: 138.1 and 120.4, 138.1 and 94.4, and 138.1 and 77.3, with a collision energy of 15V. The source temperature was 150°C, the desolvation temperature was 500°C, the desolvation gas flow was 800 L/hr, and the cone gas flow was 50 L/hr. MassLynx was used for system operation and data processing.

Reconstitution of NE1434. For some experiments, the following reconstitution procedure was performed instead of adding iron directly to enzyme assays. A 2.5 mL sample of purified NE1434 (~7 mg/mL) was deoxygenated in an anaerobic chamber by gentle stirring for 2 hours. After the first two hours, a stock of $\text{Fe}(\text{NH}_4)_2(\text{SO}_4)_2$ was suspended in deoxygenated 20 mM HEPES buffer (pH 7.5) and 2 molar equivalents of metal were added to the protein. The sample was left gently stirring in the anaerobic chamber for an additional 2 hours, and then exchanged into deoxygenated HEPES buffer using a PD-10 desalting column (Cytiva Life Sciences). The exchanged protein was stored in an anaerobic vial overnight at 4°C.

Substrate experiments. Typical *in vitro* pABA assays were set up using the method described above. Multiple reactions were set up for Fe/Fe reconstituted NE1434 containing either no exogenous substrate or 1 mM L-Tyrosine (L-Tyr), 4-hydroxybenzoic acid (pHB), *p*-hydroxyphenyl pyruvate (pHPP), or chorismate. DTT was added to each reaction which was then aerated by gentle pipetting. Reactions incubated overnight at 25°C on the benchtop and were quenched the next day with 1.5 mL of CH_3CN . Samples were then prepared for analysis by the LC-MS in the same manner described above.

Site-directed mutagenesis. NE1434 mutants were generated according to the instructions provided by the Phusion site-directed mutagenesis kit (Thermo Fischer Scientific). Primers used

for mutagenesis are listed in Table 3.1. Sanger sequencing services at Virginia Tech were used to confirm the presence of the mutation, where each mutant was then expressed and purified in the same manner as the wild type. All mutant *in vitro* assays were carried out with LB-as purified enzyme with 154 μM enzyme and 10 mM DTT in 20 mM HEPES buffer (pH 7.5).

AlphaFold structural prediction. A predicted structural model of NE1434 was generated using ColabFold v1.5.2: AlphaFold2 using MMseqs2 [8]. The NE1434 protein sequence (UniProt ID Q82UP8) was used as the query sequence and the resulting structure was exported to Pymol for visualization. An alignment to a CADD monomer (PDB: 1RCW) was performed in Pymol where CADD's protein structure was hidden, and metal ions were shown to visualize relevant residues in the presence of a presumed dimetal site in NE1434.

3.4 Results

Overexpression and purification of NE1434 in *E. coli*. NE1434 from *N. europaea* was implicated as a pABA synthase through genetic studies. However, this has yet to be confirmed through *in vitro* enzymatic experiments [2]. Thus, we sought to confirm the activity of this enzyme and gain insight into the details of the unique reaction. NE1434 containing a 6X N-terminus His-tag was overexpressed and purified from *E. coli* BL21. A typical purification had a final protein concentration around 15 mg/mL ($\sim 700 \mu\text{M}$) in 3.5 mL of 20mM HEPES buffer (pH 7.5) (Figure 3.2A). NE1434 purified from M9 yielded a typical final protein concentration of 6 mg/mL ($\sim 200 \mu\text{M}$) in buffer (pH 7.5) (Figure 3.2B).

Site-directed mutagenesis of potential self-sacrificing residues. Because NE1434 was identified as a putative self-sacrificing enzyme from sequence similarity to the known pABA

synthase, CADD, experiments were carried out to determine pABA synthase activity as well as identify prospective self-sacrificing residues. In the presence of molecular oxygen and a reducing agent (DTT), we confirmed via LC-MS that purified NE1434 produces pABA (Figure 3.3A and 3.3B). Key residues have been highlighted in CADD as possible precursors to CADD-derived pABA and are shown to be conserved in NE1434, therefore, we propose these residues (Y25, Y41, Y45, and K159) may play a role in NE1434 pABA synthase activity (Figure 3.4A) [2,4]. These initial experiments performed to analyze important residues for NE1434 catalysis were done in the absence of exogenous metal, but the results obtained are still valuable to further narrow down residues involved in the reaction (metal dependency discussed later). The largest decrease in pABA production was seen in the Y25F, Y41F, and K159R variants, suggesting that these residues play a key role in the pABA synthesis reaction in NE1434 (Figure 3.4B). Interestingly, these results are consistent with the respective residues in CADD [4], further emphasizing this may be a conserved mechanism across species.

After determining that NE1434 retained the ability to produce pABA with a reducing agent and molecular oxygen alone, we set out to confirm this self-sacrificial nature through the addition of potential pABA precursors to our assays. *In vitro* enzymatic assays with exogenous L-Tyrosine, *p*-hydroxyphenylpyruvate (HPP), *p*-hydroxybenzoate, and chorismate did not result in increased pABA production compared to reactions containing only the enzyme and the reducing agent (Figure 3.5A). Although no additional substrate seemed to increase activity, as-purified non-reconstituted NE1434 (154 μ M in the assay) only produced \sim 0.6 μ M pABA in the presence of a reducing agent. Because the overall activity of as-purified NE1434 was so low, we repeated these experiments in the presence of added iron to once again test if exogenous substrate would increase

activity. Similarly, NE1434 produced the most pABA without additional substrate, further supporting the proposed self-sacrificing nature of this enzyme.

NE1434 pABA synthase activity when expressed in various growth conditions. Our initial results discussed thus far implicated NE1434 as a self-sacrificing pABA synthase. Unfortunately, self-sacrificing enzymes present challenges to *in vitro* experimentation such as the inability to control cofactor maturation causing an inadvertent reaction during overexpression in *E. coli*. Based on the knowledge gained from experimentation with CADD, NE1434 is presumed to require an oxygenated dimetal cofactor to initiate cleavage of a tyrosine residue, thus leaving a glycine residue in its place. This reaction is inherently a 1:1 reaction, where only one monomeric unit can produce one pABA molecule. In an attempt to mitigate the amount of protein that turns over during the growth and purification process, we sought out the conditions that would limit cofactor or oxygen availability to yield a more controlled *in vitro* assay. Thus, we carried out different expression and purification methods in an effort to maximize the amount of active purified protein. The various conditions tested were: NE1434 grown in M9 minimal media (“M9”), LB + 1,10-phenanthroline (“1,10”), normal LB growth as described above (“LB”), and LB media, but purified anaerobically (“Anaerobic”). These conditions were chosen because of the limited metals, chelation of excess iron, or limited oxygen exposure, while LB was used as the baseline. *In vitro* enzymatic assays were then carried out with each condition in which two equivalents of iron were added before adding the reducing agent. Based on these results, protein grown in M9 was used for metal dependence assays (see below) in order to use a consistent growth method that was also time efficient (Figure 3.7).

Metal dependence of NE1434. Like CADD, NE1434 belongs to the emerging heme-oxygenase like diiron oxidase (HDO) family of enzymes, all of which utilize a dimetal cofactor to

activate molecular oxygen for insertion into a substrate. CADD is unique in using a Mn/Fe cofactor, while all other characterized members use a Fe/Fe cofactor. To determine the metal dependence of NE1434 catalyzed pABA production, we conducted *in vitro* enzymatic assays with NE1434 purified from M9 minimal media in the presence of different combinations of metals. The addition of 2 molar equivalents of Fe(II) consistently yielded the highest amount of NE1434-derived pABA, producing ~2 μM pABA (Figure 3.7). Although there was a small amount of pABA produced from the non-reconstituted enzyme, this is likely due to some protein being purified with an active cofactor. Overall activity of this enzyme will be considered in the discussion.

$^{18}\text{O}_2$ experiment. Previous work done by Wooldridge, Stone et. al. [5,9] identified that CADD incorporates two atoms from molecular oxygen into the final pABA product. In order to elucidate if molecular oxygen is also incorporated into NE1434-derived pABA, *in vitro* enzymatic assays with iron-reconstituted NE1434 were incubated with $^{18}\text{O}_2$ and analyzed by LC-MS. Similarly to what was shown with CADD, NE1434-derived pABA that was incubated with $^{18}\text{O}_2$ displayed a $[\text{M} + \text{H}]^+$ ion at 142 m/z, indicating that two heavy atom oxygens were incorporated into the carboxylic acid portion of pABA. The control reaction that was flushed with molecular oxygen displayed a $[\text{M} + \text{H}]^+$ ion at 138 m/z, which indicates $^{16}\text{O}_2$ was incorporated into the final product. These results correspond to what was found for CADD, classifying both of these enzymes as oxygenases, although the specifics of how these oxygen atoms are incorporated is not yet understood.

3.5 Discussion

The biochemical characterization of NE1434 was inspired by the work done to characterize its ortholog, CADD, which catalyzes a novel self-sacrificing reaction for pABA synthesis (Chapter 2). Sequence analysis of NE1434 has shown that residues involved in the CADD self-sacrificing reaction for pABA biosynthesis are conserved (Figure 3.1C); thus we propose that NE1434 is also a self-sacrificing pABA synthase that cleaves off one of its own tyrosine residues to use as a substrate. Similarly, it may also utilize an amino group from one of its lysine residues near the dimetal active site. Additionally, NE1434 is a likely metallo-oxygenase that uses its dimetal cofactor for its pABA synthase activity.

NE1434 is a probable self-sacrificing pABA synthase. As previously reported, NE1434 was indicated as a novel pABA synthase, which did not utilize chorismate or shikimate metabolites to produce pABA [2]. Notably, our *in vitro* enzymatic assays are the first to show detection of pABA production from NE1434 in the absence of exogenous pABA precursors [2]. Our initial site-directed mutagenesis study to test potential self-sacrificing residues in NE1434 displayed a comparable pattern to the respective residues from CADD (Figure 3.4B) [4]. Chapter 2 of this thesis presented that as determined by LC-MS/MS, Y27 from CADD was shown to be converted to a glycine after a typical *in vitro* reaction had taken place [5]; additionally, K152, which corresponds to K159 from *N. europaea*, was found to be replaced by aminoadipic acid, suggesting this lysine contributes its amino group to the reaction [5]. Additional analysis will need to be carried out to verify the modifications of these residues in NE1434, but our initial site-directed mutagenesis results support a conserved self-sacrificial pABA biosynthetic pathway between these two distantly related organisms.

NE1434 likely uses a diiron cofactor for pABA synthase activity. After the exciting discovery that CADD uses a Mn/Fe cofactor for pABA synthase activity, the next step was to ask if this were the case for orthologs of CADD. Our initial experiments to understand if NE1434 also requires manganese for optimal pABA synthase activity has presented a clear divide between these two enzymes. The addition of manganese to NE1434 enzymatic assays dramatically stunted any pABA production compared to the most active form seen with the addition of two molar equivalents of iron solution (per monomer) (Figure 3.7).

Unlike CADD, which is expressed by an intracellular pathogen, NE1434 is expressed by a non-pathogenic, environmental microbe. The difference in metal preferences seen between these organisms could potentially be explained by the distinct environments in which they live. Intracellular pathogens must adapt to host-immune responses in order to survive; the evolutionary substitution of manganese in place of iron has been identified as a mechanism for pathogens to better deal with reactive oxygen species (ROS) and iron depleted environments [10]. Class Ib-Id ribonucleotide reductases (RNRs) are manganese-dependent RNRs that are only expressed in pathogens unlike the class Ia RNR which can be found in all forms of life [11]. The selective presence of these class I subclasses presents the hypothesis that organisms have evolutionarily fine-tuned their metal preferences in order to adapt to host mediated immune responses. Incapable of infecting a host cell, *N. europaea* would not have encountered the same evolutionary pressure as *C. trachomatis* to adapt to host-mediated defenses such as reactive oxygen species or iron depletion [10].

Although the addition of 2x molar equivalents of iron yielded the most active form of NE1434, it should be noted that the activity is still extremely low (~1% turnover). We hypothesize that the active diiron cofactor could be present during the overexpression of NE1434, thus

initiating the reaction and creating an inert enzyme that has already completed the maximum 1:1 turnover. Another important consideration is that we have yet to confirm the true metal cofactor(s) for NE1434; more metal dependence assays with other physiologically relevant metals could help discern this ambiguity. These preliminary experiments serve to guide future work in the investigation of CADD-like self-sacrificing enzymes and the recommendations will be described in chapter 4 of this thesis.

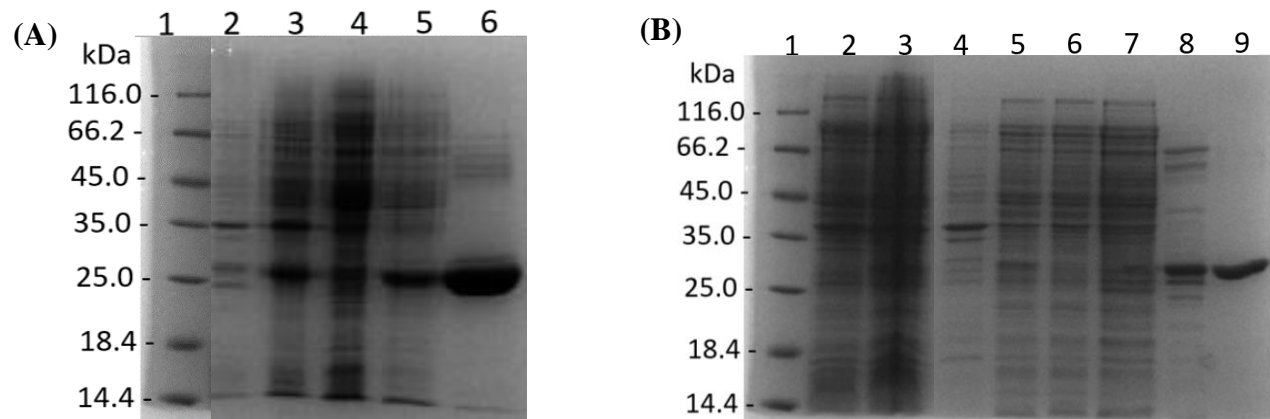


Figure 3.2: **A.** SDS-PAGE gel showing NE1434 purified from Luria-Broth medium. Left to right: (1) Protein molecular weight marker (2) insoluble fraction (3) liquid supernatant (4) flow through (5) 20 mM imidazole wash (6) elution of NE1434. **B.** SDS-PAGE gel showing NE1434 purified from M9 minimal media. Left to right: (1) Protein molecular weight marker (2) T_0 induction study (3) T_r induction study (4) insoluble fraction (5) liquid supernatant (6) flow through (7) 20 mM imidazole wash (8) 5 mL 100 mM imidazole wash (9) elution of NE1434.

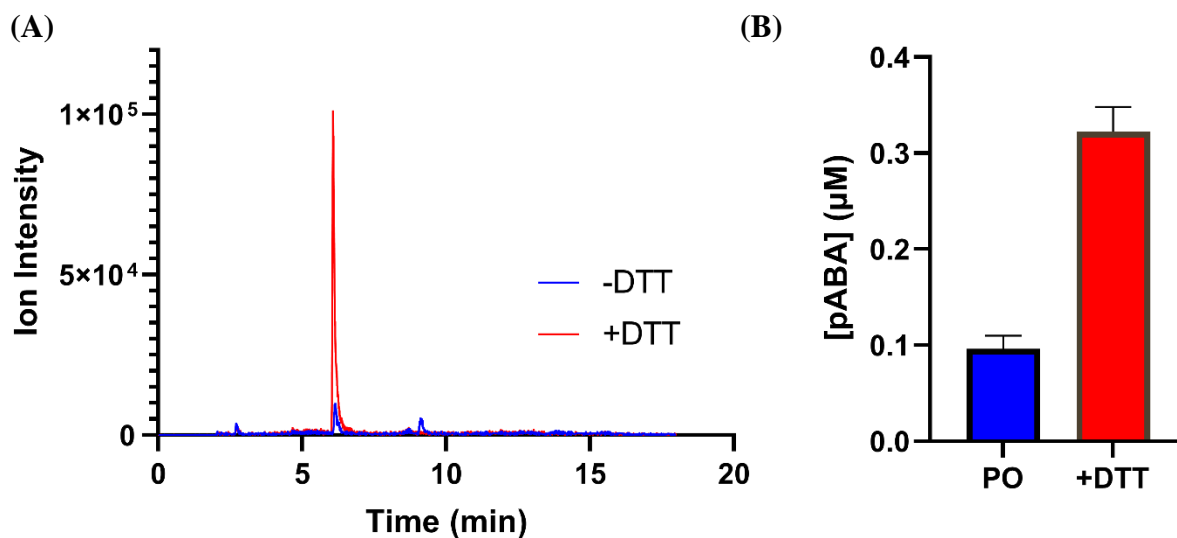


Figure 3.3: LC-MS analysis of pABA production by NE1434. **A)** Overlaid LC-MS extracted chromatograms of NE1434 pABA production with and without DTT. **B)** Corresponding quantitation of pABA for each reaction. *In vitro* enzymatic assays were carried out with 154 μM protein and 10 mM DTT. A reaction containing only as-purified NE1434 diluted in HEPES buffer is shown in blue and the reaction containing DTT is shown in red.

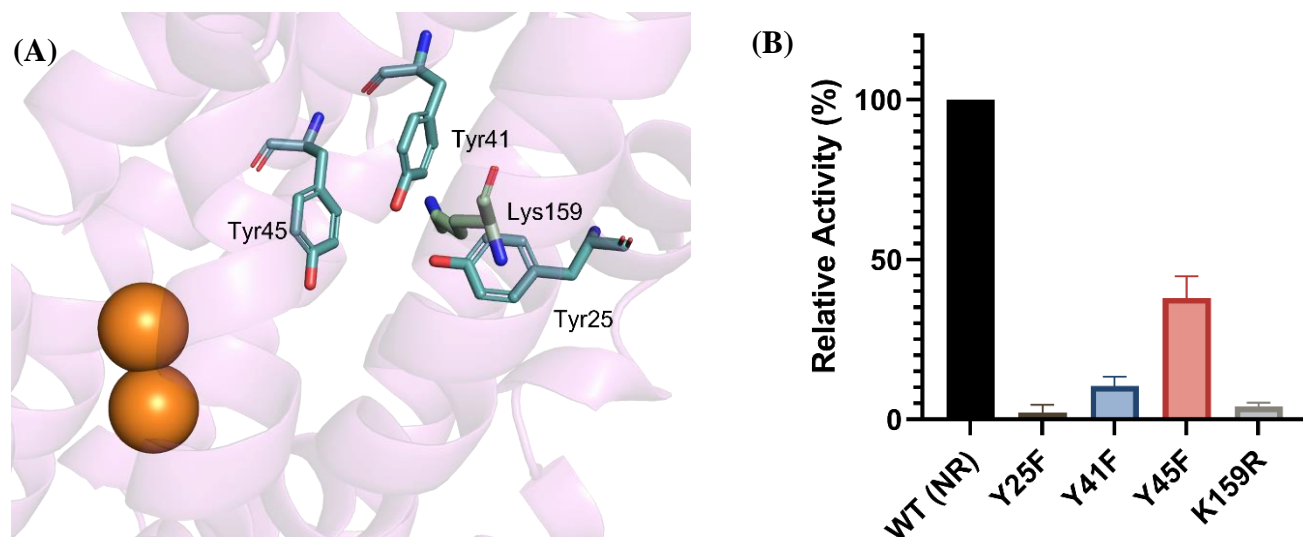


Figure 3.4: Site-directed mutagenesis studies in NE1434 **A)** Potential aromatic or amino donating residues from NE1434 shown with the dimetal site of CADD as determined by a structural alignment in Pymol. **B)** Relative activity of NE1434 mutants compared to a non-reconstituted WT. The reactions were conducted in triplicate.

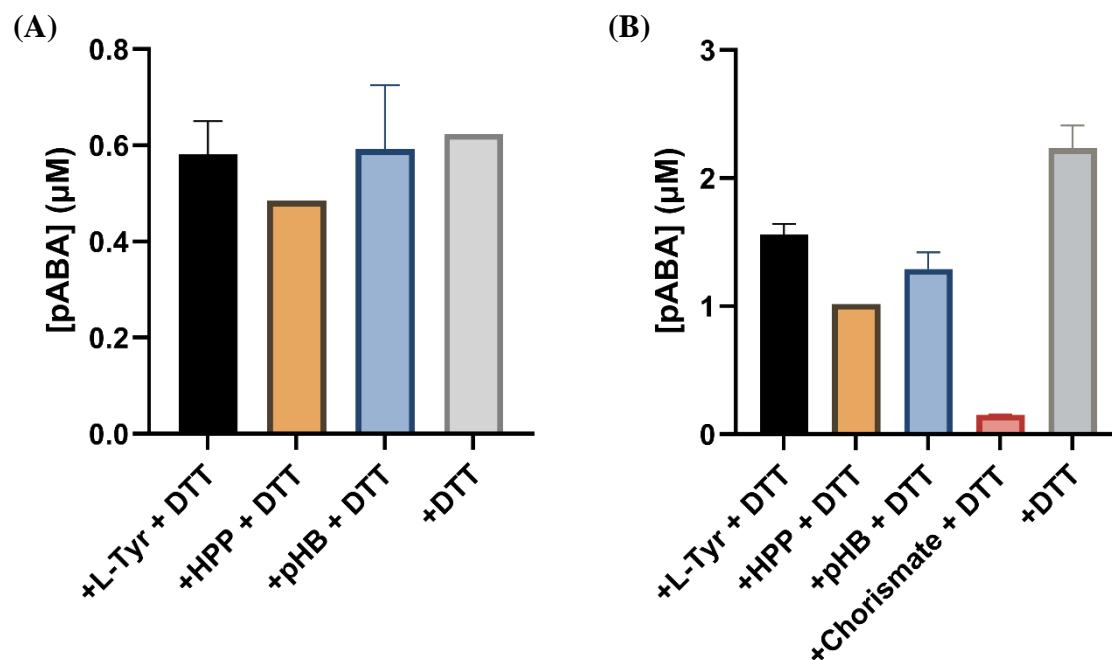


Figure 3.5: *In vitro* enzymatic assays of non-reconstituted and reconstituted NE1434 in the presence of potential pABA precursors **A)** As-purified NE1434 with the addition of exogenous substrate. **B)** NE1434 in the presence of exogenous substrate with added iron solution (reconstitution method).

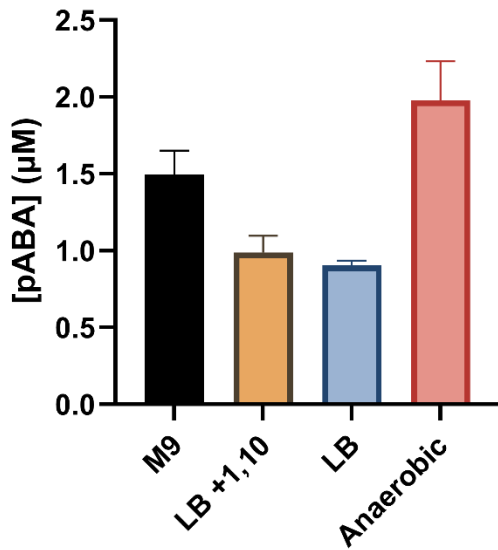


Figure 3.6: pABA synthase activity of NE1434 WT from various growth conditions and supplemented with 2X molar excess iron at the start of the reaction.

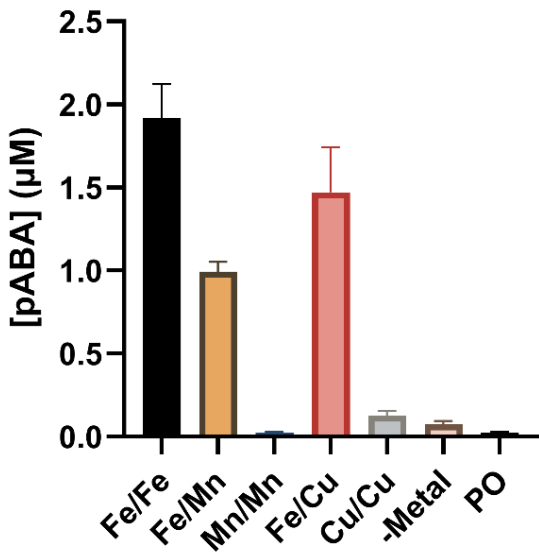


Figure 3.7: *In vitro* enzymatic assays of NE1434 purified from M9 minimal media with metal solutions added directly to the assay. Mixed metal assays were added at a 1:1 ratio and were mixed before being added to the assay. A control “protein only” (PO) reaction contained only protein in 20 mM HEPES buffer (pH 7.5).

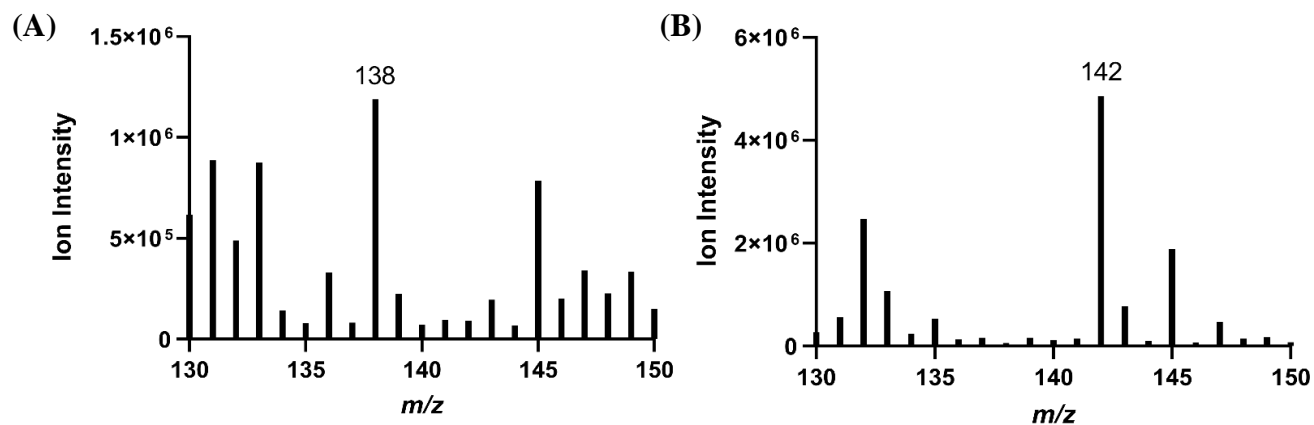


Figure 3.8: Incorporation of molecular oxygen into NE1434-derived pABA. **A)** pABA peak from Fe reconstituted NE1434 flushed with $^{16}\text{O}_2$. **B)** pABA peak from Fe reconstituted NE1434 flushed with $^{18}\text{O}_2$.

Mutation	Sequence (5' to 3')
Y25F	Fwd: cagcatccgtt <u>tc</u> attgcctggacc
	Rev: gcagcaggtgtctgcttgaatgatggaat
Y41F	Fwd: cagttacgccac <u>tc</u> gctgagcagtat
	Rev: ttcacgagtcagttgccttcggtccaggc
Y45F	Fwd: tatgctgagcag <u>tc</u> tttacaatgtg
	Rev: gtggcgtaactgttcacgagtcagttgcc
K159R	Fwd: attgctgccgtc <u>aga</u> atcgatggctg
	Rev: atcaggcacctgagattcgaacgcatgtaa

Table 3.1: Primers used to create NE1434 mutants using site-directed mutagenesis. The mutation is highlighted in red and underlined.

References:

- 1 Adams NE, Thiaville JJ, Proestos J, Juárez-Vázquez AL, McCoy AJ, Barona-Gómez F, Iwata-Reuyl D, de Crécy-Lagard V & Maurelli AT (2014) Promiscuous and Adaptable Enzymes Fill “Holes” in the Tetrahydrofolate Pathway in Chlamydia Species. *mBio* **5**, e01378-14.
- 2 Satoh Y, Kuratsu M, Kobayashi D & Dairi T (2014) New gene responsible for para-aminobenzoate biosynthesis. *J Biosci Bioeng* **117**, 178–183.
- 3 Stenner-Liewen F, Liewen H, Zapata JM, Pawlowski K, Godzik A & Reed JC (2002) CADD, a Chlamydia Protein That Interacts with Death Receptors*. *J Biol Chem* **277**, 9633–9636.
- 4 Macias-Orihuela Y, Cast T, Crawford I, Brandecker KJ, Thiaville JJ, Murzin AG, de Crécy-Lagard V, White RH & Allen KD (2022) An Unusual Route for p-Aminobenzoate Biosynthesis in Chlamydia trachomatis Involves a Probable Self-Sacrificing Diiron Oxygenase. *J Bacteriol* **202**, e00319-20.
- 5 Wooldridge R, Stone S, Pedraza A, Ray WK, Helm RF & Allen KD (2023) The Chlamydia trachomatis p-aminobenzoate synthase CADD is a manganese-dependent enzyme that uses its own amino acid residues as substrates. *FEBS Lett*.
- 6 Manley OM, Phan HN, Stewart AK, Mosley DA, Xue S, Cha L, Bai H, Lightfoot VC, Rucker PA, Collins L, Williams TI, Chang W-C, Guo Y & Makris TM (2022) Self-sacrificial tyrosine cleavage by an Fe:Mn oxygenase for the biosynthesis of *para* -aminobenzoate in *Chlamydia trachomatis*. *Proc Natl Acad Sci* **119**, e2210908119.
- 7 Rose HR, Ghosh MK, Maggiolo AO, Pollock CJ, Blaesi EJ, Hajj V, Wei Y, Rajakovich LJ, Chang W, Han Y, Hajj M, Krebs C, Silakov A, Pandelia M-E, Bollinger JM Jr & Boal AK (2018) Structural Basis for Superoxide Activation of Flavobacterium johnsoniae Class I Ribonucleotide Reductase and for Radical Initiation by Its Dimanganese Cofactor. *Biochemistry* **57**, 2679–2693.
- 8 Mirdita M, Schütze K, Moriwaki Y, Heo L, Ovchinnikov S & Steinegger M (2022) ColabFold: making protein folding accessible to all. *Nat Methods* **19**, 679–682.
- 9 Wooldridge RS CT610: A Mn-Dependent Self-Sacrificing Oxygenase in p- Aminobenzoate Biosynthesis in Chlamydia trachomatis. .
- 10 Palmer LD & Skaar EP (2016) Transition Metals and Virulence in Bacteria. *Annu Rev Genet* **50**, 67–91.
- 11 Ruskoski TB & Boal AK (2021) The periodic table of ribonucleotide reductases. *J Biol Chem* **297**, 101137.

Chapter 4:

Future Directions

Until the combination of our study and the one performed by Manley et al, [1] the substrate for CADD pABA synthase activity remained elusive. Fortunately, we were able to provide evidence of Tyr27 being the sacrificial donor for CADD's pABA synthase mechanism in addition to illustrating this is likely a conserved mechanism in the ortholog, NE1434; our study was also the first to designate a specific Lys residue (K152) as the anticipated internal amino donor. The distance from the dimetal active site to the sacrificial Tyr is roughly 14 Å, thus it is suspected CADD and its ortholog make use of a transient radical highway along conserved aromatic amino acids. The antagonistic metal preferences seen between CADD and NE1434 raise the question of how these two enzymes can employ similar chemistry with varying metal requirements. Finally, LC-MS/MS analysis of bands containing a putative cross-link from CADD *in vitro* reactions could help shed light on the complex structural rearrangements that take place in this already elaborate enzyme.

Diverging metal dependence of CADD and its ortholog, NE1434. The heme oxygenase-like diiron oxidase (HDO) superfamily is comprised of catalytically diverse enzymes, yet the enzymes in this family are linked together by their 3-helix fold that houses a dimetal cluster. CADD from *C. trachomatis* is the first member of this family that does not utilize a diiron cofactor which was previously thought to be another unifying factor for this family; instead, CADD's pABA synthase activity is determined by its ability to form a heterodinuclear Mn/Fe cofactor. The complexity of this superfamily is further exemplified from our findings that a CADD ortholog,

NE1434 from *N. europaea*, is not reliant on manganese for pABA synthase activity. To rationalize this, we draw upon the hypothesis presented for the emergence of manganese dependent class I(b-d) RNRs in pathogenic bacteria which are now better equipped to deal with iron depletion or oxidative stress; the substitution of manganese for iron in these systems eliminates the need to enter the competitive lottery for iron trafficking and acquisition within their host and gives the intruder a beneficial way to use reduced forms of oxygen [2–4]. Previous exploration of the Mn/Fe oxidase, R2lox, highlighted how minor structural rearrangements and shuffled hydrogen bonding networks dictate metal assembly [5]; thus, obtaining a crystal structure of NE1434 would guide the discussion in order to justify how CADD and NE1434 contain analogous metal coordinating residues but possess distinct metal requirements for catalysis. Furthermore, excessively low *in vitro* activity of NE1434 raises concern about prematurely labeling NE1434 as an enzyme solely reliant on iron for catalysis. It is hypothesized that our overexpression methods inadvertently create favorable cofactor maturation conditions which allow for ill-timed turnover, leaving an inert enzyme in its place; this idea can be rationalized by our findings from our LC/MS-MS study in which the “protein only” condition also contained modified peptides, but not to the same intensity as protein incubated with a reducing agent. It is crucial to first clarify metal dependence with appropriate growth conditions for NE1434 so that meaningful comparisons can be made between mutants and the wild type. Difficulties in limiting iron availability during overexpression will require more stringent methods to ensure the initial enzyme is in the apo form. It is recommended that NE1434 be grown in M9 minimal media and purified anaerobically, where the use of inductively coupled plasma atomic emission spectroscopy (ICP-AES) can give insight as to the types and relative amounts of metals present.

Defining a radical translocation pathway in a self-sacrificing pABA biosynthesis pathway. The sacrificial tyrosine in CADD (Tyr27) is located roughly ~ 14 Å away from the dimetal active site (Figure 4.1). Cleavage of this aromatic residue from the protein backbone likely mimics the long-range radical transfer (RT) seen in class I RNRs, where a series of aromatics in between the two serve as transient “stepping stones” for a radical species [6]. Mutagenesis studies have made it tempting to discount Y47, Y141, and Y170 as critical for pABA synthase activity in CADD [7], but a study that tested activity of two double mutants (Y141/170F and W92F/Y170F) suspected to be in the radical pathway found a significant decrease in pABA formation of these mutants [1]. Taking a closer look at the aligned sequences of CADD and NE1434 makes this hypothesis more appealing, due to natural occurrence of Y47F, Y141F, and Y170F in NE1434, coupled with its low *in vitro* activity [7]. Albeit not the typical use, site-directed mutagenesis could be done to essentially “restore” the RT network in NE1434 and compare the activity of these “enhanced” mutants. Additionally, these mutants could be retested with various metals to discern if the low observed activity is attributable to mismetallation or the inability to create an ideal RT network. Although mutagenesis studies aid in making speculations of the radical translocation that occurs within these enzymes, more advanced spectroscopy and radical trapping will need to be employed to better visualize this pathway. Techniques such as pulse electron paramagnetic resonance (EPR) could provide more concrete evidence of a radical pathway; mutagenesis studies in concert with this can identify signals of radical buildup due to the loss of redox potential in the altered RT network [8]. Additionally, EPR is useful for characterizing the active state of the dimetal center because it is sensitive to oxidation states of iron and manganese species. Therefore, this method would provide thoughtful insight to the radical “hopping” and cofactor radical states employed by these self-sacrificing pABA synthases.

Further investigation of a putative cross-link formed during CADD's self-sacrificing mechanism. The curious double band formation seen on an SDS-PAGE gel of CADD containing reactions has gained insight from enzymes such as galactose oxidase, which can self-assemble a Cu containing cofactor cross-link; it was demonstrated that the cross-linked form ran slightly below the non-cross-linked form [9]. The formation of the cross-link seen in galactose oxidase was dependent upon metal assembly and oxygen availability, which leads us to believe this is a plausible case for CADD. Thus, it is recommended that LC-MS/MS be used to uncover the residues involved in the putative crosslink that is formed during the CADD reaction as well as the conditions that induce its formation. Samples of each condition described in Figure 2.9 have been sent out for independent analysis, which will hopefully provide a clearer indication of the chemistry occurring during CADD's *in vitro* reaction.

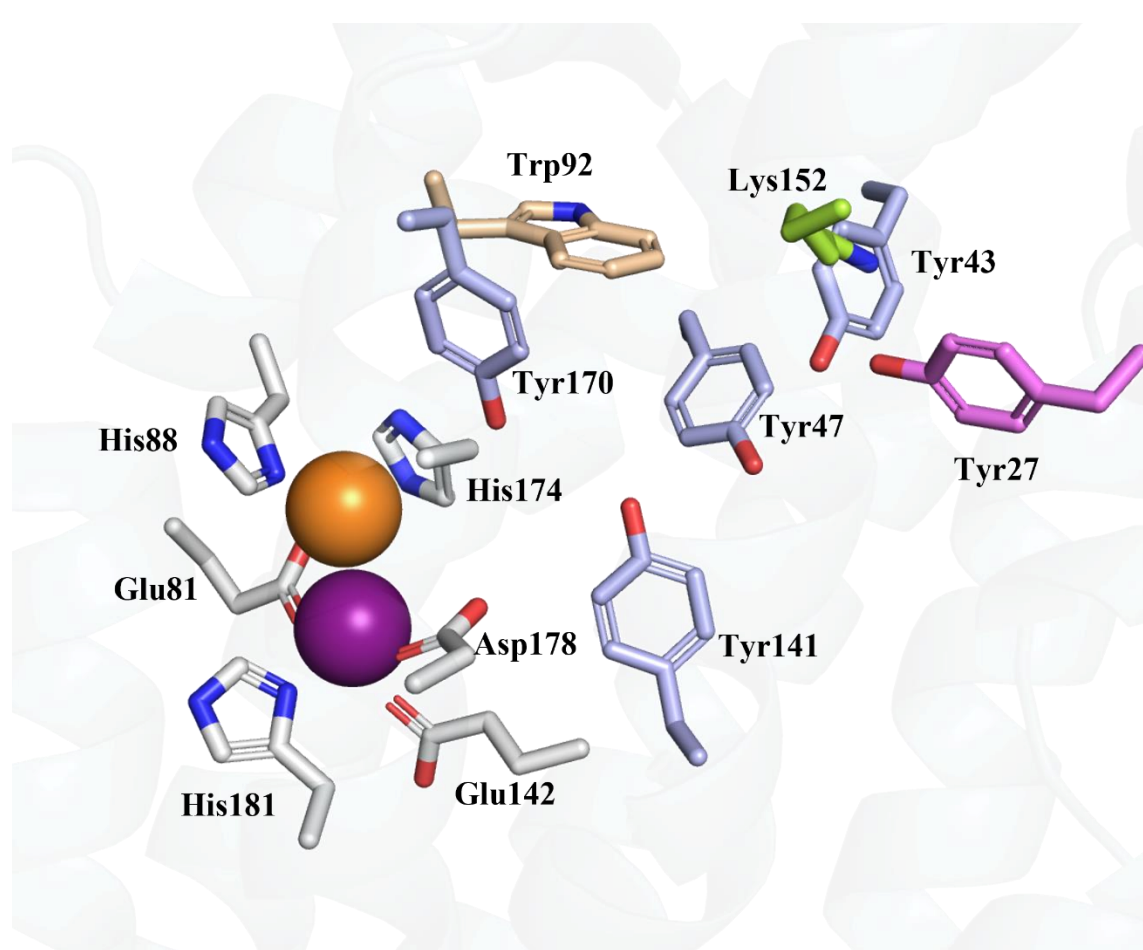


Figure 4.1: Residues of interest for a radical translocation pathway in CADD- the sacrificial tyrosine (Tyr27) shown in raspberry, non-sacrificial tyrosine residues shown in light blue, a conserved tryptophan (Trp92) shown in wheat, and an essential lysine (Lys152) shown in green.

References:

- 1 Manley OM, Phan HN, Stewart AK, Mosley DA, Xue S, Cha L, Bai H, Lightfoot VC, Rucker PA, Collins L, Williams TI, Chang W-C, Guo Y & Makris TM (2022) Self-sacrificial tyrosine cleavage by an Fe:Mn oxygenase for the biosynthesis of *para*-aminobenzoate in *Chlamydia trachomatis*. *Proc Natl Acad Sci* **119**, e2210908119.
- 2 Pokorzynski ND, Thompson CC & Carabeo RA (2017) Ironing Out the Unconventional Mechanisms of Iron Acquisition and Gene Regulation in Chlamydia. *Front Cell Infect Microbiol* **7**.
- 3 Ruskoski TB & Boal AK (2021) The periodic table of ribonucleotide reductases. *J Biol Chem* **297**, 101137.
- 4 Cotruvo JA & Stubbe J (2010) An Active Dimanganese(III)–Tyrosyl Radical Cofactor in Escherichia coli Class Ib Ribonucleotide Reductase. *Biochemistry* **49**, 1297–1309.
- 5 Kisgeropoulos EC, Griese JJ, Smith ZR, Branca RMM, Schneider CR, Högbom M & Shafaat HS (2020) Key Structural Motifs Balance Metal Binding and Oxidative Reactivity in a Heterobimetallic Mn/Fe Protein. *J Am Chem Soc* **142**, 5338–5354.
- 6 Kang G, Taguchi AT, Stubbe J & Drennan CL (2020) Structure of a trapped radical transfer pathway within a ribonucleotide reductase holocomplex. *Science* **368**, 424–427.
- 7 Macias-Orihuela Y, Cast T, Crawford I, Brandecker KJ, Thiaville JJ, Murzin AG, de Crécy-Lagard V, White RH & Allen KD (2022) An Unusual Route for p-Aminobenzoate Biosynthesis in Chlamydia trachomatis Involves a Probable Self-Sacrificing Diiron Oxygenase. *J Bacteriol* **202**, e00319-20.
- 8 Dassama LMK, Jiang W, Varano PT, Pandelia M-E, Conner DA, Xie J, Bollinger JM & Krebs C (2012) Radical-Translocation Intermediates and Hurdling of Pathway Defects in “Super-oxidized” (Mn^{IV}/Fe^{IV}) Chlamydia trachomatis Ribonucleotide Reductase. *J Am Chem Soc* **134**, 20498–20506.
- 9 Dominy JE, Hwang J, Guo S, Hirschberger LL, Zhang S & Stipanuk MH (2008) Synthesis of Amino Acid Cofactor in Cysteine Dioxygenase Is Regulated by Substrate and Represents a Novel Post-translational Regulation of Activity*. *J Biol Chem* **283**, 12188–12201.